Strength Size Effect in Asphalt Binders and Mixtures at Low Temperature

A THESIS
SUBMITTED TO THE FACULTY OF THE GRADUATE SCHOOL
OF THE UNIVERSITY OF MINNESOTA
BY

AUGUSTO CANNONE FALCHETTO

IN PARTIAL FULFILLMENT OF THE REQUIREMENTS
FOR THE DEGREE OF
DOCTOR OF PHILOSOPHY

Mihai O. Marasteanu, Adviser

Jia-Liang Le, Co-Adviser

January 2013

ACKNOWLEDGEMENTS

I would like to express my deepest gratitude to my advisor Dr. Mihai O. Marasteanu for his patience, kind support and guidance throughout the development of this thesis, and to my co-advisor Dr. Jia-Linag Le for introducing me to the size effect analysis, which is the fundamental kernel of this dissertation.

I also want to thank Dr. Lev Khazanovich and Dr. Douglas M. Hawkins for their advice and contributions and for serving as committee members. I express also my appreciation to Dr. Vaughan R. Voller for supporting me through the Dental School research project.

The financial support provided by the NCHRP IDEA program is gratefully acknowledged.

I would also like to thank Dr. Chris Williams at Iowa State University for providing accesses to their laboratory and the Minnesota Department of Transportation for providing the materials used in this dissertation.

My particular gratitude goes to Dr. Ki Hoon Moon and Mugurel I. Turos for their help at the University of Minnesota.

Finally, and above all, I am truly, deeply thankful to my Mother and my Father for supporting and encouraging me during these years.

ABSTRACT

Low temperature cracking is the prevailing failure mode in asphalt pavements built in cold regions. This phenomenon manifests as a set of surface-initiated transverse cracks which can lead to further damage due to water penetration. Good strength properties of asphalt binders and asphalt mixtures are, therefore, critical for building durable pavements. The current testing methods used to characterize asphalt binder and mixture strength require the use of very expensive and sensitive testing devices and present limitations in the extrapolation of results from laboratory specimens to larger structures such as full scale pavements.

In this thesis the strength size effect of asphalt materials is investigated with the aim of addressing the possibility of using a simple laboratory device, called Bending Beam Rheometer (BBR), for performing strength tests on small beam specimens of asphalt binders and asphalt mixtures. Using three-point bending experimental data and size effect theory for quasibrittle materials, the failure distribution of the Representative Volume Element (RVE) of asphalt binders and asphalt mixtures is evaluated, and a RVE substructure model for asphalt mixture is proposed to analyze the strength measurements obtained on small BBR beams. Forward and back calculation procedures are implemented to directly link the statistic parameters of failure distribution of one RVE to the mean size effect curve of structural strength and vice versa. The effect on strength of different cooling media used in BBR is also evaluated.

TABLE OF CONTENTS

LIST OF TABLES

LIST OF FIGURES

Chapter 1. Introduction

1.1. Background

Asphalt pavements represent approximately 94% of the 2.70 million miles of paved roads in US (*U.S. Department of Transportation - Bureau of Transportation Statistics 2010*). They are built with asphalt mixture, which is a composite material made of aggregates of different sizes bonded together with asphalt binder, a residue of oil distillation. The asphalt binder is a highly temperature susceptible material that becomes brittle at low temperatures. This characteristic makes low temperature cracking a significant distress in asphalt pavements built in cold climates and highly affects the ride quality and pavement durability. Using asphalt materials that have high strength at low temperature can significantly improve the durability of asphalt pavements and reduce the costs associated with maintaining and repairing the roads during their service life.

1.2. Problem Statement

The current test methods used to obtain strength properties of asphalt binder and asphalt mixture are Direct Tension Tester (DTT) (*AASHTO T314-07-UL 2007*) and Indirect Tensile test (IDT) (*AASHTO T322-07-UL 2007*), respectively. These procedures require expensive and sensitive testing devices available only to very few laboratories. For this reason, the selection and quality control of asphalt materials are done, in most cases, based on empirical correlations to volumetric properties (*AASHTO M323-07-UL 2007*), which can be easily measured in laboratory conditions.

In addition, asphalt materials have quasibrittle behavior at low temperatures (*Turos et al. 2012, Marasteanu et al. 2012*). Quasibrittle heterogeneous materials are

characterized by inhomogeneities that are not negligible compared to the structure size (*Bažant and Pang 2007, Le et al. 2011*). For this type of materials, size effect can be significant. Previous studies have shown that IDT, due to specimen and testing geometry, presents non-unique and irregular strength size effect (*Rocco et al. 1995, Rocco 1996, Bažant and Planas 1998*), which significantly limits the possibility of extrapolating the laboratory results to the larger asphalt pavement structures.

1.3 Objective and Research Approach

Understanding strength size effect of asphalt materials is fundamental for predicting the field response and performance of asphalt pavements. In this dissertation, the size dependence of the strength of asphalt binders and asphalt mixtures is investigated, with the objective of evaluating the possibility of obtaining and extrapolating relevant material properties by testing small size specimens with the Bending Beam Rheometer (BBR) (*AASHTO T313-10-UL 2010*). This device is currently used for creep tests on asphalt binders and asphalt mixtures (*Marasteanu et al. 2009*), and is less expensive than DTT (*AASHTO T314-07-UL 2007*) and IDT (*AASHTO T322-07-UL 2007*).

The research approach used in this thesis is based on an extensive experimental work consisting of multiscale strength tests on specimens of asphalt binders and asphalt mixture, and on the use of the size effect theory for quasibrittle materials (*Bažant and Planas 1998, Bažant and Pang 2007, Bažant et al. 2009, Le et al. 2011*). According to this theory, the type of strength distribution changes as the size of the structure increases (*Bažant and Pang 2007, Bažant et al. 2009, Le et al. 2011*). Quasibrittle structures of positive geometry, for which the peak load is reached as macro-crack initiates from one

representative volume element (RVE), can be statistically modeled as a finite chain of RVEs according to the finite weakest link model (WLM) (*Bažant and Pang 2007, Bažant et al. 2009, Le et al. 2011*). Therefore, the cumulative distribution function (cdf) of the strength of one material RVE is needed to fully predict the failure probability of the entire structure. The RVE cdf of strength is described by a Gaussian cdf core, onto which, a remote Weibull cdf tail is grafted on the left. At structure level, the strength distribution can be obtained by the joint probability theorem which results into a convoluted size effect on the mean structural strength (*Bažant and Pang 2007*, *Le et al. 2011*).

1.4. Organization

This thesis is divided into six Chapters. Chapter 2 includes a general review of asphalt binder and asphalt mixture characteristics and internal structures, and of the current and recently developed strength test methods for both materials. This chapter also presents a review of the size effect theory of strength for quasibrittle materials. In Chapter 3 the experimental phase and analysis used to evaluate asphalt binder strength is outlined. Chapter 4 provides a general approach to strength size effect for asphalt mixture including forward and backcalculation procedures for the evaluation of the material failure distribution and mean size effect analysis. Chapter 5 presents the work conducted to investigate the asphalt mixture strength obtained from BBR tests. Chapter 6 contains summary and conclusions of this thesis.

Chapter 2. Literature Review

First, a description of asphalt binder microstructure is presented. Next a short overview on asphalt mixture is provided. This is followed by a review of the current specifications for asphalt binder and asphalt mixture strength test procedures at low temperatures and of the alternative testing methods proposed in literature. This chapter concludes with a review of the strength size effect theory for quasibrittle materials.

2.1. Asphalt Binder

The first record on the use of asphalt binder for road application dates back to Nabopolassar, King of Babylon (Circa 600 BC) (*Abraham 1960*). However, its use disappeared until the early 19th century, when natural sources of this material were discovered (*Lay 1992*). Currently, asphalt binder is obtained as vacuum residue of oil distillation, and 95% of the total production is used for paving purposes (*Lesueur 2009*). Asphalt binder is generally defined as a "virtually involatile, adhesive and waterproofing material derived from crude petroleum, or present in natural asphalt, which is completely or nearly completely soluble in toluene, and very viscous or nearly solid at ambient temperatures" (*EN 12597 2000, Lesueur 2009*). The density of asphalt binder is typically between 1.01 and 1.04 g/cm^3 depending on the crude source. Asphalt binder exhibits a glass transition around T=-20 °C, although it varies in a range from 5°C down to -40°C depending essentially on the crude source (*Read and Whiteoak 2003*).

Asphalt binder mainly consists of carbon (typically 80–88% in weight) and hydrogen atoms (8–12% in weight) with a hydrocarbon content superior to 90% and a hydrogen-to-carbon molar ratio H/C around 1.5. This H/C ratio is intermediate between

that of aromatic structures (benzene has H/C=1) and that of saturate alkanes (H/C~2). Heteroatoms such as sulfur (0–9%), nitrogen (0–2%) and oxygen (0–2%) and traces of metals including vanadium, up to 2000 parts per million (ppm), and nickel (up to 200 ppm) are also present (*Branthaver et al. 1994*). Average molecular structures have been proposed for asphalt binders used during the SHRP study (*Jennings et al. 1992*). However, binder properties can be better investigated by separating the molecules into different chemical families, depending on their size and solubility in polar, aromatic or non-polar solvents (*Lesueur 2009*). Corbett (*1969*) was the first in separating asphalt binder in the so called SARA fractions, Saturates, Aromatics, Resins and Asphaltenes, resulting into a binder structure made of a chemical continuum with a gradual increase of molar mass, aromatic content and polarity from saturates to asphaltenes (Figure 2.1).

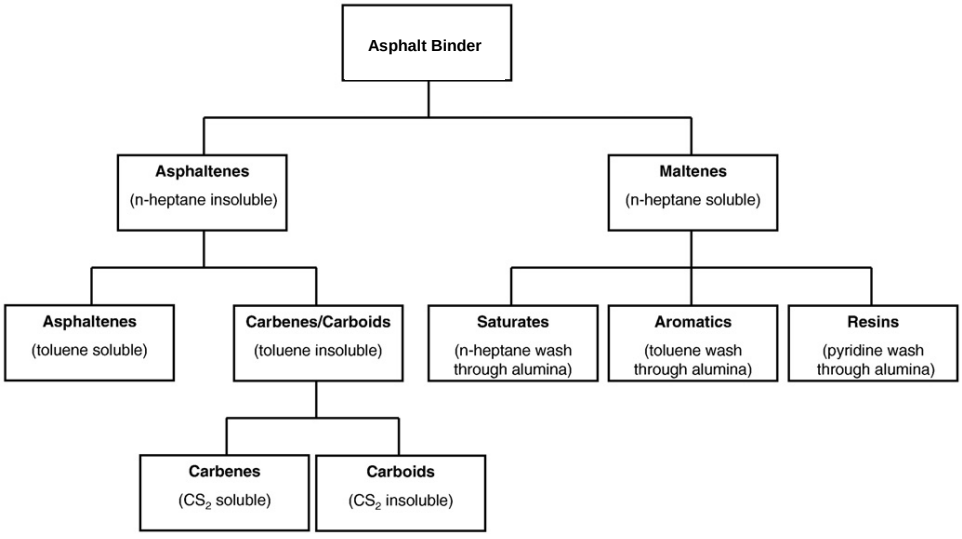

Figure 2.1. SARA fractions of asphalt binder (*Speight 2004*)

Saturates (5–15% of the asphalt binder weight) form an almost colorless liquid and present a very low glass transition temperature around -70°C, which is typically 40°C

below the glass transition of their original binder. Aromatics (naphthene aromatics) are the most abundant components of a binder, together with the resins, since they amount for 30–45% of the total weight; they form a yellow to red liquid at room temperature. Resins (30% to 45% in weight) are generally dark and semi-solid or solid. They are fluid when heated, and become brittle at low temperature. Asphaltenes (5 to 20% in weight) have a dark brown color, and play a viscosity building role in the material. Ultra-Violet fluorescence (*Mullins 1998*) shows that they contain fused aromatic rings, with a structure made of 4–10 rings connected to aliphatic chains. Because of the condensed aromatic rings structures, asphaltenes form planar molecules that can associate through π–π bonding to form parallel-like stacks showing dimensions in the range of 2-5 nm. When put in a solvent, the asphaltenes still associate and the aggregation (Figure 2.2) leads to micelles formation in a process that is the basis of the colloidal structure of asphalt binder (*Lesueur 2009*).

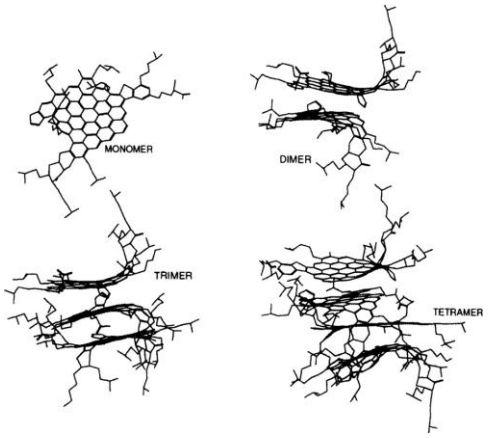

Figure 2.2. Aggregation process of asphaltenes (*Dickie and Yen 1967*)

2.1.1. Asphalt Binder Structure

The first colloidal models for asphalt binder, in which asphaltenes are very close in structure to free carbon and form a colloidal suspension within the maltene phase, was proposed by Rosinger (*1914*) and Nellensteyn (*1924*). The colloidal model was further developed by Pfeiffer and Saal (*1940*), who separated asphalt binder in two categories: sol and gel. Sol binders present Newtonian behavior, while gel binders are highly non-Newtonian (Figure 2.3).

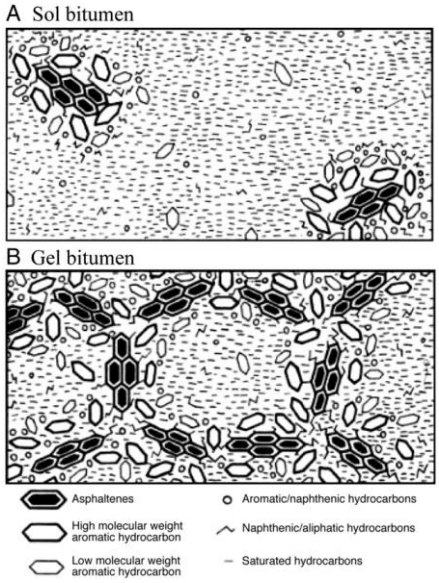

Figure 2.3. Original colloidal models (*Read and Whiteoak 2003*)

Asphalt binder is described as a colloidal dispersion of asphaltenes micelles in the maltenes. The resins, that are the polar components of the maltenes, play a stabilizer role for asphaltene micelles. Lesueur et al. (*1996*) showed, through viscoelastic analysis, the existence of asphaltenes micelles that exhibit a Brownian motion at higher temperatures. Further proof of the existence of asphaltenes is given by the fact that asphalt binder undergoes a glass transition at a temperature very close to that of its aromatics. This

suggests that the asphaltenes exist as dispersed solid particles, and do not directly participate to the glass transition (*Turner and Branthaver 1997*). Asphaltenes micelles are generally described as spherical objects; however, a more open molecular assembly with low fractal geometry (Figure 2.4) was also proposed (*Gawrys and Kilpatrick 2004*).

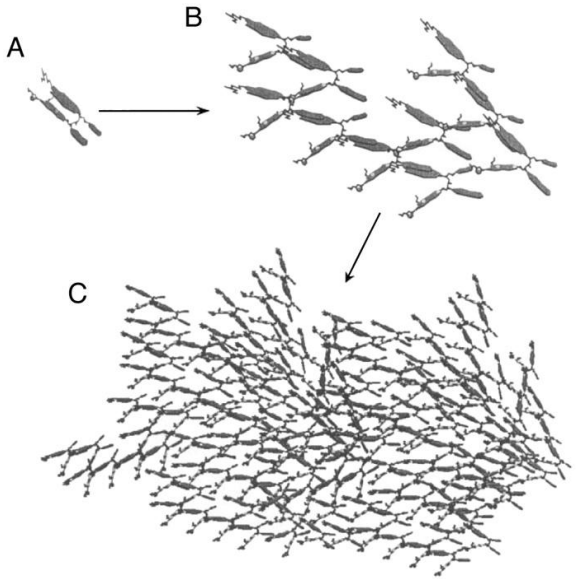

Figure 2.4. Fractal model with asphaltenes aggregate with size ca. 12–15nm (*Gawrys and Kilpatrick 2004*)

The stabilizing role of the resins in asphaltenes micelles is not well understood; however, Koots and Speight (*1975*) confirmed that, without the resins, the asphaltenes would precipitate from the oily asphalt binder components.

Different assembly structure organizations of the asphaltenes micelles were hypothesized based on the different experimental setup used. For example, based on Atomic Force Microscopy(AFM) scanning, a “bee” structure (Figure 2.5 (a)) was found

for gel binder (*Loeber et al. 1996*) with an average height between 22 and 85 nm and a typical distance between strips of order 150 nm (*Masson et al. 2006*).

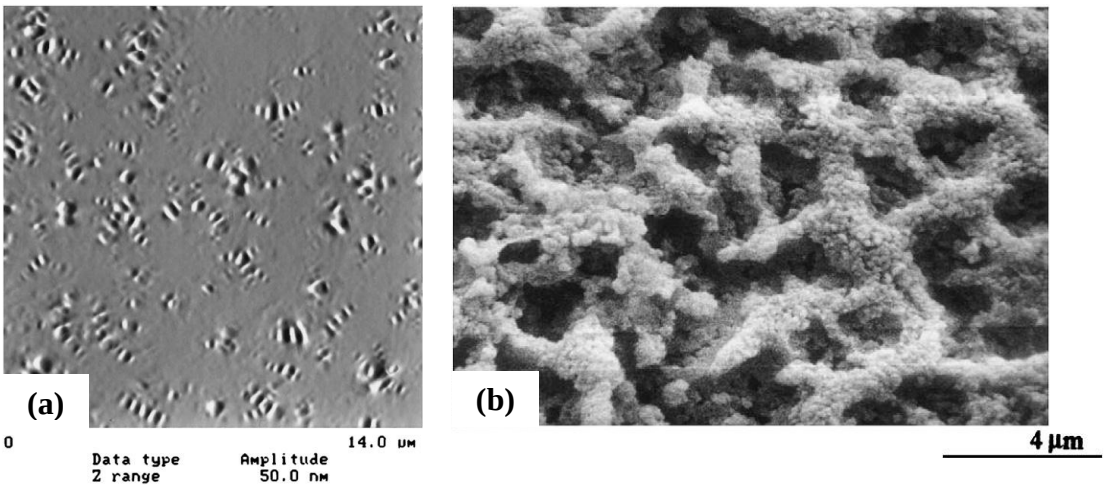

Figure 2.5. (a) Asphalt binder "bee" structure with typical size 1µm (b) SEM gel-binder (*Loeber et al. 1996*)

In a different research effort (*Jäger et al. 2004*), binder structures with flake-like domains of diameter of 1µm were found, while Scanning Electron Microscope (SEM) observations on gel binders showed connecting particles of asphaltene of diameter around 100 nm (Figure 2.5 (b)) (*Loeber et al. 1996*). The surfactant effect of resins as asphaltenes stabilizer was investigated by Storm et al. (*1993*) and a solvation parameter *K* was introduced to quantify the increase in volume fraction of solid phase due to the adsorbed resins.

In addition to the nanostructure arising from the asphaltenes, linear alkanes present within asphalt binder can crystallize (*Lesueur* 2009). The effects of wax crystallizations on the structure of binder are not clear yet, however, wax crystals display different geometries depending on the crude source and crystallization conditions with typical sizes of order of 1-10µm (Figure 2.6) (*Lu et al. 2005*).

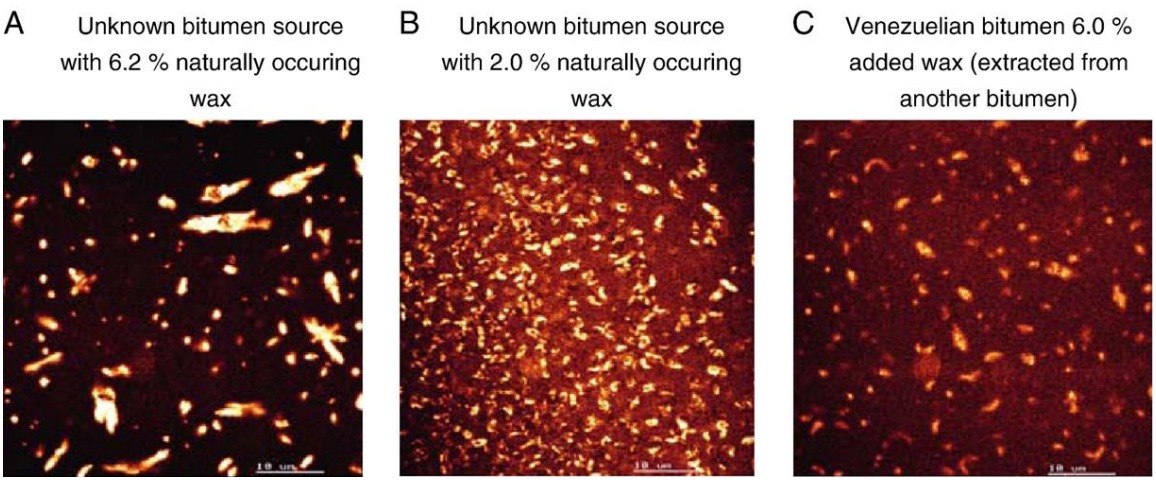

Figure 2.6. Wax crystallization in asphalt binder (*Lu et al. 2005*)

Waxes typically crystallize in asphalt binders at temperatures starting from 90°C down to the glass transition temperature, and most binders for paving applications have amounts of paraffin-like crystalline components less than 5% by weight.

2.1.2. Aging

The structure of asphalt binder is quite complex with slow temperature dependent evolution that is strictly associated to its internal molecular organization (*Lesueur 2009*). Additionally, the molecules may irreversibly experience chemical aging, which consists of a combination of oxidation reactions, polymerization, and lighter components evaporation (*Bell 1989, Read and Whiteoak 2003*). Chemical aging leads to a global hardening of the material (*Read and Whiteoak 2003*) and increased cracking susceptibility (*Isaccson and Zeng 1998*). Two aging conditions are identified for asphalt binder used for paving purposes. The first one, called short-term aging, consists in a rapid chemical aging upon mixing the hot asphalt binder, in thin film, with the hot aggregate to produce asphalt mixture. This is generally reproduced in laboratory through the Rolling

Thin Film Oven Test (*AASHTO T240-09-UL 2009*). The second, long-term aging consists of an in-situ aging during the service life of the pavement. Pressure Ageing Vessel Test (*AASHTO R028-09-UL 2009*) is the current experimental procedure used to simulate long term aging.

2.2. Asphalt Mixture

Asphalt mixtures are composite materials consisting of three phases: asphalt binder, aggregate, and air voids. A typical volumetric composition of this material is 5% of air voids, 20% of asphalt binder, and 75% of aggregate (*NCAT 2009*); at the macroscopic level aggregate particles of various sizes and shapes are distributed in matrix of asphalt binder (Figure 2.7).

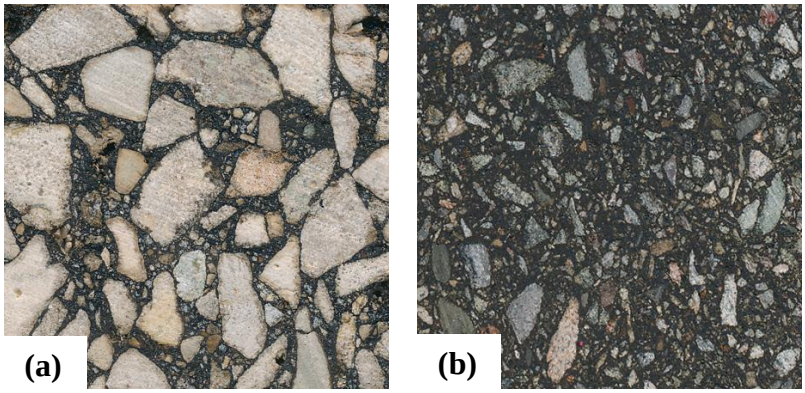

Figure 2.7. Two asphalt mixtures with different aggregate grain size (*Marasteanu et al. 2012*)

Similarly to other composite materials, the properties of asphalt mixture are related to the properties of its components. The aggregate phase is generally considered linear elastic and the asphalt binder is considered viscoelastic, which results in a viscoelastic

composite material with properties depending also on temperature (*Monismith and Secor 1962*).

Mineral filler is the fine part of the aggregates fraction usually identified as the material passing the 200 sieve in the US (0.075mm). Generally filler adds up to 2-12% (*Lesueur 2009*) of the aggregate component of asphalt mixtures and when mixed with binder forms a suspension (*Rigden 1947*), called mastic. However, in the case of the so-called active fillers, specific binder/filler interactions come into play giving rise to quite different behavior resulting into a much significant stiffening effect. This is the case of lime, fly ash and kaolin (*Craus 1979*). For this type of materials, the combined effect of an adsorption layer of asphaltenes around the mineral and the high porosity of some active filler contribute to the increase in stiffness (*Petersen et al. 1987*).

Different model were proposed to describe the properties of asphalt mixture. Micromechanical models (*Hirsch 1962, Milton 1981, Torquato 2002, Christensen et al. 2003*) were used to schematize asphalt mixture either as a two or three-phase composite, and to predict the response of the material based on the properties of the components. Analogical models were proposed (*Huet 1963, Di Benedetto et al. 2004, Cannone Falchetto et al. 2011*) for the rheological behavior of asphalt binders and asphalt mixtures.

Descriptions of the microstructure of asphalt mixture were also recently proposed based on Digital Image Processing (DIP) and *n*-point correlation functions (*Berryman 1985, Torquato 2002*). Asphalt mixture was generally described as a random heterogeneous material (*Velasquez 2009*). In a different study it was found that the spatial distribution of aggregate phase presents a random pattern even when recycled asphalt

material is added to the mixture (*Cannone Falchetto et al. 2012a, 2012b*); however an increase in the autocorrelation length of the aggregate phase was observed in recycled mixture (*Cannone Falchetto et al. 2012b*).

2.3. Strength Tests Methods for Asphalt Materials at Low Temperature

2.3.1. Asphalt Binder

Currently, asphalt binder low temperature behavior is characterized using the Bending Beam Rheometer (BBR) (*AASHTO T313, 2010*) and the Direct Tension Tester (DTT) (*AASHTO T314, 2007*). BBR is used to perform low-temperature creep tests on beams of asphalt binders conditioned at the desired temperature for 1 hour in ethanol (C_2H_6O). The DTT is used to perform low-temperature uniaxial tension tests at a constant strain rate of 3% on dog-bone shaped specimen of asphalt binder conditioned at the desired temperature for 1 hour in potassium acetate (CH_3CO_2K) (Figure 2.8). The average stress and strain at failure are obtained from the four highest values out of six replicates.

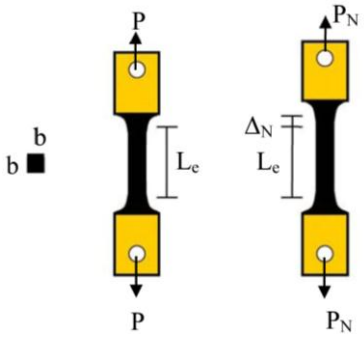

Figure 2.8. DTT strength scheme (*Marasteanu et al. 2012*)

DTT failure stress σ_N (nominal strength) and failure strain ε_N are calculated according to equations [2.1] and [2.2].

$$\sigma_N = \frac{P_N}{A} \quad [2.1]$$

$$\varepsilon_N = \frac{\delta_N}{L_e} \quad [2.2]$$

where σ_N is expressed in MPa, P_N is the failure load (N), A=bxb is the original cross section of the specimen (mm^2), b=6mm is the side of the specimen, ε_N is the strain at failure, δ_N is the elongation at failure and L_e is the effective gage length (33.8mm).

DTT was used by different authors to investigate asphalt binder strength (*Marasteanu et al. 2007, Khedoe et al. 2008*). DTT was modified by introducing two symmetric notches at the middle of the sample to perform double edge notched tension (DENT) fracture tests (*Zofka et al. 2007*). As expected, significant differences were found due to the presence of notches in the DENT specimens.

Beam geometry was also used to investigate the failure of asphalt binder. Three point bending tests for notched beam were proposed by several authors in the past (*Lee and Hesp 1994, Hoare and Hesp 2000, Anderson et al. 2001, Olard and Di Benedetto 2004*) and more recently (*Portillo and Cebon 2008, Velasquez et al. 2011*). However, only recently a new method was presented to obtain asphalt binder nominal strength with a modified BBR on unnotched beams (125mm x 12.5mm x 6.25 mm) (*Marasteanu et al. 2012*) (Figure 2.9).

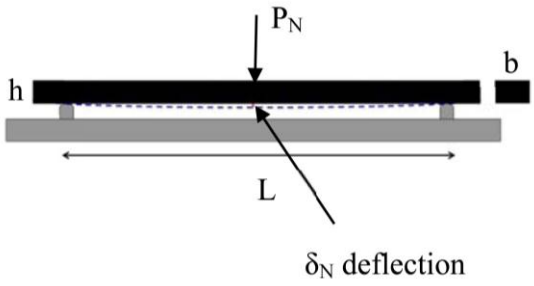

Figure 2.9. BBR strength scheme (*Marasteanu et al. 2012*)

The BBR nominal strength (maximum stress at peak load) and corresponding strain at the bottom of the thin beam were computed according to equations [2.3] and [2.4].

$$\sigma_N = \frac{3P_N L}{2bh^2} \quad [2.3]$$

$$\varepsilon_N = \frac{6\delta_N h}{L^2} \quad [2.4]$$

where σ_N is the nominal strength (MPa), ε_N is the strain at failure, P_N is the failure load (N), L=101.6mm is beam span, b=12.5mm is the width of the beam, h=6.25mm is the thickness of the beam and δ_N is the deflection of the beam corresponding to the maximum load. In the same work, the authors compared the BBR strength results with DTT values through simple geometry and stress field corrections. Weibull distribution (*Weibull 2009*) was used to convert BBR results to uniaxial stress for a specimen with the same volume of DTT. It was found that DTT strength is much higher (4 to 5 times) when compared to BBR measurements obtained in ethanol, while strengths are comparable when BBR tests are performed in potassium acetate as for DTT. Another important finding was, therefore, the significant impact of cooling medium on asphalt binder strength (*Dongré and*

D'Angelo 1998) due to environmental stress cracking effects on the material (*Arnold 1995, Moskala 1998*).

2.3.2. Asphalt Mixture

Indirect Tension Test (IDT) (*AASHTO T322-07-UL 2007*) is used to determine asphalt mixture strength at low temperature. Test is performed on cylindrical specimens that are 40mm thick and 150mm in diameter (Figure 2.10).

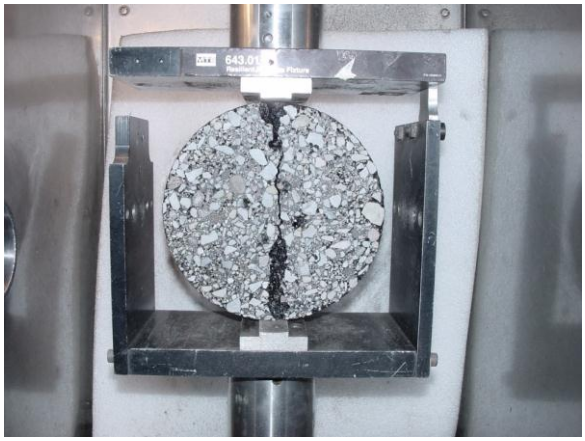

Figure 2.10. IDT - Indirect Tensile Test

Loading is diametrically applied at a constant displacement rate of 12.5 mm/min until failure occurs. Tensile strength is calculated according to equation [2.5]:

$$\sigma_{IDT} = (2P / \pi \cdot bD) \qquad [2.5]$$

where P is the failure load at which the difference between vertical and horizontal deformation is maximum and b and D are the thickness and the diameter of the specimen respectively. To avoid damage to the LVDT's, P is usually assumed as the peak load; for this reason Christensen et al. (*2004*) proposed a correction formula to evaluate the tensile nominal strength obtained with this method. Past research effort showed that Indirect

Tensile test, also known as the Brazilian strength test and Split tensile strength test is dominated by a non-unique and irregular size effect (*Sabnis and Mirza 1979, Chen and Yuan 1980, Hasegawa et al. 1985, Kim 1989, Bažant et al. 1991, Rocco et al. 1995*) that significantly limits the possibility of extrapolating the experimental results to larger structures. The complexity of the observed behavior was explained with the lack of material scale reference, with the rate dependence of the splitting strength tests and, especially, with the high sensitivity of this type of test to the boundary conditions, such as the loading strip to specimen diameter ratio *h*/*D* (*Bažant and Planas 1998, Rocco 1996*).

Uniaxial Tension Test (*EN 12697-46 2012*) or Direct Tension strength test can be also used to obtain the nominal strength of asphalt mixture. Rectangular or cylindrical specimens are glued to the loading plates through an epoxy compound, and load is applied until failure. DT is not widely used due to specimen alignment difficulties (*Khedoe et al. 2008, Hase and Oelkers 2009, Koh et al. 2009*); for this reason, eccentricity corrections may be needed.

More recently, *Turos et al.* (2012) investigated the use of a three-point bending test on small asphalt mixture beams. The new experimental method is based on a modified Bending Beam Rheometer capable of applying load at different rates; BBR nominal strength was computed according to equation [2.3].The new experimental procedure was compared with the current standard strength test methods, IDT and DT, through a simplified size effect approach based on pure Weibull failure distribution (*Bažant and Planas 1998*). The authors found that BBR mixture strength is similar to IDT strength. However, due the simplified approach used for the analysis, the dimension

of the representative volume element (RVE) of asphalt mixture and its failure distribution were not investigated.

2.4. Size Effect on Structural Strength

Size effect and scaling of materials properties were first discussed by Leonardo da Vinci (*1500s*) and later by Galileo Galilei (*1638*), but only after 1650s major advances were achieved (*Mariotte 1686*). Significant progress in probabilistic and experimental investigation of size effect was obtained when extreme value statistics and weakest link model (WLM) for a chain were formulated by Fréchet (*1927*) and Fisher and Tippet (*1928*). However, the capstone of statistical size effect was first laid by Weibull in 1939 (*Weibull 1939*); he proposed for the tail of the extreme value distribution of the strength of a small material element a power law (*Weibull 1939, Bažant 2005*). Weibull theory applies to structures that fail at the initiation of a macrocrack with small fracture process zone (FPZ) and minimal stress redistribution (*Bažant 2005*). However, this is not true for quasibrittle materials such as Portland cement concrete and asphalt mixture for which the size of the inhomogeneities is not negligible compared to the structure size (*Bažant and Planas 1998, Bažant 2005, Bažant and Pang 2007, Bažant et al. 2009, Le et al. 2011*). In the recent past, several research efforts were attempted to model the behavior of this class of materials based on linear elastic fracture mechanics (LEFM) (*Leicester 1969, Walsh 1972*), cohesive crack model (*Hilleborg et al. 1976*) and fractal characteristics of cracks at different scales (*Carpinteri and Chiaia 1995*).

More recently, an energetic statistic approach to strength size effect was successfully proposed by Bažant and co-workers (*Bažant and Novák 2000, Bažant and*

Pang 2007, Bažant et al. 2009, Le et al. 2011). According to this theory two limiting failure behaviors can be identified: plastic (or ductile) and perfectly brittle. In the first case the failure distribution and thus the cumulative distribution function (cdf) of structural strength follows Gaussian statistics given by the weighted sum of the strength contributions from all the representative volume elements (RVEs) of the material constituting the failure surface (*Le et al. 2011*). The WLM (*Bažant and Planas 1998, Bažant and Pang 2007, Bažant et al. 2009, Le et al. 2011*) can be used to describe perfectly brittle failure in which the structure failure is triggered by the failure of one RVE; for very large structures this type of failure follows the Weibull distribution (*Weibull 1939*). However, for quasibrittle materials failure changes from quasi-plastic to brittle as the structure size increases (*Bažant and Pang 2007, Bažant et al. 2009, Le et al. 2011*), and thus, the strength cdf of the structure is size dependent.

Such a size effect formulation is used to analyze and evaluate the experimental strength results obtained in this thesis. The following sections of this chapter provide a short overview and a theoretical background on size effect theory for quasibrittle materials.

2.4.1. Size Effect Types

According to the deterministic theories of elasticity and plasticity, geometrically similar structures do not present size effect, and their nominal strength, is defined as:

$$\sigma_N = \frac{cP_{\max}}{bD} \qquad [2.6]$$

where, σ_N is the nominal strength of the structure P_{max} is maximum load that the structure can sustain, D is the structure characteristic size (scaling dimension), b is the third

dimension of the of the structure (b=constant), c is a dimensionless constant which may depend on structure shape but not on size, such that σ_N represents the maximum elastic principal stress in a notchless structure (*Bažant and Pang 2007*). However, for quasibrittle structures the failure criterion includes a material characteristic length, l_0, and two main types of strength size effect can be identified. Type I size effect, which is the only one considered in this thesis, occurs in notchless structures failing at macrocrack initiation from one representative volume element (RVE) of the material (*Bažant and Pang 2007*). Figure 2.11(a) presents type I size effect: m is the Weibull (*Weibull 1939, Bažant and Pang 2007*) modulus and n indicates the scaling dimension(s). Type II occurs in structures containing a large notch or a stress-free (fatigued) crack formed before reaching the peak load (*Bažant and Pang 2007*) (Figure 2.11(b)).

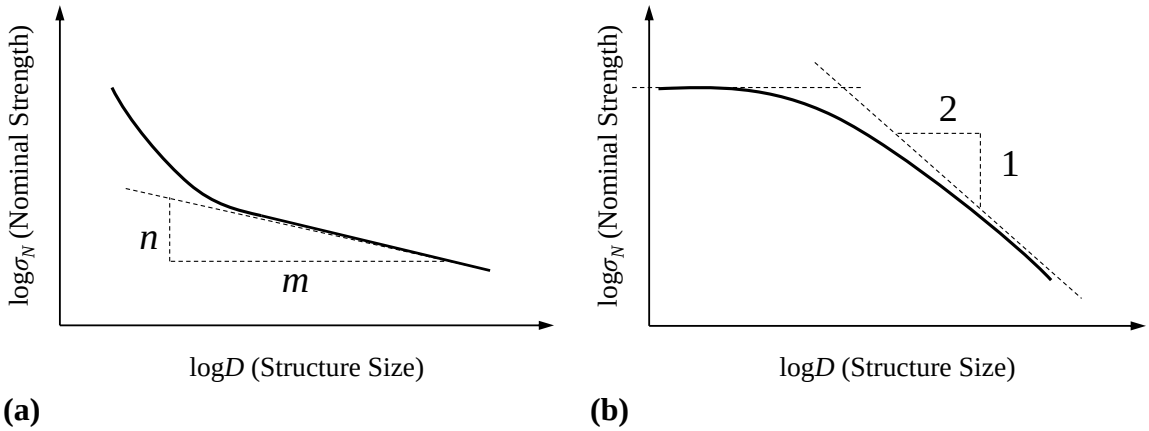

Figure 2.11. (a) Type I and (b) Type II size effect on structural strength

Type I size effect is typical of uniaxial and flexural failures, in which the RVE size is comparable with the thickness of the microcracking boundary zone where energy release and stress redistribution occur before the formation of a macrocrack. For structures in the small and medium size limit, the Type I size effect can be derived from

the Taylor series expansion of the energy release function at zero crack length. At large size limit, the size effect is governed by the Weibull statistics (*Bažant and Pang 2007*).

Type I size effect can be alternatively derived from the WLM (*Bažant and Pang 2007*). Due to the non-negligible dimension of the RVE the structure is statistically modeled as a finite chain of RVEs where the strength distribution of one RVE can be obtained from fracture mechanics of nano-cracks propagating by small, activation-energy controlled, random jumps through a nano-structure (*Bažant and Pang 2007, Le et al. 2011*).

In order to relate the strength cdf of a nano-scale element to the strength cdf of an RVE at the macro-scale a statistical multiscale transition framework based on a hierarchical model consisting of bundles (Fiber Bundle Model) and chains (Weakest Link Model) can be used (*Bažant and Pang 2007, Le et al. 2011*).

2.4.2. Weakest Link Model

According to the WLM, which statistically models the localization of failure into one FPZ at one location (*Le et al. 2011*), the structure can be represented as a chain of small materials elements, RVEs (Figure 2.12).

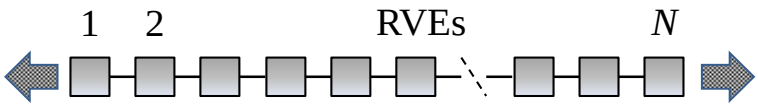

Figure 2.12. Weakest link model: chain of *N* RVEs

Each RVE, which is the smaller material volume that triggers the entire structure failure, represents an element of the structure model. Grassl and Bažant (*2009*) recently

demonstrated through discrete element simulation that the auto-correlation length of the random field of the structural strength is approximately equal to the RVE size. Therefore, assuming the statistical independence of the random strength of the RVEs and based on the joint probability theorem, the failure probability of the entire structure P_f made of N RVEs can be obtained as (*Bažant and Pang 2007, Le et al. 2011*):

$$P_f(\sigma_N) = 1 - \prod_{i=1}^{N} \left[1 - P_1(s_i \sigma_N)\right] \qquad [2.7]$$

where P_1 is the cumulative distribution function (cdf) of strength of one RVE, σ_N is the nominal strength of the structure, s_i is the dimensionless stress field (function of the coordinate vector **x**) such that $\sigma_N s_i$ corresponds to the maximum elastic principal stress at the center of i^{th} RVE. Based on experiments, Weibull (*Weibull 1939*) realized that the left tail of the cdf of one RVE follows a power law:

$$P_1 = \left[\sigma_N / s_0\right]^m \qquad [2.8]$$

where m is the Weibull moduls of the material (shape parameter) and s_0 is a material constant (scale parameter). Equation [2.7] can be rewritten in logarithm form and by approximating $\ln(1-x) \approx -x$ the following expression can be obtained (*Bažant and Pang 2007, Le et al. 2011*):

$$P_f(\sigma_N) = 1 - \exp\left\{-\sum_i^N \left(\frac{\sigma_N \langle s_i \rangle}{s_0}\right)^m\right\} = 1 - \exp\left\{-\int_V \left(\frac{\sigma_N \langle s(\mathbf{x}) \rangle}{s_0}\right)^m \frac{dV(\mathbf{x})}{l_0^n}\right\} \qquad [2.9]$$

where l_0 is the characteristic dimension of the material RVE, n represents the scaling dimension(s), $s(\mathbf{x})$ is the positive dimensionless stress field for the coordinate vector $\mathbf{x}(x,y)$ and $V(\mathbf{x})$ is the volume of the structure. Based on equation [2.9] the mean strength of the entire structure can be calculated as:

$$\bar{\sigma}_N = s_0 \Gamma\left(1+\frac{1}{m}\right)\left(\frac{l_0}{D}\right)^{n/m}\left[\int_V \langle s(\xi)\rangle^m \mathrm{d}V(\xi)\right]^{-1/m} \qquad [2.10]$$

where $\boldsymbol{\xi} = \mathbf{x}/D$ is the normalized coordinate vector, and $\Gamma(x)$ is the Eulerian gamma function. The coefficient of variation, ω_N (CoV), can then be derived from expression [2.9] as (*Bažant and Planas 1998, Bažant and Pang 2007*):

$$\omega_N = \sqrt{\frac{\Gamma(1+2/m)}{\Gamma^2(1+2/m)} - 1} \qquad [2.11]$$

2.4.3. Fiber Bundle Model

Fiber bundle model (or parallel coupling) is a basic statistical model, which statistically represents the load redistribution for a partially damage material microstructure (*Bažant and Pang 2007, Le et al. 2011*) (Figure 2.13).

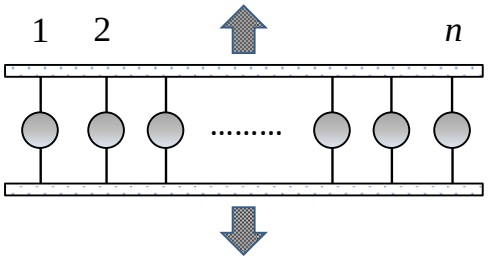

Figure 2.13. Bundle of fibers model

Different sharing rule for load redistribution after a fiber breaks were proposed (*Daniels 1945*, *Phoenix and Tierney 1983*, *Mahesh and Phoenix 2004*). A physically meaningful and simple approach is to derive load sharing of fibers after breaking from the assumption that all the fibers are subjected to the same strain ε (*Bažant and Pang 2007*).

Fibers are assumed to respond in elastic manner till the strength limit is reached; same cross section A, same elastic modulus E and same strength cdf $F(\sigma)$ are assigned to

each fiber. Three types of fiber behaviors can be identified after reaching the strength limit of the fiber: (a) brittle, when the stress drops suddenly to zero, (b) plastic, in which case the fiber plastically deforms at a constant stress σ_i, and (c) softening, when the fiber presents a post peak softening (*Bažant and Pang 2007*, *Le et al. 2011*) (Figure 2.14).

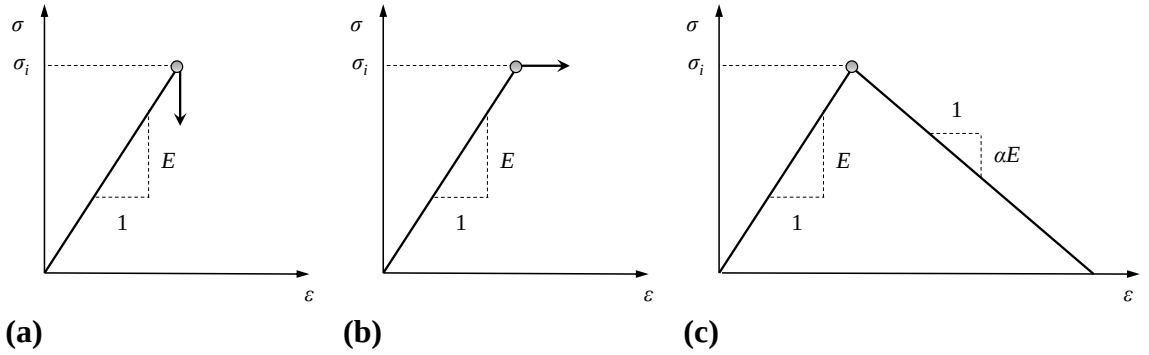

Figure 2.14. (a) Brittle (b) plastic and (c) softening fibers behaviors

2.4.3.1. Brittle Bundle

The cumulative distribution function of strength σ of a bundle made on n brittle fibers can be derived from the following recursive formula (*Daniel 1945*):

$$G_n(\sigma) = \sum_{k=1}^{n} (-1)^{k+1} \binom{n}{k} F^k(\sigma) G_{n-k}\left(\frac{n\sigma}{n-k}\right) \qquad [2.12]$$

where fibers are numbered k = 1, 2...n in the order of increasing random values of strength σ_k, $F_k(\sigma) = [F(\sigma)]^k$, $\sigma > 0$, $G_0 = 1$, $G_n(\sigma)$ is the strength cdf of the entire bundle with n fibers. When the strength cdf of each fiber has a power-law left tail with same exponent p, then the cdf of strength of brittle bundle has also a power-law tail, and its exponent is np. In this case $F_k(\sigma) = \sigma^{kp}$ and expression [2.12] can be rewritten as (*Bažant and Pang 2007*):

$$G_n(\sigma) = \left[(-1)^{n+1} G_0 + \sum_{k=1}^{n-1} (-1)^{k+1} \binom{n}{k} \left(\frac{n\sigma}{(n-k)s_{n-k}} \right)^{(n-k)p} \right] \sigma^{np} = \left(\frac{\sigma}{s_n} \right)^{np} \quad [2.13]$$

where s_{n-k} and s_n are scale parameters. It is clear that parallel couplings can raise the power-law tail exponent from 1 on the nano-scale to any value, m, on the RVE scale (*Bažant and Pang 2007*).

2.4.3.2. Plastic Bundle

In case of plastic fibers, the maximum load of the bundle is given by the sum of the random independent values of strength σ_k (k = 1, 2 ... n) of the fibers of the bundle. Based on the Central Limit Theorem (CLT) (*Bulmer, 1967, Soong 2004, Moore et al. 2009*) and assuming that all σ_k have finite variance, the sum $Y = \left[\sum_{k=1}^{n} \sigma_k \right]_{n \to \infty}$ converges to the Gaussian probability density function (pdf) except in the tail. According to Bouchaud and Potters (*2000*) the tail outside the Gaussian core and the tails of the distribution of σ_k must be of the same type. Therefore, if the tail of each fibers follows a power-law, so must do the tail of the mean (*Bažant and Pang 2007*). For a bundle of two plastic fibers with stresses σ_1 and σ_2 and governed by a power law tails of exponent multiple of p, the pdf $f(\sigma)$ of the entire bundle can be written according to the CTL as (*Bažant and Pang 2007*):

$$f(\sigma) = \int_0^{\sigma} f_1(\sigma_1) f_2(\sigma - \sigma_1) \mathrm{d}\sigma_1 \quad [2.14]$$

where f_1 and f_2 are the pdf of the two fibers composing the bundle and $\sigma = \sigma_1 + \sigma_2$ is the maximum load on the bundle. Based on a simplified power series approach Bažant and Pang (*2007*) demonstrated that corresponding cdf of the bundle $F(\sigma)$ has a power law tail,

and that the length of the power-law tail of the cdf for elastic–plastic bundle is about two to three times longer than the corresponding elastic–brittle bundle tail.

2.4.3.3. Softening Bundle

Softening bundle presents fibers with a bi-linear behavior which is depicted by Figure 2.14(c). Each fiber in the bundle has an elastic modulus E and a softening modulus that can be expressed as a multiple of E: $E_s = \alpha E$.

Recently Le et al. (*2011*) proposed a simple analytical proof for the additivity of the tail exponent and for the Gaussian convergence for large bundles with softening fibers. Assuming a bundle made of two fibers, with random strengths (variables) σ_1 and σ_2, and $\sigma_1 \leq \sigma_2$, respectively, the total peak stress in the bundle can be derived as:

$$\sigma_b = 0.5 \max_{\varepsilon} \left[s_1(\varepsilon) + s_2(\varepsilon) \right] \qquad [2.15]$$

where σ_b is the peak stress in the bundle, s_1 and s_2 are the stress in the two fibers for the corresponding strain ε. According to the value of the parameter α two cases are identified (*Le et al. 2011*):

Case 1 $0 \leq \alpha \leq 1$

$$\text{if } (1+\alpha)\sigma_1/\alpha > \sigma_2 \quad \text{then} \quad \sigma_b = 0.5[(1+\alpha)\sigma_1 + (1-\alpha)\sigma_2] \qquad [2.16]$$

$$\text{if } (1+\alpha)\sigma_1/\alpha \leq \sigma_2 \quad \text{then} \quad \sigma_b = 0.5\sigma_2 \qquad [2.17]$$

Case 2 $\alpha > 1$

$$\text{if } (1+\alpha)\sigma_1/\alpha > \sigma_2 \quad \text{then} \quad \sigma_b = \sigma_1 \qquad [2.18]$$

$$\text{if } (1+\alpha)\sigma_1/\alpha \leq \sigma_2 \quad \text{then} \quad \sigma_b = \max(\sigma_1, 0.5\sigma_2) \qquad [2.19]$$

The two extreme cases of brittle bundle (*Daniels 1945*) and plastic bundle (*Bažant and Pang 2007*) can be derived by setting $\alpha = \infty$ and $\alpha = 0$, obtaining a peak stress of the bundle corresponding to $\sigma_b = \max(\sigma_1, 0.5\sigma_2)$ and $\sigma_b = 0.5(\sigma_1 + \sigma_2)$, respectively. Assuming that the strength of the bundle is smaller than a stress value S ($\sigma_b \leq S$) the strength of each fiber is limited to the two domains $\Omega_2(S)$ derived from equations [2.16] – [2.19] (Figure 2.15) (*Le et al. 2011*).

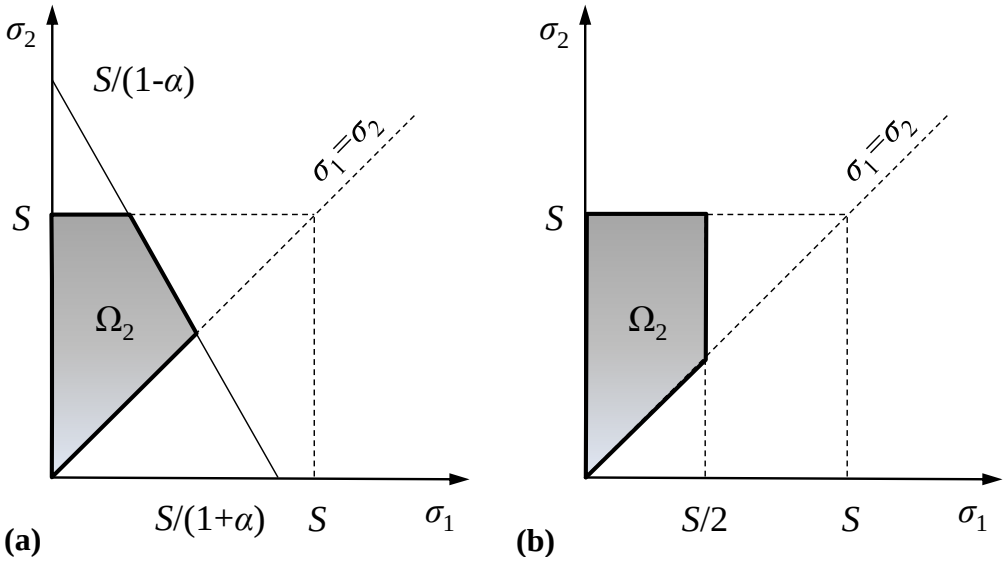

Figure 2.15. (a) Case 1 and (b) case 2 strength domains of fibers

Given the independence of the fibers' strength and by the joint probability theorem, the cdf of the average bundle strength can be expressed as:

$$G_2(S) = 2\int_{\Omega_2(S)} f_1(\sigma_1) f_2(\sigma_2) \mathrm{d}\sigma_1 \mathrm{d}\sigma_2 \qquad [2.20]$$

where $f_1(\sigma_1)$ and $f_2(\sigma_2)$ are the pdf of the two fibers composing the bundle. For fibers with a power law tail such as $P_i(\sigma) = (\sigma / s_0)^{p_i}$, and assuming $y_i = \sigma_i/S$, the tail of the cdf of the two-fiber bundle can be expressed as:

$$G_2(S) = 2S^{(p_1+p_2)} \int_{\Omega_2(1)} \frac{p_1 p_2}{s_0^{p_1+p_2}} y_1^{p_1-1} y_2^{p_2-1} \mathrm{d}y_1 \mathrm{d}y_2 \qquad [2.21]$$

where $\Omega_2(1)$ represent the domain $\Omega_2(S)$ normalized by S. Therefore, the cdf of the bundle follows a power-law tail of exponent p_1+p_2 (*Le et al. 2011*). A general expression of the bundle cdf for n fibers was also proposed by Le et al. (*2011*). The behavior of the softening bundle is intermediate between that of a brittle and plastic bundle; the extension of the bundle tail ranges from $P_{tn} \sim (P_{t1}/n)^n$ and $(P_{t1}/3n)^n$, where P_{t1} is the extension of the tail for one fiber and n is the number of fibers in the bundle.

2.4.4. RVE Gaussian-Weibull Grafted cdf model

Chain and bundle models can be used to reconstruct the mathematical model of one RVE. Based on recent studies (*Bažant and Pang 2007, Bažant et al. 2009, Le et al. 2011*) the failure probability of one RVE can be derived from atomistic fracture mechanics and a statistical multi-scale transition models. As already mentioned, the transition from the nano-scale to the macro-scales of the RVE can be accomplished through a hierarchical assembly of statistical chains and bundles (*Bažant and Pang 2007, Bažant et al. 2009, Le et al. 2011*). Figure 2.16 provides an example of hierarchical model of RVE structure.

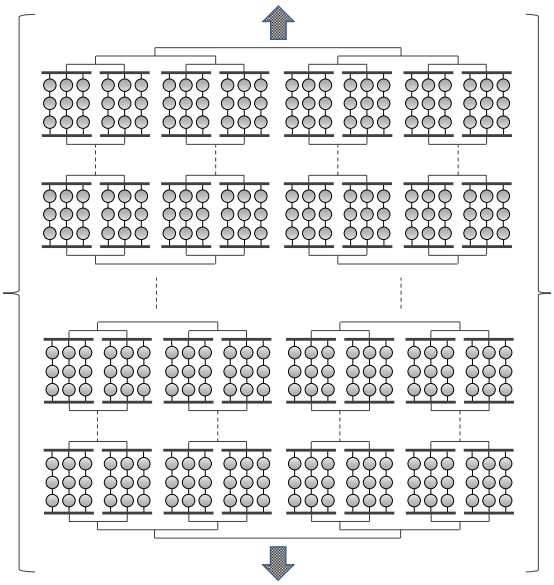

Figure 2.16. Example of RVE hierarchical model

Based on this framework, the strength distribution of one RVE can be approximated by a Weibull cdf tail grafted on the left into a Gaussian cdf at a point with a probability between 10^{-4} and 10^{-2}. The grafted cdf of strength of one RVE can be expressed as (*Bažant and Pang 2007, Bažant et al. 2009, Le et al. 2011*):

$$P_1(\sigma) = 1 - \exp[-(\sigma / s_0)^m] \approx \langle \sigma / s_0 \rangle^m \qquad (\sigma_N \le \sigma_{gr}) \qquad [2.22a]$$

$$P_1(\sigma) = P_{gr} + \frac{r_f}{\delta_G \sqrt{2\pi}} \int_{\sigma_{gr}}^{\sigma_N} \exp\left\{ -\left[\frac{(\sigma' - \mu_G)^2}{2\delta_G^2} \right] \right\} d\sigma' \qquad (\sigma_N > \sigma_{gr}) \qquad [2.22b]$$

where σ is the maximum elastic principal stress at the center of the RVE, m is the Weibull modulus, s_0 is a scale parameter of the Weibull tail, $\langle x \rangle = \max(x, 0)$, μ_G and δ_G are the mean and the standard deviation of the Gaussian core. P_{gr} and σ_{gr} are the grafting probability and the grafting stress between the Gaussian and Weibull parts of the distribution, respectively, and r_f is a scaling factor ensuring that Weibull-Gaussian

grafted cdf is normalized: $P_1(\sigma\rightarrow\infty)=1$. The continuity of the probability density function (pdf), $p_1(\sigma) = dP_1(\sigma)/d\sigma$, of the grafted distribution is then imposed by the following condition $p_1(\sigma_{gr}^{+}) = p_1(\sigma_{gr}^{-})$. Therefore, six statistical parameters, m, $s0$, μ_G, δ_G, r_f and $P(\sigma_{gr}) = P_{gr}$ are used to describe the failure distribution of one RVE; however, due to normalization and continuity conditions, only four of these parameters are independent, and thus suffice to fully define the RVE strength cdf, $P_1(\sigma)$. The physical meaning of the Weibull modulus, m, is the minimum number of cuts needed to separate the RVE hierarchical model into two distinct parts; this correspond to the number of cracks needed to break the RVE (*Bažant and Pang 2007*). For this reason, the Weibull modulus needs to be an integer number.

The strength distribution of the entire structure can be calculated by mean of the joint probability theorem (WLM) [2.7] and equations [2.22a] and [2.22b]. This results in a cdf of the structural strength that consists itself of two parts: below the grafting point the failure distribution still presents a Weibull cdf, while above the grafting stress, it follows a chain of Gaussian elements. For larger structures the Weibull distribution penetrates into the Gaussian part eventually becoming completely dominant. Based on the strength cdf, the mean structural strength, $\bar{\sigma}_N$, for structures of different sizes can be obtained as (*Bažant and Pang 2007, Bažant et al. 2009, Le et al. 2011*):

$$\bar{\sigma}_N = \int_0^1 \sigma_N dP_f = \int_0^\infty [1 - P_f(\sigma_N)] d\sigma_N \qquad [2.23]$$

However, a closed form does not exist for equation [2.23] and a numerical solution is, therefore, needed to determine the effect of structure size, D, on mean strength for geometrically similar specimens. Based on asymptotic matching Bažant and co-workers

(*Bažant and Novák 2000, Bažant and Pang 2007, Bažant et al. 2009, Le et al. 2011*) proposed an approximate expression for the size dependence of the mean strength:

$$\bar{\sigma}_N = \left[\frac{C_1}{D} + \left(\frac{C_2}{D} \right)^{rn/m} \right]^{1/r} \qquad [2.24]$$

where m is the Weibull modulus, n is the number of dimensions to be scaled (n = 1, 2 and 3). C_1, C_2 and r can be determined using the following asymptotic conditions for small and large-size of the mean strength size effect curve: $[\bar{\sigma}_N]_{D \to l_m}$, $[d\bar{\sigma}_N / dD]_{D \to l_m}$ and $[\bar{\sigma}_N / D^{n/m}]_{D \to \infty}$, where l_m represents the smallest structure size used in the scaling and for which the finite WLM is valid. Equation [2.24] was found to fit very well Type I size effect curve (Figure 2.12(a)) for various types of quasibrittle materials (*Bažant and Novák 2000, Bažant and Pang 2007, Bažant et al. 2009, Le et al. 2011*).

Chapter 3. Asphalt Binder Strength

This chapter presents the work conducted to investigate the possibility of obtaining the bending strength of asphalt binder using a modified Bending Beam Rheometer (BBR) device (*AASHTO T313-10-UL 2010*). Using a test protocol recently developed (*Marasteanu et al. 2012*), the effect of factors such as binder type, aging, cooling medium and conditioning time, on the mean strength obtained in three-point bending tests is analyzed. Then, a comparison of the current Direct Tension Tester (DTT) (*AASHTO T314-07-UL 2007*) procedure with the BBR strength test method is performed first through statistical tools and then with size effect theory. Size effect type and failure distribution of the BBR strength of asphalt binder are also addressed.

3.1. Materials and Experimental Procedure

Two asphalt binders were used in this study: a plain PG 58-28 binder, identified as Citgo, and a modified Elvaloy PG58-34 binder, identified as MIF. Both asphalt binders were short and long term aged according to the Rolling Thin-Film Oven Test (RTFOT) procedure (*AASHTO T240-09-UL 2009*) and to the Pressurized Aging Vessel (PAV) method (*AASHTO R028-09-UL 2009*), respectively.

All tests were performed at one temperature equal to the binder PG lower limit + 4°C. A new device, provided by Canon Instrument Company and named TE-BBR Pro, was used to perform three-point bending strength tests on small asphalt binder beams (101.60mm x 12.50mm x 6.25mm) (Figure 3.1). The loading frame of the new machine is equipped with a proportional valve bearing system capable of a much more complex

control of the pressure, such as applying constant loading rates on the test specimens to perform strength tests. The load cell capacity is 44N.

Figure 3.1. TE-BBR Pro device

Three different cooling media were used for BBR strength tests to investigate the influence of the cooling fluid on the failure stress: ethanol (E), potassium acetate (PA) and air (A). Two different conditioning times, 1h and 20h, were used to evaluate the effect of storage time on binder strength.

DTT tests (*AASHTO T 314-07-UL 2007*) were also performed on the same two asphalt binders only in PAV condition (*AASHTO R028-09-UL 2009*). One conditioning time of 1h and one cooling medium, potassium acetate, were used.

To obtain meaningful comparisons of the BBR and DTT strength data, the loading procedure for the BBR strength tests was set such that DTT and BBR times to failure were similar. Different loading rates were selected based on preliminary calibration tests to match the BBR and DTT times to failure, which were 15s to 20s for

the two asphalt binders used. This procedure minimizes the loading rate effect (*Bažant and Gettu 1992, Bažant and Jirasek 1993, Bažant and Li 1997, Bažant and Planas 1998*) and imposes a constant loading rate of the fracture process zone (FPZ). This is based on the fact that the cohesive law, governing the fracture process zone (FPZ) propagation, is time dependent and, consequently, rate dependent. By selecting similar times to failure for the two tests, the FPZ propagation occurs at a similar rate. A similar approach was used by others when comparing measurements of fracture energy obtained from three point bending tests on Portland cement concrete performed both in load and displacement control (*Swartz and Siew 1987*).

The BBR nominal strength (maximum stress at peak load) σ_N and corresponding strain ε_N at the bottom of the BBR beam were calculated according to equations [2.3] and [2.4]. Figure 3.2a and equations [3.1] and [3.2] recall the procedure presented in Chapter 2 (*Marasteanu et al. 2012*).

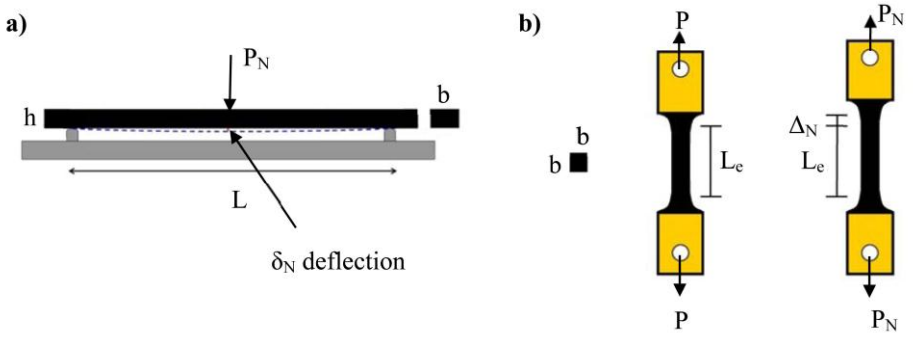

Figure 3.2. BBR (a) and DTT (b) strength tests (*Marasteanu et al. 2012*)

$$\sigma_N = \frac{3P_N L}{2bh^2} \qquad [3.1]$$

$$\varepsilon_N = \frac{6\delta_N h}{L^2} \quad [3.2]$$

where σ_N is the nominal strength (MPa), ε_N is the strain at failure, P_N is the maximum measured load (N), L is the span length (101.6 mm), b is the width of the beam (12.5 mm), h is the thickness of the beam (6.25 mm) and δ_N is the deflection (mm) of the beam corresponding to maximum load P_N.

DTT (Figure 3.2b) failure stress σ_N and failure strain ε_N were calculated as specified in the current AASHTO standard (*AASHTO T 314-07-UL, 2007*):

$$\sigma_N = \frac{P_N}{A} \quad [3.3]$$

$$\varepsilon_N = \frac{\delta_N}{L_e} \quad [3.4]$$

where σ_N is the nominal strength (MPa), P_N is the failure load (N), A=bxb is the original area of the cross section (mm^2), b = 6 mm, ε_N is the failure strain, δ_N is the elongation at failure (mm) and L_e is the effective gage length (33.8mm).

In this thesis, the analyses were based on mean strength and histogram testing. Mean strength represents the average strength value for a specific type of strength test performed on a sufficient number of specimen replicates which provides reliable and consistent results. For example, DTT mean strength is obtained by averaging the strength values of four replicates (*AASHTO T 314-07-UL 2007*). Histogram testing is a strength tests performed on a larger number of replicates. The strength results can be analyzed in the Weibull plane (*Weibull, 1939, Bažant and Pang 2007*) to identify the type of failure distribution of the material strength (brittle, quasibrittle, ductile) and, hence, can be used to predict the size dependence of strength (*Bažant and Pang 2007, Le et al. 2011*).

3.2. BBR Mean Strength

BBR mean strength tests were performed on Citgo and MIF binders at T=-24ºC and T=-30ºC, respectively, using three different cooling media (E, PA and A), two different aging conditions (RTFOT and PAV) and two conditioning times (1h and 20h). BBR nominal strength was calculated according to equation [3.1] and the mean was obtained over five beams replicates per each testing condition. Table 3.1 provides the experimental design of the BBR strength tests.

Table 3.1. BBR experimental design

Independent Variable	Type / Description
Binder Type	**1** – Citgo; **2** – MIF (Control)
Aging	**1** – RTFOT; **2** – PAV (Control)
Cooling Medium	**1** – PA; **2** – Air; **3** – E (Control)
Conditioning Time	**1** – 20h; **2** – 1h (Control)

Figures 3.3 and 3.4 present the bar charts of the mean strength of the two asphalt binders investigated for all the factor-level combinations given in Table 3.1. CoV stands for Coefficient of Variation.

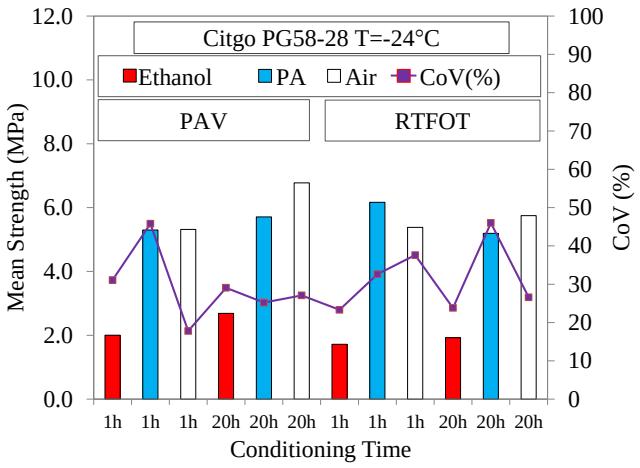

Figure 3.3. BBR mean strength for asphalt binder Citgo, PG 58-28

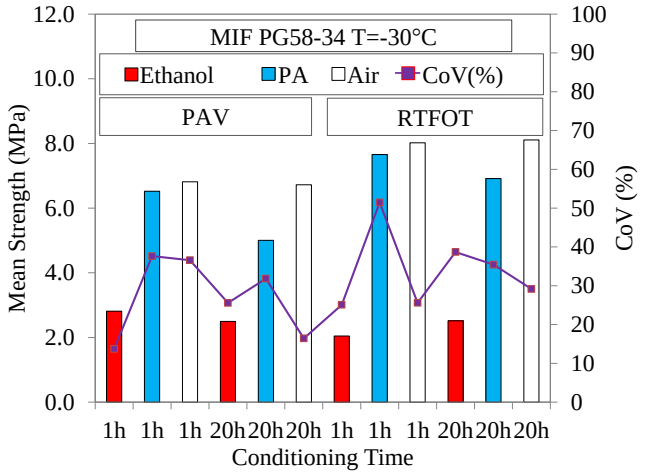

Figure 3.4. BBR mean strength for asphalt binder MIF, PG 58-34

Visual inspection of figures 3.3 and 3.4 clearly indicates there is a significant difference between the strength measured in ethanol compared to the values obtained in potassium acetate and air, which look comparable. Moreover, higher CoV's are observed for mean strength tests performed in potassium acetate. The next two figures (3.5 and 3.6) present an example of stress-strain curves for the two PAV aged asphalt binder after 1h of isothermal conditioning.

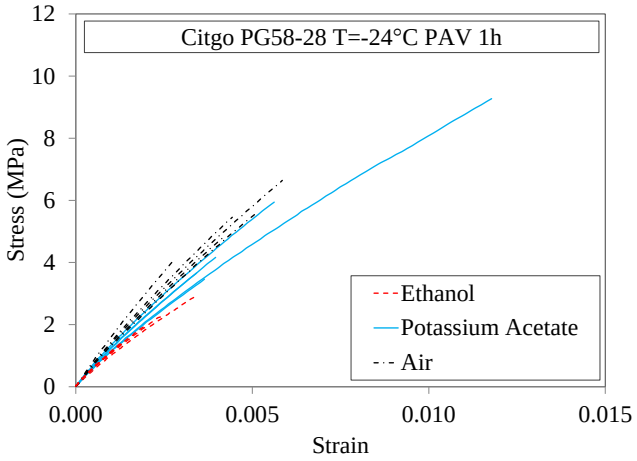

Figure 3.5. BBR stress-strain curve for asphalt binder Citgo PG 58-28

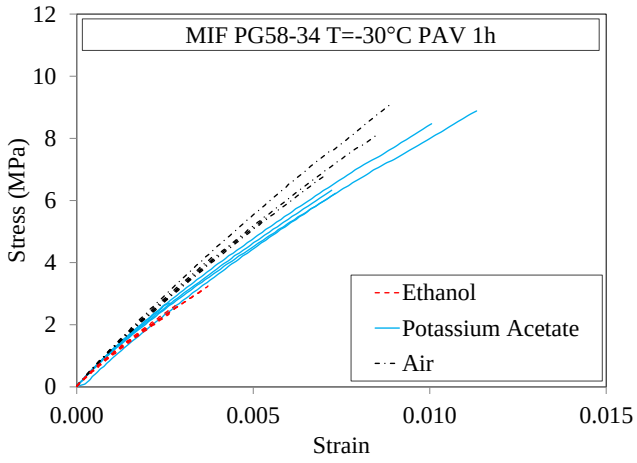

Figure 3.6. BBR stress-strain curve for asphalt binder MIF PG 58-34

An increase in asphalt binder strength, moving from the tests performed in ethanol, to potassium acetate and air, with a larger dispersion of the results in potassium acetate, are observed in Figures 3.5 and 3.6. Similarly to the bar charts, much larger strength values are obtained in PA and air compared to ethanol, while similar measurements are found for PA and air.

3.2.1. Statistical Analysis of BBR Mean Strength

The type of failure distribution of asphalt binder strength is unknown and, therefore, specific statistical tools are needed to evaluate the effect of binder type, aging, cooling medium and conditioning time (Table 3.1) on the response. To better take into account this issue, a non-parametric statistical analysis (*Moore et al. 2009*), based on the ranking of the strength values and on Analysis of Variance (ANOVA) (*Oehlert 2000*), was used to evaluate the significance of the factors used in the experimental design (Table 3.1). A significance level of 0.05 was set for the analysis. Table 3.2 summarizes the output of the statistical analysis for the statistically significant factors.

Table 3.2. BBR statistical analysis results

Factor	Coefficients	Estimate	*t*	*p*-value
Binder Type	Citgo PG 58-28	-1.222	-10.9	**10E-08**
	MIF PG 58-34	-0.832	-7.4	**10E-08**
Cooling Medium	Ethanol	Control	-	-
	Potassium Acetate	1.450	10.6	**10E-08**
	Air	1.631	11.9	**10E-08**

ANOVA shows that factors such as aging and conditioning time are not statistically significant. All the other *p*-values are very small, and below the computational digit limit, providing evidence of high significance of the factors. No intercept is needed by the statistical model. The response is binder dependent, and strongly affected by the cooling medium, with much higher values for potassium acetate and air. Furthermore, the Tukey–Kramer method (*Oehlert 2000*), which is a single-step multiple comparison, shows there is no statistical difference in mean strength between specimens tested in potassium acetate and air, confirming the visual analysis of the bar charts (Figure 3.3 and 3.4). Based on the statistical results, it may be hypothesized that the use of ethanol leads to environmental stress cracking (ESC), as found in other research efforts (Arnold 1995, Moskala 1998).

3.3. DTT Mean Strength

For comparison purposes with BBR data, DTT strength tests were also performed on Citgo and MIF asphalt binders at the same two temperature used for BBR strength tests (T=-24ºC and T=-30ºC), after PAV aging and 1h of isothermal storage in potassium acetate. According to AASHTO T314-07-UL (*2007*), six replicates are tested and the highest four strength values are used to compute the material mean strength. However, in this thesis eight replicates were tested and used to determine the mean nominal strength

of the asphalt binder according to equation [3.3]; based on different studies (*Bažant and Pang 2007, Le et al. 2011*), the tail of the failure probability of strength (cumulative distribution function – cdf), located in the low stress failure domain, plays a fundamental role in governing the failure of the material. Therefore, significant error is generated by disregarding the lower strength measurements especially when the dimension of the representative volume element (RVE) of the material is small compared to the specimens size, as may be in the case of asphalt binder. Table 3.3 presents the results of the DTT mean strength for the two asphalt binder considered. CoV represents the coefficient of variation.

Table 3.3. DTT strength results

Binder PG	Aging	T (ºC)	Cooling Medium	Strain Rate (%)	Nominal Strength (MPa)	CoV (%)
Citgo PG 58-28	PAV	-24	PA	3	3.9	16
MIF PG 58-34	PAV	-30	PA	3	5.5	11

3.4. Statistical Comparison of BBR and DTT Mean Strength

Figure 3.7 provides a visual comparison between the BBR strength results in ethanol, potassium acetate, and air, and DTT mean strength for the standard (*AASHTO T314-07-UL 2007*) testing condition: PAV aging, 1h isothermal storage in PA.

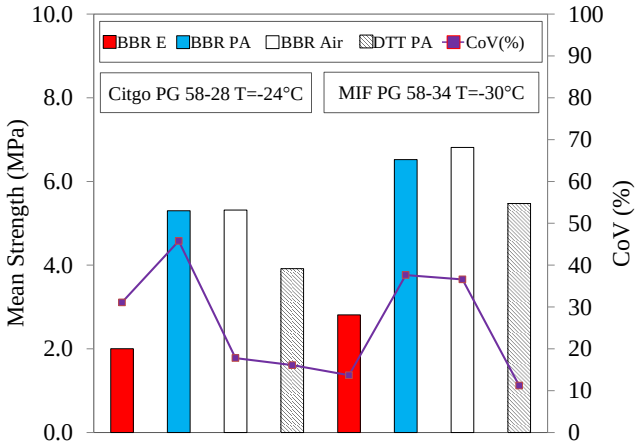

Figure 3.7. BBR vs. DTT mean strength bar chart for asphalt binder Citgo PG 58-28 and MIF PG 58-34

Significant difference between the mean nominal strength obtained with DTT and the three-point bending tests (BBR) values can be observed. To further evaluate this, ANOVA is used to perform the statistical comparison between the mean strength obtained from the two types of test. Asphalt binder type was set as block (*Oehlert 2000*) since in the previous statistical analysis of BBR strength, Citgo and MIF were found statistically different. Cooling medium (potassium acetate, air and ethanol) and test type (DTT and BBR) were set as factors. Table 3.4 presents the results of the statistical analysis.

Table 3.4. DTT vs BBR mean strength statistical analysis

Parameter	Coefficients	Estimate	*t*	*p*-value
-	Intercept	-1.331	-5.7	**10E-08**
Binder	MIF PG 58-34	Control	-	-
	Citgo PG 58-28	-0.685	-5.3	**10E-08**
Test	DTT	Control	-	-
	BBR	0.426	2.3	**0.024**
Cooling Medium	Ethanol	Control	-	-
	Potassium Acetate	1.680	8.4	**10E-08**
	Air	1.690	8.8	**10E-08**

ANOVA results indicate that binder type (block) and cooling medium are statistically significant at a 0.05 level. DTT and BBR mean strengths are statistically different. This result is not entirely surprising since the specimens used in the two tests have different volumes and are subjected to different stress fields (uniaxial vs. flexural). For this reason a detailed investigation of the influence of volume, geometry and stress field on mean strength and on failure distribution is presented in next section.

3.5. Size Effect and Failure Distribution of Asphalt Binder Strength

BBR and DTT are performed under different types of loading, three-point bending and direct tension, and the volumes of the specimens are significantly different: 9922 mm^3 and 1946 mm^3 for BBR and DTT, respectively. Therefore, the dependence of structural strength on the structure size, geometry and stress field must be taken into account with different experimental and mathematical tools.

In the recent past, Bažant and co-workers (*Bažant and Pang 2007, Le et al. 2011*) proposed a theoretical framework to analyze the size dependence of structural strength (see Chapter 2) based on strength cdf and on experimental histogram testing (*Bažant and Pang 2007*). This type of approach was used by different authors for various types of materials (*Bažant and Novák 2000, Bažant 2005, Bažant and Pang 2007, Bažant et al. 2009, Le et al., 2011, Le et al., 2012*). In this section, size effect theory (*Bažant and Pang 2007*) and histogram strength testing are used to compare BBR and DTT strength results.

3.5.1. BBR Strength Histogram Tests on Asphalt Binders

In a previous research (*Marasteanu et al. 2012*) DTT and BBR strength tests were compared using the same cooling medium: potassium acetate. However, this fluid is

highly corrosive for the laboratory equipment and may not represent the real field conditions. Since the statistical analysis conducted on the BBR mean strength (section 3.2.1.) showed there is no significant difference between the mean strength values measured in air and potassium acetate, BBR histogram testing was performed only in air on PAV aged asphalt binders Citgo (PG 58-28) and MIF (PG 58-34). Testing temperature was set to low PG+4°C, and 1h isothermal storage was used to match the DTT conditions, except for the cooling medium (section 3.3.).

BBR strength histogram testing was performed on a larger number of replicates, 20 and 21 for Citgo and MIF, respectively, and mean strength calculated according to equation [3.1]. The same loading procedure, adopted for mean strength tests, was used. Table 3.5 summarizes the mean strength results of BBR histogram tests.

Table 3.5. BBR mean strength from histogram testing

Binder PG	Aging	Temperature (ºC)	Cooling Medium	Loading Rate (N/min)	Nominal Strength (MPa)	CoV (%)
Citgo PG 58-28	PAV	-24	Air	76	5.8	14
MIF PG 58-34	PAV	-30	Air	64	8.3	17

Strength histograms (Figures 3.8 and 3.9) were plotted in the Weibull scale based on the midpoint position method (*Rinne 2009*). According to this procedure the strength histogram plot can be obtained by first ranking the strength values in ascending order, i = 1...N, where i is the rank and N is the total number of tested specimens. Next, the strength cdf can be calculated as $P_f(\sigma_N^B) = (i - 0.5)/N$.

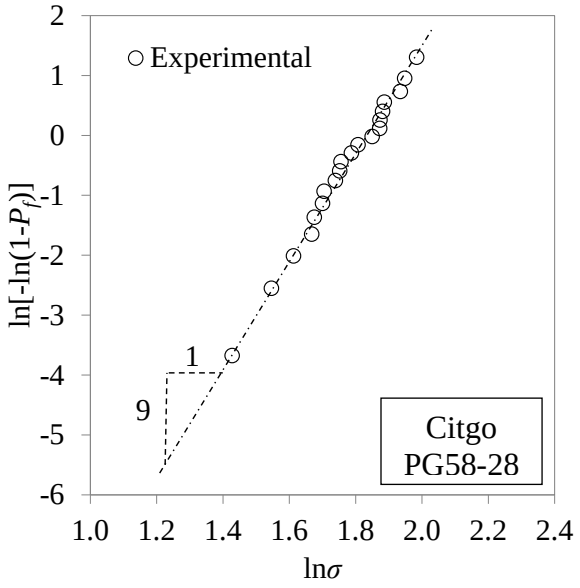

Figure 3.8. BBR strength histogram for asphalt binder Citgo PG 58-28

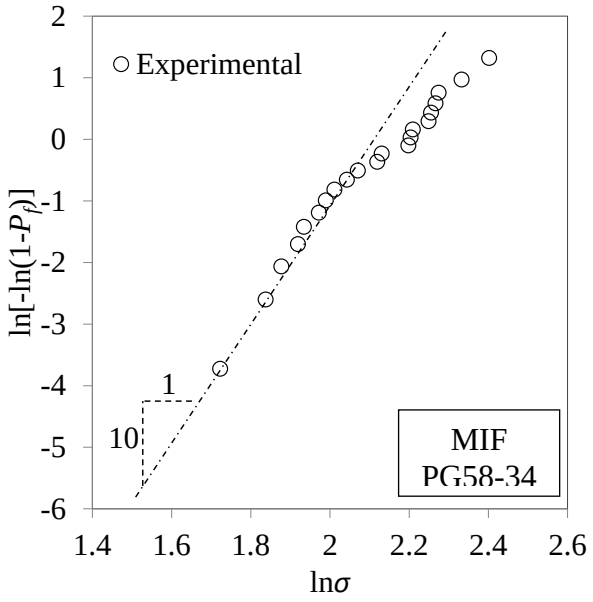

Figure 3.9. BBR strength histogram for asphalt binder MIF PG 58-34

The strength histograms show that the two asphalt binders have significantly different behaviors, which result into two different failure distributions, with binder MIF

deviating from a straight line pattern (Figure 3.9). Therefore, two distinct analyses are used to compare the BBR strength with the corresponding DTT results for each binder investigated.

3.5.2. BBR-DTT Size Effect Analysis for Citgo Binder

The strength histogram of Citgo binder (Figure 3.8) clearly follows a straight line suggesting that the BBR strength is mainly located in the brittle failure domain. The RVE dimension (l_0) of the material was assumed negligible compared to the structure size (BBR beam): for unmodified binder the size of the inhomogeneities (binder constituents) is on the nano-scale (*Lesueur 2009*). Therefore, what matters for the failure probability of the structure is the tail part of the strength distribution of one RVE (equation [2.22a]), which is fully described by the power-law Weibull statistics (*Bažant and Pang 2007, Bažant et al. 2009, Le et al. 2011*).

It can be assumed that BBR and DTT specimens share the same failure mechanism, where the peak load is reached once a macro-crack initiates from one representative volume element (RVE). Therefore, the structure can be statistically represented by a chain of RVEs. The failure probability can be further calculated based on the joint probability theorem (see Chapter 2):

$$1-P_f(\sigma_N)=\prod_{i=1}^{N}\left[1-P_1(\sigma_i)\right] \qquad [3.5]$$

or

$$\ln[1-P_f(\sigma_N)]=\sum_{i=1}^{N}\ln\left[1-P_1(\sigma_i)\right] \qquad [3.6]$$

where P_f is the failure probability of the entire structure, σ_N is the nominal strength of the structure, P_1 is the cumulative distribution function (cdf) of strength of one RVE, and σ_i is the maximum elastic principal stress at center of the i^{th} RVE. Since, as previously mentioned, the tail of the strength distribution of one RVE must follow a power-law, $P_1=(\sigma_i/s_0)^m$ (*Bažant and Pang 2007*), and by using the approximation $\ln(1-x) = -x$ for small value of x, expression [3.6] can be re-written as:

$$P_f = 1 - \exp\left\{ -\sum_{i=1}^{n} [s(x_i)]^m (\sigma_N / s_0)^m \right\} \qquad [3.7]$$

where $s(x_i)$ is the dimensionless stress field such that $\sigma_i = s(x_i)\sigma_N$, s_0 is a constant (scale parameter of the Weibull distribution) and m is a material constant called Weibull modulus (or shape parameter).

Since the structure size is much larger than the RVE size, the sum can be replaced by an integral over the volume V of the specimen (*Bažant and Pang 2007*):

$$P_f = 1 - \exp\left\{ -\left\{ \int_V [s(x)]^m dV(x) \right\} (\sigma_N / s_0)^m \right\} \qquad [3.8]$$

Equation [3.8] indicates that the distribution of structural strength follows the classical two-parameter Weibull distribution (*Weibull 1939*). This is expected due to the previous assumption on the RVE size and is confirmed by the linear pattern of Figure 3.8.

Based on equation [3.8], mean strength can be easily calculated as:

$$\bar{\sigma}_N = s_0 \Gamma(1+1/m) \left\{ \int_V [s(x)]^m dV(x) \right\}^{-1/m} \qquad [3.9]$$

where $\Gamma(x)$ is the Eulerian gamma function:

$$\Gamma(x) = \int_0^{\infty} t^{x-1} e^{-x} dt \qquad [3.10]$$

where x is the argument of the gamma function and t is the integration variable. The integral term of equation [3.9] represents the effect of structure size, as well as stress field, on the mean structural strength in the brittle failure domain. By using simple elastic stress field for BBR and DTT, together with equation [3.9], the mean strength of BBR specimen σ_N^B can be converted into the mean strength of DTT specimen σ_N^U.

$$\frac{\sigma_N^B}{\sigma_N^U} = \left[2 \cdot (1+m)^2\right]^{(1/m)} \left(\frac{V_U}{V_B}\right)^{1/m} \qquad [3.11]$$

where V_U and V_B are the volumes of DTT and BBR specimens subjected to tensile stress, respectively. In order to apply equation [3.11], the only parameter required is the Weibull moduls, m. This can be simply obtained as the slope of the experimental strength histogram rounded to the closest integer; a value of m = 9 was obtained for the strength histogram of Figure 3.8. Table 3.6 shows the comparison between predicted and measured DTT strength for asphalt binder Citgo (PG 58-28).

Table 3.6. Comparison between DTT vs. BBR strength for binder Citgo (PG 58-28)

Binder	T	Measured Mean Strength (MPa)		Ratio	Corrected Mean Strength (MPa)	Ratio
	(ºC)	BBR	DTT	(%)	BBR to DTT	(%)
Citgo PG58-28	-24	5.8	3.9	149.0	3.7	**94.3**

The prediction obtained from equation [3.11] is very close to the experimental DTT mean strength, with a difference of almost 6%, which is well below the experimental error. Therefore, transformation [3.11] allows the conversion of three-point

bending strength obtained with BBR into uniaxial strength, when the failure distribution can be approximated as brittle.

3.5.2. BBR-DTT Size Effect Analysis for MIF Binder

The strength histogram of MIF binder (Figure 3.9) deviates at the top from a straight line, and thus from a pure brittle failure, showing a curvilinear pattern. Such a pattern can be observed for many other quasibrittle materials (*Gross 1996, Munz and Fett 1999, Tinschert et al. 2000, Lohbauer et al. 2002*), and it indicates that the asphalt binder presents a quasibrittle failure distribution. Due to the binder modification (Elvaloy), the RVE dimension, l_0, is not negligible compared to the BBR beam size.

Different microstructures can be identified for modified asphalt binders depending on the dispersion of the modifier in the binder matrix (B*onemazzi et al. 1996, PIARC 1999, Lesueur 2009*). The most probable structures are those showed in Figures 3.10a and 3.10b.

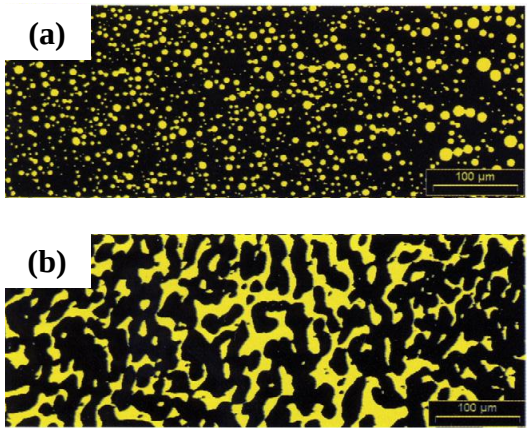

Figure 3.10. Different microstructures of modified binders: (a) ARP and (b) PRP (*Lesueur 2009*)

The first one represents a continuous Asphaltene-Rich Phase (ARP), while the second exhibit a continuous morphology Polymer-Reach Phase (PRP) (*Lesueur 2009*). The PRP structure presents a characteristic dimensions ranging between 10 and 200 μm. Bažant and Pang (*2007*) showed that, for quasibrittle materials, the RVE size is roughly equal to 2-3 times the size of material inhomogeneity or grain size. Based on this condition and on the binder structures proposed by Lesueur (*2009*), an RVE characteristic size l_0 = 170 μm, which corresponds to an RVE volume V_0=0.005 mm^3, was assumed for the following analysis.

In order to convert the flexural BBR strength into the corresponding uniaxial DTT value, at least four independent parameters (e.g. μ_G, δ_G, m and s_0) characterizing the failure distribution of the material RVE (see Chapter 2), which is given by the system of equations [3.12a] and [3.12b], must be determined.

$$P_1(\sigma) = 1 - \exp[-\langle \sigma / s_0 \rangle^m] \approx \langle \sigma / s_0 \rangle^m \qquad (\sigma_N \le \sigma_{gr}) \qquad [3.12a]$$

$$P_1(\sigma) = P_{gr} + \frac{r_f}{\delta_G \sqrt{2\pi}} \int_{\sigma_{gr}}^{\sigma_N} \exp\left\{ -\left[\frac{(\sigma' - \mu_G)^2}{2\delta_G^2} \right] \right\} d\sigma' \qquad (\sigma_N > \sigma_{gr}) \qquad [3.12b]$$

where σ is the maximum elastic principal stress at the center of the RVE, m is the Weibull modulus, s_0 is a scale parameter of the Weibull tail, $\langle x \rangle$ = max(x, 0), μ_G and δ_G are the mean and the standard deviation of the Gaussian core. P_{gr} and σ_{gr} are the grafting probability and the grafting stress between the Gaussian and Weibull parts of the distribution, respectively, and r_f is a normalizing factor.

Therefore, the BBR specimens can be physically represented as a finite chain of RVEs, and the finite weakest link model (WLM), mathematically described by the joint probability theorem (equation [2.7]), can be used. The BBR beam can be subdivided into

N RVEs; each RVE has a failure probability which depends on the corresponding elastic stress at its center, and which is calculated according to equations [3.12a] and [3.12b]. Since the BBR beam presents constant width b = 12.5 mm, the characteristic RVE size, l_0, was rescaled as $l_0 = \sqrt{V_0 / b} = 20\,\mu\text{m}$ for discretization purposes (Figure 3.11).

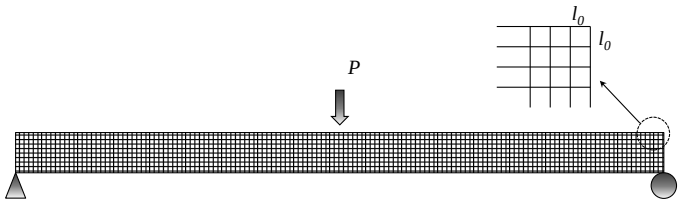

Figure 3.11. RVE discretization scheme of the BBR beam

Finally, the four parameters of the RVE cdf were obtained by fitting equations [2.7] together with [3.12a] and [3.12b] to the experimental strength histogram shown in Figure 3.9b. Figure 3.12 presents the experimental strength histogram and the WLM prediction (solid line) for binder MIF (PG 58-34).

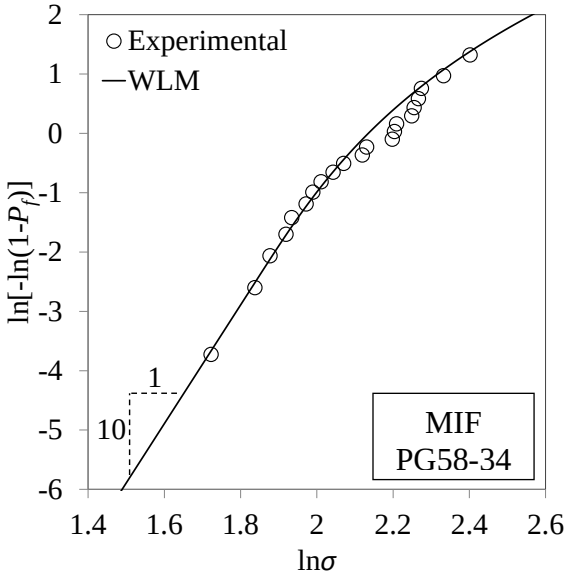

Figure 3.12. Strength histogram and WLM prediction for binder MIF PG 58-34

The WLM (equation [2.7]) fits very well the experimental strength data. The values of the parameters of the RVE cdf are: μ_G = 417.9MPa and δ_G = 128.85MPa for the Gaussian core and m=10 (Weibull modulus) s_0 =19.45MPa (scale parameter) for the Weibull tail. The predicted histogram (solid line) shows that the cdf of structural strength changes gradually from Weibull to a chain of Gaussian elements, and thus, from brittle to ductile failure as the failure stress increases. The mean structural strength can be obtained using the following equation (see Chapter 2, equation [2.23]):

$$\bar{\sigma}_N = \int_0^1 \sigma_N \mathrm{d}P_f = \int_0^\infty [1 - P_f(\sigma_N)]\mathrm{d}\sigma_N \qquad [3.13]$$

For the BBR specimen, the integration provides a value $\bar{\sigma}_N = 8.4$ MPa which is very close to the experimental mean value $\bar{\sigma}_N = 8.3$ MPa.

Finally, the RVE cdf obtained from BBR strength histogram and the WLM can be used to calculate the corresponding uniaxial DTT strength. Since DTT geometry and the type of stress field are known (Figure 3.2b and equation [3.3]) the WLM (equation [2.7]) and the RVE grafted distribution can be applied once more to predict both DTT mean strength and failure distribution. Table 3.7 presents the comparison between predicted and measured DTT strength for asphalt binder MIF (PG 58-34). Figure 3.13 shows the predicted strength histogram of DTT (dashed line) and the histogram of DTT specimens with smaller and larger number of RVEs (solid lines).

Table 3.7. Comparison between DTT vs. BBR strength for binder MIF (PG 58-34)

Binder	T	Measured Mean Strength (MPa)		Ratio	Corrected Mean Strength (MPa)	Ratio
	(ºC)	BBR	DTT	(%)	BBR to DTT	(%)
MIF PG58-34	-30	8.3	5.5	151.0	5.3	**96.4**

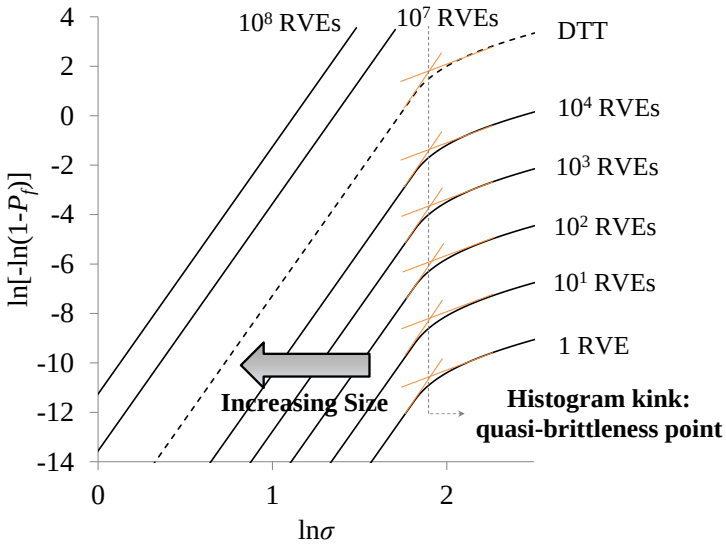

Figure 3.13. WLM prediction of the DTT strength histogram for binder MIF, PG 58-34

From table 3.8, it can be observed that there is a minimal difference (about 4%) tbetween the DTT mean strength predicted through the WLM and the experimental DTT value. It must be noticed that it is not possible to assume a perfectly brittle failure for the MIF binder, as is the case of the unmodified Citgo binder, because this would lead to a severe under prediction of the DTT mean strength with an error of almost 30%. This further supports the experimental results obtained from the strength histogram that indicate a quasibrittle behavior of the MIF modified binder, which is different than the brittle failure distribution of strength of the plain Citgo binder.

An even more interesting behavior can be observed in Figure 3.13. The DTT failure distribution is not yet in a full brittle domain and, therefore, quasibrittleness is exhibited also by the DTT test, at least for specimen dimensions specified by the current standard (*AASHTO T314-07-UL 2007*). Nevertheless, by increasing the size of the DTT

specimen, the cdf of the entire structure is eventually governed by a pure brittle failure represented in the Weibull plane by a straight line. The position of the kink, representing the location of the quasibrittleness of the material, in the DTT predicted histogram, (Figure 3.13) is aligned vertically (dashed line). As the specimen size increases the kink point moves upward eventually vanishing when the brittle failure behavior becomes totally dominant.

3.5.2.1. BBR Type I Size Effect of Asphalt Binder MIF PG 58-34

Since the BBR strength of asphalt binder MIF presents a quasibrittle failure, it is expected to observe Type I size effect for its structural strength. Based on the WLM model and on equation [3.13] it is possible to predict the mean structural strength of beam of asphalt binder with the same thickness to span ratio of BBR (1:16.256) for a discrete number of a sizes. However, equation [3.13] does not present a closed form of the size dependence of the structural strength. Alternatively equation [2.24] can be fitted to the predicted strength values and, hence, obtain an approximate expression of $\bar{\sigma}_N = \bar{\sigma}_N(D)$, where D is the characteristic size of the specimens, which was assumed to be the thickness of the BBR beam. Figure 3.14 shows the mean strength prediction points obtained with the WLM and the fitting of equation [2.24].

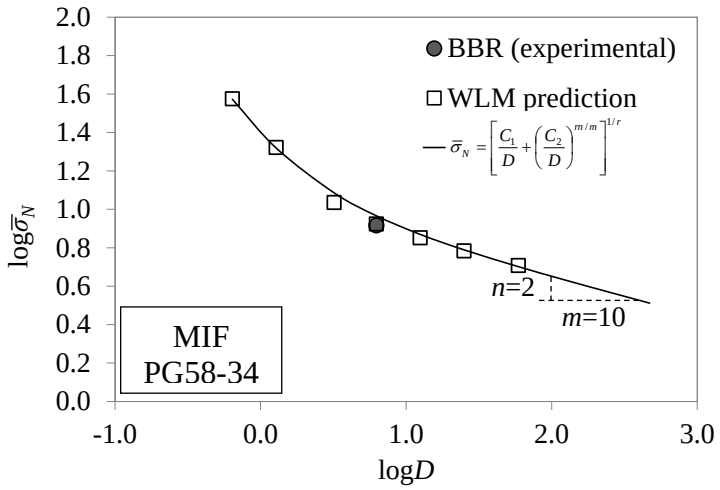

Figure 3.14. Type I size effect of BBR structural strength for binder MIF 58-34

The mean strength size effect plot of Figure 3.14 indicates that asphalt binder MIF follows a Type I size effect and that equation [2.24] provides a good approximation as demonstrated in other studies (*Bažant and Novák 2000, Bažant and Pang 2007, Bažant et al. 2009, Le et al. 2011*). The values of the constants obtained from fitting equation [2.24] are: C_1 = 1.68, C_2 = 167379.04, r = 0.50 and m = 10 (Weibull modulus determined from strength histogram).

Chapter 4. Strength Size Effect of Asphalt Mixture

The aim of this dissertation is to evaluate the possibility of obtaining and extrapolating relevant strength properties of asphalt materials by testing small size specimens with the Bending Beam Rheometer (BBR). In Chapter 3, it was demonstrated that, in the case of asphalt binder, such an objective is achievable by using strength size effect analysis. Asphalt binder presents a RVE size that is very small compared to the BBR beam characteristic dimension (thickness). However, this may not be true for asphalt mixture due to the aggregate skeleton. Therefore, a preliminary investigation on the strength size effect of asphalt mixture is necessary for identifying the analysis tools which can be used for extrapolating experimental strength values, and that can be then applied to the BBR asphalt mixture test results (Chapter 5).

For such a purpose, in this chapter, a multiscale experimental approach is selected, and a single asphalt mixture with sufficiently small RVE size is used. Forward and inverse solutions to the analysis of the strength size effect of asphalt mixture are then implemented. A set of closed form equations is first derived to directly link the statistical parameters characterizing the RVE failure distribution to the size effect of mean structural strength and vice versa. The new formulation is then used to predict the mean strength curve of asphalt mixture from the experimental data obtained through histogram strength testing on three-point bending beams. Then, the statistical parameters of the material RVE are back-calculated from the mean strength data obtained on asphalt mixture specimens of different size and geometry, through the same set of equations previously derived. Finally, the forward and inverse formulations are compared and discussed.

4.1. Relations between Strength Distribution of one RVE and Mean Strength Size Effect Curve

In Chapter 2 the theoretical background on strength size effect for quasibrittle material was presented. Based on such a theoretical framework six parameters, m, s_0, μ_G, δ_G, r_f and P_{gr}, can be identified in the grafted cumulative distribution function of strength of one RVE (*Bažant and Pang 2007, Bažant et al. 2009, Le et al. 2011*):

$$P_1(\sigma) = 1 - \exp[-(\sigma / s_0)^m] \approx \langle \sigma / s_0 \rangle^m \qquad (\sigma_N \le \sigma_{gr}) \qquad [4.1a]$$

$$P_1(\sigma) = P_{gr} + \frac{r_f}{\delta_G \sqrt{2\pi}} \int_{\sigma_{gr}}^{\sigma_N} \exp\left\{ -\left[\frac{(\sigma' - \mu_G)^2}{2\delta_G^2} \right] \right\} d\sigma' \qquad (\sigma_N > \sigma_{gr}) \qquad [4.1b]$$

where σ is the maximum elastic principal stress at the center of the RVE, m is the Weibull modulus (*Weibull 1939*), s_0 is a scale parameter of the Weibull tail, $\langle x \rangle = \max(x, 0)$, μ_G and δ_G are the mean and the standard deviation of the Gaussian core. P_{gr} and σ_{gr} are the grafting probability and the grafting stress between the Gaussian and Weibull parts of the distribution respectively and r_f is a normalizing factor. However, due to continuity and normalization conditions, only four of these parameters are independent. Therefore, the cdf of one RVE can be fully described by a set of four parameters: two for the Weibull tail, m and s_0, and two for the Gaussian core, μ_G and δ_G.

The strength distribution, P_f, of a structure of positive geometry made of N RVEs can then be calculated using the finite weakest link model (WLM) (*Bažant and Pang 2007, Le et al. 2011*):

$$P_f(\sigma_N) = 1 - \prod_{i=1}^{N} \left[1 - P_1(s_i \sigma_N) \right] \qquad [4.2]$$

where P_1 is the cumulative distribution function of strength of one RVE, σ_N is the nominal strength of the structure, s_i is the dimensionless stress field (function of the coordinate **x**) such that $\sigma_N s_i$ is equal to the maximum elastic principal stress at the center of i^{th} RVE.

The statistical parameters of the RVE cdf can be calibrated from histogram strength testing (*Bažant and Pang 2007, Bažant et al. 2009, Le et al. 2011*), when the dimension of the material RVE, l_0 is known. Recent studies showed that RVE size of quasibrittle materials is about two to three times the size of the material inhomogeneities (*Bažant and Pang 2007*). For materials such as asphalt mixture, l_0 can be obtained through digital image analysis (*Cannone Falchetto et al. 2012a*) or directly from sieve size analysis as was done in this dissertation.

Five parameters, n, m, r, C_1 and C_2, are needed to describe the mean strength size effect curve according to the following approximate equation (Chapter 2 equation [2.24]) proposed by Bažant and co-workers (*Bažant and Novák 2000, Bažant and Pang 2007, Bažant et al. 2009, Le et al. 2011*):

$$\bar{\sigma}_N = \left[\frac{C_1}{D} + \left(\frac{C_2}{D} \right)^{rn/m} \right]^{1/r} \qquad [4.3]$$

where m is the Weibull modulus, n is the number of dimensions to be scaled (n = 1, 2 and 3). C_1, C_2 and r can be determined using the following asymptotic conditions for small and large-size of the mean strength size effect curve: $[\bar{\sigma}_N]_{D \to l_m}$, $[d\bar{\sigma}_N / dD]_{D \to l_m}$ and $[\bar{\sigma}_N / D^{n/m}]_{D \to \infty}$, Parameter l_m represents the smallest structure size for which the finite WLM is applicable; for very small-size structures the stress distribution is highly

nonlinear within one RVE and, therefore, it is not accurate to use the average stress of the RVE for evaluating the failure probability.

The scaling dimension, n is known a priori: in this thesis a 2D scaling was selected and, thus, n=2. The Weibull modulus, m, is a parameter common to both the RVE cdf expression, equation [4.1a], and to the mean strength curve, equation [4.3]. When histogram testing is performed m can be obtained as the slope of the lowest straight part of the histogram in the Weibull scale (*Bažant and Pang 2007, Bažant et al. 2009, Le et al. 2011*); m can be also estimated from the slope of the mean strength size effect curve for large structures (*Bažant and Pang 2007, Bažant et al. 2009, Le et al. 2011*). Therefore, by knowing the cdf parameters of one RVE, only three parameters, r, C_1 and C_2, need to be estimated for the mean strength function (equation [4.3]), and vice versa for the RVE grafted distribution (s_0, μ_G and δ_G).

According to the WLM (equation [4.2]) the tail of the strength cdf of one RVE controls the overall failure distribution of the entire structure for large-size limit; based on equation [4.1a] this presents a power law: $P_1 \approx \langle \sigma_N \rangle^m / s_0^m$. Equation [4.2] can be rewritten in logarithm form, and by approximating $\ln(1-x) \approx -x$, the following expression can be obtained (*Bažant and Pang 2007, Le et al. 2011*):

$$\ln[1 - P_f(\sigma_N)] = -\sum_i^N \left(\frac{\sigma_N \langle s_i \rangle}{s_0} \right)^m \qquad [4.4]$$

and rearranged as:

$$P_f(\sigma_N) = 1 - \exp\left\{ -\sum_i^N \left(\frac{\sigma_N \langle s_i \rangle}{s_0} \right)^m \right\} = 1 - \exp\left\{ -\int_V \left(\frac{\sigma_N \langle s(\mathbf{x}) \rangle}{s_0} \right)^m \frac{\mathrm{d}V(\mathbf{x})}{l_0^n} \right\} \qquad [4.5]$$

where l_0 is the dimension of the material RVE, $\langle s(\mathbf{x})\rangle$ is the positive dimensionless stress field for the coordinates $\mathbf{x}(x, y)$ and $V(\mathbf{x})$ is the volume of the structure. At large- size limit the failure probability is governed by the Weibull distribution (equation [4.5]). This is expected since the RVE size becomes negligible compare to the entire structure; this is in agreement with the classical extreme value statistics (*Fréchet 1927, Fisher and Tippett 1928, Gumbel 1958, Ang and Tang 1984, Haldar and Mahadevan 2000*). From equation [4.5] the mean strength of very large structures can be calculated as (*Bažant and Planas1998, Bažant and Pang 2007, Bažant et al. 2009, Le et al. 2011*):

$$\bar{\sigma}_N = s_0 \Gamma\left(1+\frac{1}{m}\right)\left(\frac{D_0}{D}\right)^{n/m} \qquad [4.6]$$

where $D_0 = l_0\left[\int_V \langle s(\boldsymbol{\xi})\rangle^m \mathrm{d}V(\boldsymbol{\xi})\right]^{-1/n}$, $\boldsymbol{\xi} = \mathbf{x}/D$ is the normalized coordinate, and $\Gamma(x)$ is the Eulerian gamma function. For very large structure rn/m<<1 and equation [4.3] can be also rewritten as:

$$\bar{\sigma}_N = (C_2 / D)^{n/m} \qquad [4.7]$$

By equating equations [4.6] and [4.7] it is possible to obtain parameter C_2 in terms of the Weibull scale parameter s_0:

$$C_2 = D_0\left[s_0\Gamma\left(1+\frac{1}{m}\right)\right]^{m/n} \qquad [4.8]$$

By inverting expression [4.8] is also possible to obtain the value of the scale parameter s_0, when the value of C_2 is known from the mean strength size effect curve:

$$s_0 = \left(\frac{C_2}{D_0}\right)^{n/m}\Gamma^{-1}\left(1+\frac{1}{m}\right) \qquad [4.9]$$

The remaining two parameters, r and C_1, can be associated to the Gaussian core parameters, μ_G and δ_G, of the RVE cdf of strength, by considering the following asymptotic conditions at the small-size limit:

$$\bar{\sigma}_N\big|_{D\to l_m} = \left[\frac{C_1}{l_m} + \left(\frac{C_2}{l_m}\right)^{rn/m}\right]^{1/r} \qquad [4.10]$$

$$\left.\frac{\mathrm{d}\bar{\sigma}_N}{\mathrm{d}D}\right|_{D\to l_m} = -\frac{1}{r}\left[\frac{C_1}{l_m^2} + \frac{nr}{ml_m}\left(\frac{C_2}{l_m}\right)^{rn/m}\right]\left[\frac{C_1}{l_m} + \left(\frac{C_2}{l_m}\right)^{rn/m}\right]^{1/r-1} \qquad [4.11]$$

where l_m represents the smallest structure size that has physical meaning. Recently, Le et al. (*2012*) demonstrated that l_m has to account for a sufficient numbers of RVEs in order to use the elastic stress field for obtaining realistic calculation of failure probability. In a recent computational research effort, Le et al. (*2012*) demonstrated that in order to apply the WLM to three-point bending geometry, the beam should have a minimum depth of about 4 RVEs.

The mean strength of a structure can also be calculated as:

$$\bar{\sigma}_N = \int_0^1 \sigma_N \mathrm{d}P_f = \int_0^\infty [1\text{-}P_f(\sigma_N)]\mathrm{d}\sigma_N \qquad [4.12]$$

However, as mentioned in Chapter 2, a closed form expression does not exist for equation [4.12], and a numerical solution is, therefore, needed to determine the effect of structure size, D, on mean strength for geometrically similar specimens. Nevertheless, by substituting equation [4.2] into equation [4.12] is possible to express the structure mean strength as:

$$\bar{\sigma}_N = \int_0^\infty [1-P_f(\sigma_N)]\mathrm{d}\sigma_N = \int_0^\infty \prod_{i=1}^{N} [1-P_1(s_i\sigma_N)]\mathrm{d}\sigma_N \qquad [4.13]$$

where N is the total number of RVEs in the structure.

Therefore, a first equation relating r and C_1 to the parameters of the failure cdf of one material RVE can be obtained by equating equation [4.10] to equation [4.13]:

$$\int_0^{\infty} \prod_{i=1}^{N} [1 - P_1(s_i \sigma_N)] \mathrm{d}\sigma_N = \left[\frac{C_1}{l_m} + \left(\frac{C_2}{l_m} \right)^{rn/m} \right]^{1/r} \qquad [4.14]$$

A second condition for determining r and C_1 can be obtained from the asymptotic slope of the size effect curve at the small-size limit. The slope of the mean size effect curve can be calculated as the derivative of equation [4.3]:

$$\frac{\mathrm{d}\bar{\sigma}_N}{\mathrm{d}D} = \frac{\mathrm{d}}{\mathrm{d}D}\left(\int_0^1 \sigma_N \mathrm{d}P_f \right) = \frac{\mathrm{d}}{\mathrm{d}D}\left(\int_0^{\infty} [1 - P_f(\sigma_N)] \mathrm{d}\sigma_N \right) = -\int_0^{\infty} \frac{\mathrm{d}P_f}{\mathrm{d}D} \mathrm{d}\sigma_N \qquad [4.15]$$

The failure probability of the entire structure $P_f(\sigma_N)$ can be expressed using the logarithm of the WLM (equation [4.2]) and by integrating over the volume of the structure as:

$$P_f(\sigma_N) = 1 - \exp\left\{ \sum_i^N \ln[1 - P_1(s_i \sigma_N)] \right\} = 1 - \exp\left\{ \int_V \ln[1 - P_1(s(\mathbf{x})\sigma_N)] \frac{\mathrm{d}V(\mathbf{x})}{l_0^n} \right\} \qquad [4.16]$$

Expression [4.16] can be further manipulated using a system of normalized coordinates, $\boldsymbol{\xi} = \mathbf{x}/D$:

$$\frac{\mathrm{d}\bar{\sigma}_N}{\mathrm{d}D} = \int_0^{\infty} \frac{\mathrm{d}}{\mathrm{d}D}\left[\exp\left\{ \frac{D^n}{l_0^n} \int_V \ln[1 - P_1(s(\boldsymbol{\xi})\sigma_N)] \mathrm{d}V(\boldsymbol{\xi}) \right\} \right] \mathrm{d}\sigma_N \qquad [4.17]$$

$$\frac{\mathrm{d}\bar{\sigma}_N}{\mathrm{d}D} = \frac{nD^{n-1}}{l_0^n} \int_0^{\infty} [1 - P_f(\sigma_N)] \left(\int_V \ln[1 - P_1(s(\boldsymbol{\xi})\sigma_N)] \mathrm{d}V(\boldsymbol{\xi}) \right) \mathrm{d}\sigma_N \qquad [4.18]$$

$$\frac{\mathrm{d}\bar{\sigma}_N}{\mathrm{d}D} = \frac{n}{D} \int_0^{\infty} [1 - P_f(\sigma_N)] \ln[1 - P_f(\sigma_N)] \mathrm{d}\sigma_N \qquad [4.19]$$

Substituting equation [4.13] into equation [4.19] the following expression of the cdf of the material RVE, $P_1(s_i \sigma_N)$, can be written:

$$\frac{\mathrm{d}\bar{\sigma}_N}{\mathrm{d}D} = \frac{n}{D}\int_0^{\infty} \prod_{i=1}^{N}[1-P_1(s_i\sigma_N)] \sum_{i=1}^{N} \ln[1-P_1(s_i\sigma_N)]\mathrm{d}\sigma_N \qquad [4.20]$$

Therefore, the second equation for relating r and C_1 to the parameters of the failure cdf of one RVE can be derived by equating equations [4.11] to equation [4.20]:

$$\frac{n}{D}\int_0^{\infty} \prod_{i=1}^{N}[1-P_1(s_i\sigma_N)] \sum_{i=1}^{N} \ln[1-P_1(s_i\sigma_N)]\mathrm{d}\sigma_N = \\ = -\frac{1}{r}\left[\frac{C_1}{l_m^2} + \frac{nr}{ml_m}\left(\frac{C_2}{l_m}\right)^{rn/m}\right]\left[\frac{C_1}{l_m} + \left(\frac{C_2}{l_m}\right)^{rn/m}\right]^{1/r-1} \qquad [4.21]$$

For small structures (at the small-size limit), made of a limited number of RVEs, it can be observed that the Weibull tail of the strength failure probability is very short, ending at a value in the range of 10^{-3} or lower. Therefore, the cdf of strength can then be entirely approximated by the Gaussian core, and hence, by a pure Gaussian distribution. It is then acceptable to replace P_1 with the cdf of the standard Gaussian normal distribution Φ_G, with mean and standard deviation equal to μ_G and δ_G, respectively. Therefore expressions [4.14] and [4.21] can be rewritten as:

$$\int_0^{\infty} \prod_{i=1}^{N}[1-\Phi_G(s_i\sigma_N,\mu_G,\delta_G)]\mathrm{d}\sigma_N = \left[\frac{C_1}{l_m} + \left(\frac{C_2}{l_m}\right)^{rn/m}\right]^{1/r} \qquad [4.22]$$

$$\frac{n}{D}\int_0^{\infty} \prod_{i=1}^{N}[1-\Phi_G(s_i\sigma_N,\mu_G,\delta_G)] \sum_{i=1}^{N} \ln[1-\Phi_G(s_i\sigma_N,\mu_G,\delta_G)]\mathrm{d}\sigma_N = \\ = -\frac{1}{r}\left[\frac{C_1}{l_m^2} + \frac{nr}{ml_m}\left(\frac{C_2}{l_m}\right)^{rn/m}\right]\left[\frac{C_1}{l_m} + \left(\frac{C_2}{l_m}\right)^{rn/m}\right]^{1/r-1} \qquad [4.23]$$

where $\Phi_G(s_i\sigma_N,\mu_G,\delta_G) = (2\pi)^{-1/2}\int_{-\infty}^{s_i\sigma_N} \exp[-(x-\mu_G)^2/2\delta_G^2]\mathrm{d}x$ and $s_i\sigma_N$ is the maximum principal stress at the center of the i^{th} RVE.

Therefore, r and C_1 can be calculated by solving the system of equations given by [4.22] and [4.23]. Together with C_2, derived from equation [4.9], the Weibull modulus m and by knowing the scaling factor (n=2 for this study), it is possible obtaining the set of five parameters required to describe the effect of structure size, D, on mean strength for geometrically similar specimens, according to the approximated equation [4.3].

The same set of equations can be also used to obtain the four parameters of the RVE cdf, m, s_0, μ_G and δ_G, when the mean strength curve parameters of equation [4.3] are know from experimental mean strength tests.

4.2. Materials and Experimental Procedure

An asphalt mixture prepared with an asphalt binder (7.4% by weight) having performance grade PG 64-34 (*AASHTO M320-10-UL 2010*), and with a blend of aggregates consisting of taconite aggregates (55% of MIN TAC tailings and 10% of ISPAT tailings) and pit sand (35%) was used for the experimental phase. Based on the sieve size analysis, the RVE dimension was estimated as double of the material inhomogeneities, which correspond to the nominal average aggregate size. For the particular asphalt mixture considered in this study, an average aggregate size of 1.22 mm and an RVE volume of V_0=14.4mm^3 were determined, respectively.

A comprehensive set of tests, consisting of both histogram tests and mean strength tests at a low temperature, was performed to validate the proposed methods for predicting the mean strength curve from the strength cdf of a material RVE and vice versa. In order to determine the four parameters (m, s_0, μ_G and δ_G) characterizing the strength cdf of the RVE, histogram tests were first performed on single-size beam

specimens (specimen series *C* in Table 4.1 and Figure 4.1) in three-point bending (3PB) configuration. A second series of strength histogram tests was also performed on beams of a smaller size to verify the WLM (specimen series *B* in Table 4.11 and Figure 4.1). In the case of the back-calculation of the RVE cdf from the mean strength size effect curve, both strength histograms were used for validating the RVE parameters through the WLM.

Besides histogram testing, mean strength tests were also conducted on specimens of different size to obtain the mean size effect curve. However, due to the limitations imposed by the dimensions of the climatic chamber attached to the testing machine, it was not possible fabricating and testing beam specimens that were large enough for the size effect analysis under three-point bending. One way for overcoming this difficulty was to consider a different specimen geometry (or loading configuration), which would cause a different stress field and consequently a different failure probability for a given load. Therefore, it is possible equating the mean nominal strengths of structures of different geometries by changing their sizes, which would effectively lead to a large specimen size. For example, considering a Weibull cdf, a concrete beam in direct tension is equivalent to a beam with a depth 50 times larger under pure bending (*Bažant and Planas 1998*) and 1250 times larger in three-point bending. The volume conversion across different structural geometries has to be based on the finite WLM. In this thesis, it was chosen to use direct tension (DT) specimen of the largest possible size that could fit into the climatic chamber to maximize the number of RVEs in the specimen, so that the strength cdf of DT specimen would follow the two-parameter Weibull distribution. By doing so, a closed-form expression for calculating the equivalent size of the three-point bending beam can be easily derived.

Test specimens were cut from twenty-six slabs of asphalt mixture (380 mm long by 200 mm wide) compacted to 7% air voids using a Linear Kneading Compactor (LKC). In order to optimize asphalt mixture preparation and specimens cutting, two different slab thicknesses (50 mm and 75 mm) were set. In this dissertation, 2D scaling was used; all beams were prepared with the same span-to depth ratio of 1:6, constant width (in the transverse direction) b = 40 mm and a scaling ratio $1:\sqrt{3}:3$ (Figure 4.1 and Table 4.1). For DT test, a single specimen size was used. Table 4.1 summarizes the details of the test specimens, while Figure 4.1 shows the four specimens used.

Table 4.1. Specimens' details

Specimen ID	Replicates #	Dimensions (*L* x *D* x *b*)	Test Type	Mean/Histogram
A	12	100 x 16.7x 40 mm	3PB	Mean
B	28	173 x 28.9 x 40 mm	3PB	Histogram
C	30	300 x 50 x 40 mm	3PB	Histogram
D	7	255 x 55 x 55 mm	DT	Mean

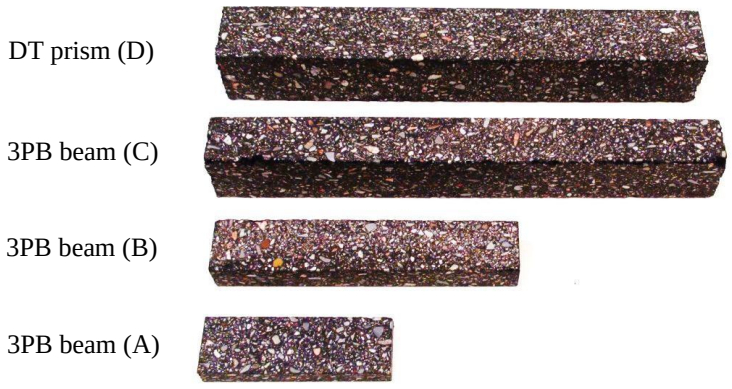

Figure 4.1. DT prism and beam specimens

The depth of the beam and the width of the prism were selected as the characteristic dimension *D* for the three-point bending and DT specimens, respectively (Fig. 4.2).

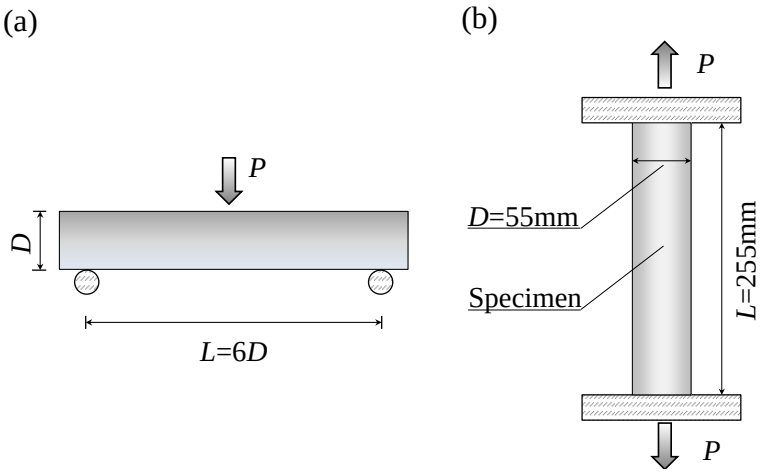

Figure 4.2. (a) Schematic of three-point bending and (b) direct tension tests

The testing temperature was set to T=−24°C (low PG+10°C), which is very close to the glass transition temperature of the asphalt binder used to prepare the mixture. Liquid nitrogen was used to obtain the desired testing temperature, with an accuracy of ±1°C. Tests were performed using a MTS servo-hydraulic system equipped with a 100 kN load cell. Prior to testing, specimens were conditioned for three hours.

The three-point bending fixtures could accommodate testing of different beam sizes by simply varying the distance between the supports. For DT tests, the specimens were glued with an epoxy compound to a set of plates that were screwed to the loading frame. Both three-point bending and DT tests were conducted in load-control mode since only the peak load was of interest in this study. In order to impose a constant loading rate on the fracture process zone, a time to failure of about 5 minutes was set for all specimen

sizes and geometries. Therefore, different loading rates were used for different specimen sizes and geometries. Before the actual tests, several preliminary tests were performed to determine the loading rate for each specimen geometry and size.

4.3. Forward Analysis: Calculation of Mean Strength Curve Parameters from RVE cdf

The nominal strength of three-point bending σ_N^B and direct tension σ_N^T were calculated according to:

$$\sigma_N^B = \frac{3P_{\max}L}{2bD^2} = \frac{9P_{\max}}{bD} \quad [4.24]$$

$$\sigma_N^T = \frac{P_{\max}}{bD} \quad [4.25]$$

where P_{max} is the peak load, L is the length of the beam, D is the characteristic size (the thickness of the beam or the width of the prism) and b is the beam width for three-point bending (b = 40mm) or the prism thickness (b = 55mm) for DT specimens. A summary of the strength tests results for all the specimens is shown in Table 4.2.

In order to calculate the probability distribution of nominal strength for beam series *B* and *C*, the strength values were ranked in ascending order, $i = 1, ..., N$, where i is the rank and N is the total number of tested specimens. According to the midpoint position method (*Rinne 2009*), the strength cdf can be calculated as:

$$P_f(\sigma_N^B) = \frac{i-0.5}{N} \quad [4.26]$$

Table 4.2. Tests results

Specimen ID	*A*	*B*	*C*	*D*
Nominal Strength (MPa)	12.8	10.1	9.6	6.4
	12.9	10.4	9.8	7.1
	13.6	10.6	10.0	8.0
	13.8	10.8	10.1	8.4
	13.8	11.0	10.3	8.9
	14.2	11.3	10.4	9.2
	14.5	11.7	10.5	9.3
	14.5	11.9	10.7	
	14.8	12.1	10.8	
	15.1	12.2	10.9	
	15.2	12.4	10.9	
	16.3	12.4	11.0	
		12.5	11.1	
		12.5	11.2	
		12.6	11.3	
		12.7	11.4	
		12.9	11.5	
		12.9	11.6	
		13.0	11.7	
		13.1	11.8	
		13.4	11.9	
		13.5	12.0	
		13.5	12.0	
		13.6	12.1	
		13.6	12.2	
		13.7	12.4	
		13.8	12.6	
		14.0	12.7	
			12.8	
			13.4	
Mean Nominal Strength (MPa)	14.3	12.4	11.4	8.2

Figure 4.3 presents the measured strength histograms on the Weibull scale. It is seen that the lower portion of the histogram follows a straight line and the upper portion of the histogram exhibits a clear nonlinearity on the Weibull scale.

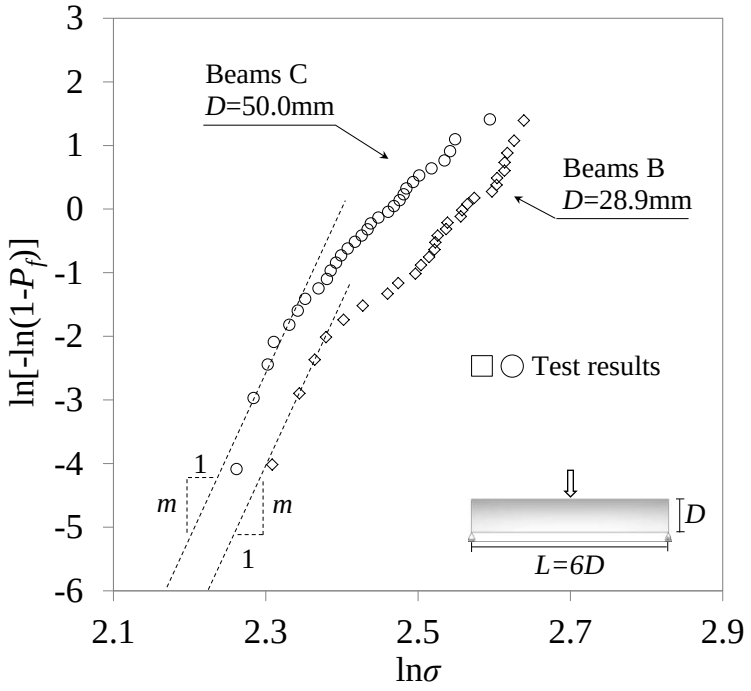

Figure 4.3. Experimental strength histograms for beam series *C* and *B*

Such type of histogram cannot be fitted by the two-parameter Weibull distribution. In contrast, the WLM can well explain this type of strength histograms, where the lower portion is dictated by the Weibull distribution, whereas the upper portion can be described as a chain of Gaussian elements. Such a two-segment strength cdf has also been seen in other quasibrittle materials, such as Portland cement mortar, engineering and dental ceramics, as summarized in Pang et al. (*2008*), Bažant et al. (*2009*), and Le et al. (*2011*).

To calibrate the strength cdf of one RVE from the cdf of structural strength, the RVE size has to be known. By considering that the macro-crack, causing the structure failure, develops across the entire width of the beam, it is possible to limit the analysis to 2D scaling: the effective RVE size for 2D beam can be calculated as $l_0 = \sqrt{V_0 / b} = 0.6$

mm. Therefore, the strength cdf of one RVE can be calibrated by the optimum fit of the strength histogram of beam series *C*. The detailed fitting algorithm was presented in Le and Bažant (*2009*). The following parameters values were estimated for the cdf of RVE strength: m=26, s_0 =12.68MPa, μ_G =44.49MPa and δ_G =14.89MPa.

Based on the WLM, (equations [4.1] and [4.2]), the strength cdf of beam series *B* can also be calculated. Figure 4.4 shows that the prediction by the WLM agrees very well with the measured strength histogram of beam series *B*, which further verifies the calibration of the strength cdf of one RVE and the finite WLM. As shown later, the finite WLM is further verified by the mean size effect analysis, which is more stringent compared to matching the strength histogram of specimens of a single size.

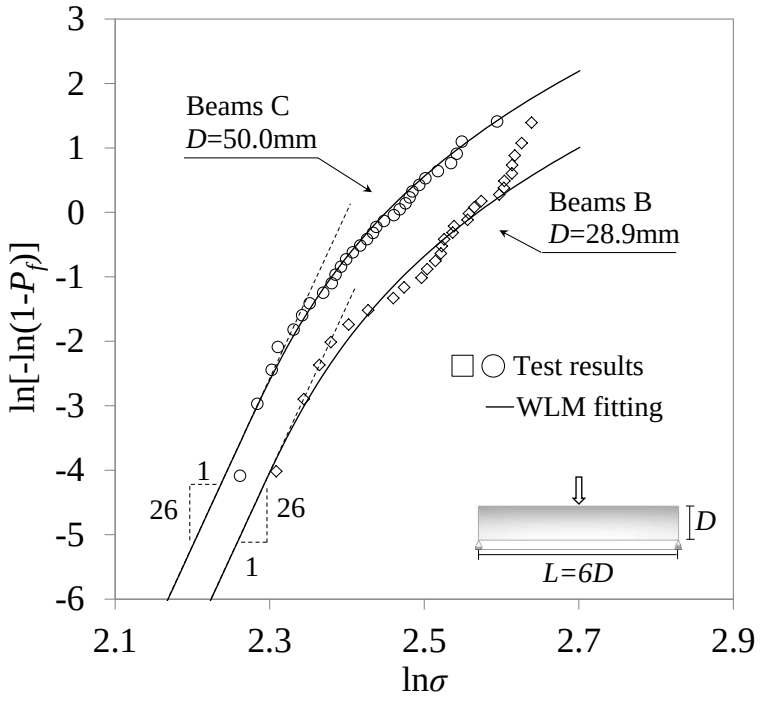

Figure 4.4. WLM fitting and prediction of experimental strength histograms for beam series *C* and *B*

By knowing the strength cdf of one RVE is then possible to determine the parameters describing the mean strength size effect curve, equation [4.3]. Since the scaling factor n=2 and the Weibull modulus m=26 are known only r, C_1 and C_2 need to be estimated. C_2 can be directly calculated by rewriting equation [4.8] for a beam specimen with a 2D scaling and thickness to span ratio 1:6:

$$C_2 = \frac{(m+1)l_0}{\sqrt{3}}\left[s_0\Gamma\left(1+\frac{1}{m}\right)\right]^{m/2} = 1.56\text{x}10^{15} \qquad [4.27]$$

Parameters r and C_1 can be obtained based on equations [4.22] and [4.23] for structures at the small size limit, which, based on recent findings, can be limited to 4 RVEs for three-point bending beams (*Le et al. 2012*). Considering a beam made of 4 x 24 RVEs (Figure 4.5), and based on elastic beam theory, two layers of RVEs are subject to tensile stress.

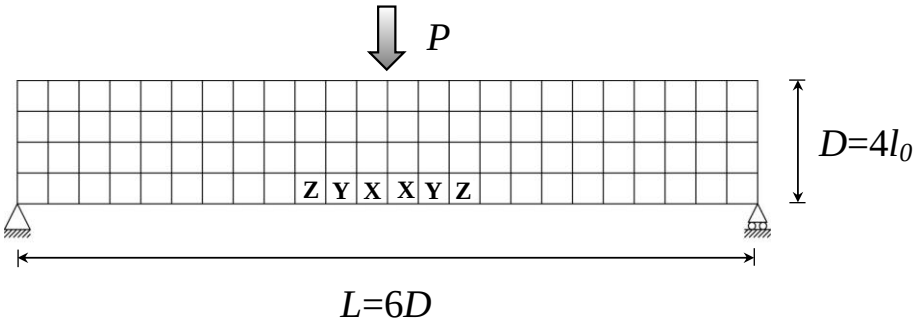

Figure 4.5. Three-point bending specimen (4 RVEs) at the small-size limit

Due to the stress linearity, the stress at the center of the bottom layer of RVEs is double compared to that in the RVEs layer adjacent to the neutral axis. Considering the bottom layer of RVEs, the average stress decreases by 9.5% and 26% as moving from the central

RVEs (RVEs "X" Fig. 4.5) to the side RVEs "Y" and "Z", respectively. Since the Weibull modulus of the asphalt mixture considered in this study is quite high (m=26), the failure probability of one RVE is expected to drop sharply with the decreasing applied stress. Therefore, it is expected that only the bottom-layer RVEs "X" and "Y" contribute to the failure probability of the entire beam and, thus, equations [4.22] and [4.23] can then be rewritten for two RVEs as:

$$\int_0^{\infty} \prod_{i=1}^{2} [1-\Phi_G(s_i\sigma_N, \mu_G, \delta_G)]^2 \mathrm{d}\sigma_N = \left[\frac{C_1}{4l_0} + \left(\frac{C_2}{4l_0} \right)^{2r/m} \right]^{1/r} \qquad [4.28]$$

$$\frac{1}{l_0} \int_0^{\infty} \left\{ \prod_{i=1}^{2} [1-\Phi_G(s_i\sigma_N, \mu_G, \delta_G)]^2 \sum_{i=1}^{2} \ln[1-\Phi_G(s_i\sigma_N, \mu_G, \delta_G)] \right\} \mathrm{d}\sigma_N = \\ = -\frac{1}{r} \left[\frac{C_1}{16l_m^2} + \frac{2r}{4l_0 m} \left(\frac{C_2}{4l_0} \right)^{2r/m} \right] \left[\frac{C_1}{4l_0} + \left(\frac{C_2}{4l_0} \right)^{2r/m} \right]^{1/r-1} \qquad [4.29]$$

where l_0=0.6mm is the 2D rescaled RVE as previously defined, s_1 = 0.718, and s_2 = 0.656. The above system of equations can be easily solved, giving r = 1.00 and C_1 = 45.34. The value of r is in the typical range of 0.5 to 2 (*Bažant 2005*), and is in very good agreement with the work of Bažant and Li (*1995*) on the modulus of rupture of concrete beams.

It is now possible to compare the predicted mean strength curve, given by equation [4.3], with the experimental mean nominal strength data. However, the results obtained from the DT mean strength need to be converted into the corresponding equivalent 3PB beam to be next used for evaluating the size dependence of the mean nominal strength. The DT specimen used in this investigation (Table 4.1) has a volume of 756,000mm^3, which consists of almost 5.25x10^4 RVEs (V_0=14.4mm^3). Such a large

number of RVEs ensures that the failure cdf of DT specimens is fully governed by the Weibull distribution, and, therefore, by the two parameters m (Weibull modulus) and s_0 (*Bažant and Pang 2007, Le et al. 2011*). Therefore, the mean strength of DT, $\bar{\sigma}_N^T$, can be written as:

$$\bar{\sigma}_N^T = N_T^{-1/m} s_0 \Gamma\left(1+\frac{1}{m}\right) \quad [4.30]$$

where N_T is the number of RVEs in the direct tension specimen and m and s_0 are the previously determined Weibull parameters. The failure distribution of the equivalent three-point bending beam is obtained as:

$$P_f(\sigma_N^B) = 1 - \exp[-N_{eq,B}(\sigma_N^B / s_0)^m] \quad [4.31]$$

where $N_{eq,B}$ is the equivalent number of RVEs of the beam. $N_{eq,B}$ can be calculated based on the elastic stress distribution for a three-point bending beam as:

$$N_{eq,B} = \frac{b}{l_0^3}\int_V [(\sigma(\boldsymbol{x})/\sigma_N^B)]^m \mathrm{d}V(\boldsymbol{x}) = \frac{1}{2(m+1)^2}\frac{V}{V_0} \quad [4.32]$$

where V is the volume of the beam. Given $N_{eq,B}$ the mean strength of the beam can be written as:

$$\bar{\sigma}_N^B = N_{eq,B}^{-1/m} s_0 \Gamma\left(1+\frac{1}{m}\right) \quad [4.33]$$

The equivalent characteristic size, D_{eq} (thickness), of the three-point bending beam, which has a nominal strength equal to $\bar{\sigma}_N^T$, is obtained by equating equations [4.30] and [4.33]:

$$D_{eq} = \sqrt{\frac{2(m+1)^2 N_T V_0}{6b}} = 2143\text{mm} \quad [4.34]$$

Such a large value for D_{eq} is not entirely surprising, since both geometry and stress field are changed when converting the DT specimen into its equivalent 3PB beam.

It is finally possible to plot all four experimental mean strength points in a $\log D$ - $\log \bar{\sigma}_N$ plane and compare them with the predictions obtained by equation [4.3] using the previously determined parameters, m, r, C_1 and C_2. Figure 4.6 presents the experimental data, the mean strength predicted by the WLM and the mean strength curve predicted by equation [4.3]; the last circle point on the right represents the equivalent 3PB size of the DT specimen.

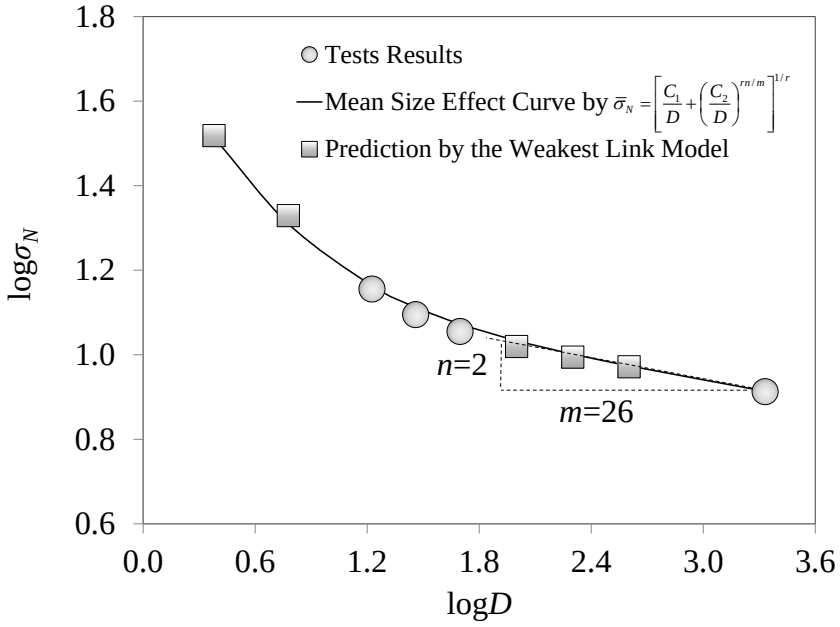

Figure 4.6. Mean strength curve: experimental data, WLM predictions and equation [4.3] predictions

It can be observed there is a very good agreement between tests results and the predicted size dependence of the mean nominal strength obtained from equation [4.3]. This result verifies the values of the mean strength curve calibrated from the cdf of the

material RVEs through histogram testing. By using the WLM, the mean strength for different beam sizes was also calculated, showing that the predicted points lie on the size effect curve. Such a result also indicates that equation [4.3] provides a good approximation of the exact size effect curve calculated from the finite WLM.

4.4. Inverse Analysis: Back-Calculation of the Strength Distribution Parameters of One RVE from Mean Strength Curve

The previously derived set of equations, [4.9], [4.22] and [4.23], which relate the parameters of the RVE cdf (equations [4.1a] and [4.1b]) to the mean strength curve parameters of equation [4.3], can be used to determine the strength distribution of one RVE from mean strength experimental data obtained on specimens of different sizes.

The Weibull modulus was assumed as known from the previous section and set as m=26. In section 4.5.2 a simple method on how to determine m from the mean size effect curve will be presented.

The parameters of the mean size effect curve can be determined by directly fitting equation [4.3] to the experimental mean strength data. Since m=26 is known, and the scaling dimension n=2 is imposed by 2D scaling problem, only r, C_1 and C_2 need to be estimated; non-linear fitting can be used for such a purpose. However, C_2 can be estimated in an alternative way, based on the measured mean strength of direct tension specimens. Equation [4.30] directly yields the value of the Weibull scaling parameter s_0 = 12.68MPa, which is also one of the four parameters of the RVE cdf. Equation [4.8] can then be used to calculate C_2 as:

$$C_2 = \frac{(m+1)l_0 s_0^{m/2}}{\sqrt{3}} \Gamma^{m/2}\left(1+\frac{1}{m}\right) \qquad [4.35]$$

Based on the previous assumption (section 4.3), for which the macro-crack leading to failure develops across the entire width of the beam, the effective RVE size can be rescaled as $l_0 = \sqrt{V_0 / b} = 0.6$ mm; therefore, from equation [4.35] a value of C_2 = 1.56×10^{15} can be calculated.

Finally, r and C_1 can be obtained using non-linear fitting methods, and by imposing a limit range for r (0.5 - 2.5); the following values were estimated: r = 1.01 and C_1 = 49.49. As in section 4.3, the value of r agrees very well with the previous theoretical study by *Bažant and Li* (*1995*). Figure 4.7 shows the experimental mean strength results and the fitting of equation [4.3].

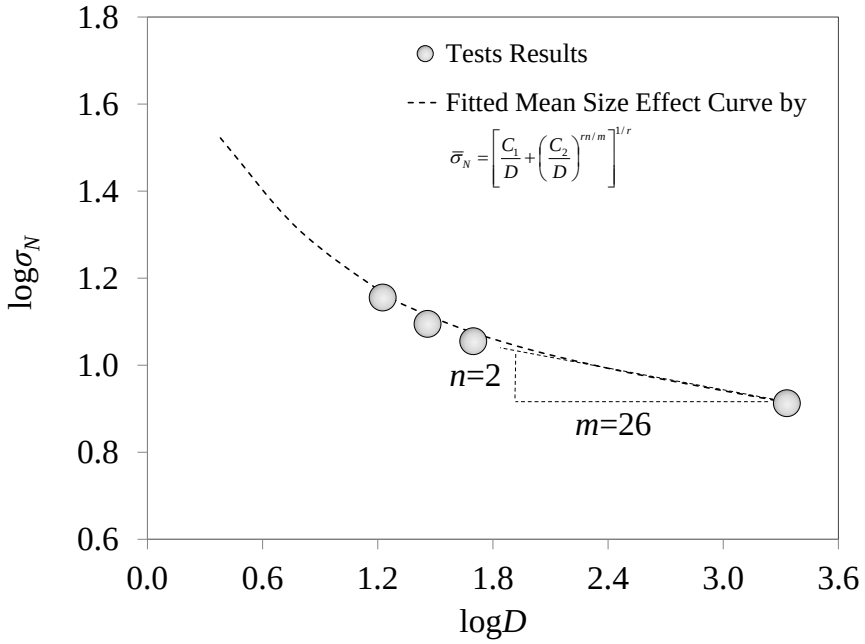

Figure 4.7. Mean strength curve: experimental data and equation [4.3] fitting

By Knowing r, C_1, C_2, n and m, it is possible to use equations [4.28] and [4.29], together with a beam geometry having a small-size limit $D = 4l_0$ (figure 4.6), for

obtaining the remaining two statistical parameters characterizing the strength distribution of one RVE: μ_G, and δ_G. It must be recalled that s_0 =12.68MPa was indirectly found from the mean strength of the DT specimens. The system of equations [4.28] and [4.29] can be numerically solved, yielding μ_G = 45.24MPa and δ_G = 14.82MPa.

The numerical solution of such a system of equations can be obtained by minimizing the value of the following function, $H(\mu_G, \delta_G)$:

$$H(\mu_G, \delta_g) = \left|F_1(\mu_G, \delta_G) - A\right| + \left|F_2(\mu_G, \delta_g) - B\right| \qquad [4.36]$$

where $F_1(\mu_G, \delta_G)$ and $F_2(\mu_G, \delta_G)$ are the left-hand sides of equations [4.28] and [4.29], respectively, and constants A and B are the numerical value of the right-hand sides of equations [4.28] and [4.29] calculated based on the calibrated values of r, C_1, C_2, and m. Figure 4.8 shows the 2D projection of $H(\mu_G, \delta_G)$.

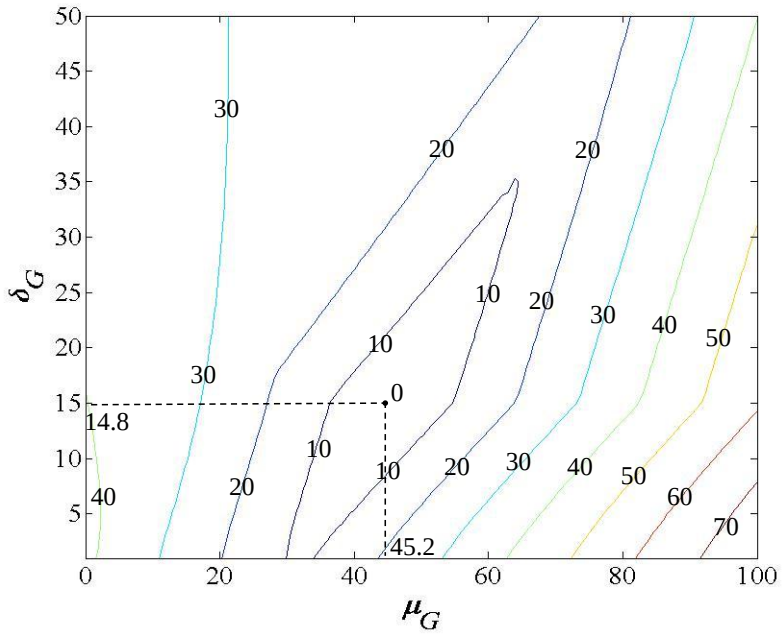

Figure 4.8. 2D projection of $H(\mu_G, \delta_G)$

It is clear that, for the range of feasible values of μ_G and δ_G, there is only one solution point for $H(\mu_G, \delta_G) = 0$. Figure 4.8 provides also an indirect verification of the values of r and C_1 determined by solving the same system of equations for the forward analysis in section 4.3.

The four parameters m, s_0, μ_G and δ_G can be finally used with equations [4.1a] and [4.1b] to obtain the strength cdf of one RVE. With the finite WLM (equation [4.2]), it is then possible to predict the strength distributions of beam series *B* and *C*, having size D = 28.9 mm and D = 50 mm, respectively. Figure 4.9 shows the comparison between the predicted and measured strength distributions.

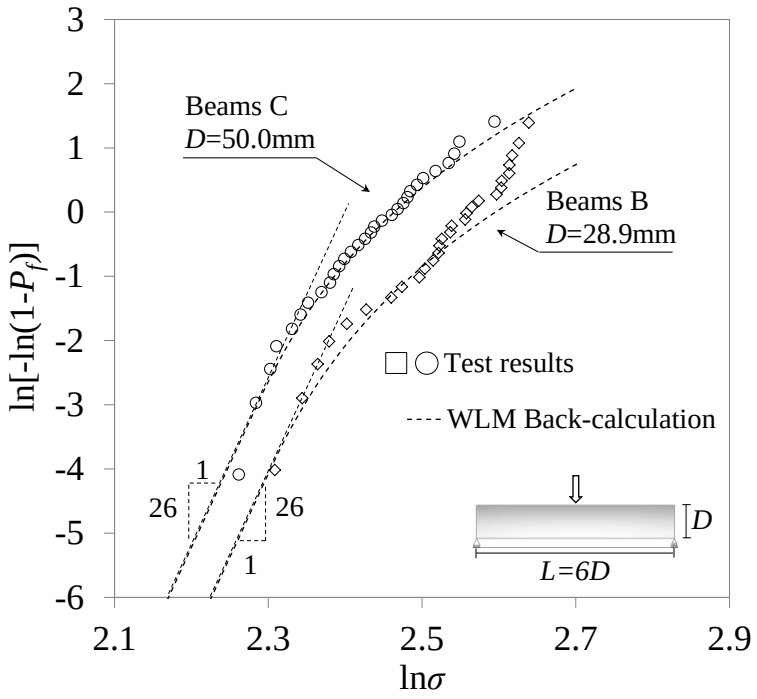

Figure 4.9. WLM back-calculation prediction of experimental strength histograms for beam series *B* and *C*

Predictions and experimental values agree very well for both beam sizes. This clearly verifies the values of the statistical parameters calibrated from the mean size effect curve.

4.5. Discussion and Comparison of Forward and Inverse Approach to Size Effect Analysis

4.5.1. Verification of the Finite Weakest Link Model

The capability of the finite WLM to capture the deviation from the two-parameter Weibull distribution of the strength histogram of single size structures made of quasibrittle materials was previously demonstrated by various authors (*Bažant and Pang 2007, Pang et al. 2008, Bažant et al. 2009, Le and Bažant 2009, Le et al. 2011*). By measuring the strength histograms of beams of two sizes, the work performed in this dissertation provides an exhaustive validation of the finite WLM. Figures 4.3, 4.4 and 4.9 clearly demonstrate the size dependence of the grafted strength distribution experimentally obtained through a proper choice of specimen sizes and number of replicates. Moreover, the good agreement between measured strength distribution obtained on beams of two sizes and the corresponding predictions clearly demonstrates that the finite WLM can well capture the size effect of the strength cdf for quasibrittle structures.

Batdorf (*1982*) alternatively proposed to consider the two-parameter Weibull distribution with a scale effect on the Weibull modulus to explain the size dependence of the strength distribution of quasibrittle structures; such a formulation results in a non-Weibullian size effect on mean structural strength. However, the experimental strength histograms obtained in this thesis, which have trends similar to those observed for other quasibrittle structures, cannot be fitted by the two-parameter Weibull distribution. By

contrast, the finite WLM considers a constant Weibull modulus, and the size effect on the type of strength cdf naturally arises from the finite number of RVEs.

4.5.1.1. Three-parameter Weibull Distribution

The size effect analysis performed and the results of sections 4.3 and 4.4 clearly show that the strength histogram of asphalt mixtures at low temperatures cannot be predicted by the classical two-parameter Weibull distribution. This can be observed in the strength histogram of other quasibrittle materials, such as engineering and dental ceramics (*Pang et al. 2008, Le et al. 2011*). Alternatively, the three-parameter Weibull distribution, which includes a stress threshold, σ_0, can be considered as fitting solution for the strength histogram of quasibrittle materials (*Stanley and Inanc 1985, Duffy et al. 1993, Gross 1996*).

According to the three-parameter Weibull statistics, the failure distribution of a structure can be written as:

$$P_f(\sigma_N) = 1 - \exp\left(- \int_V \left\langle \sigma_N s(\mathbf{x}) - \sigma_0 \right\rangle^{m_w} / s_w^{m_w} \, \mathrm{d}V(\mathbf{x}) \right) \qquad [4.37]$$

where σ_0 is the strength threshold, m_w is the Weibull modulus for three-parameter Weibull distribution, s is the scale parameter. The values of the three parameters can be obtained by fitting the experimental strength histograms of beam series *B* and *C* (Figure 4.10): σ_0 = 8.8MPa, m_w =1.4 and s_w =110MPa.

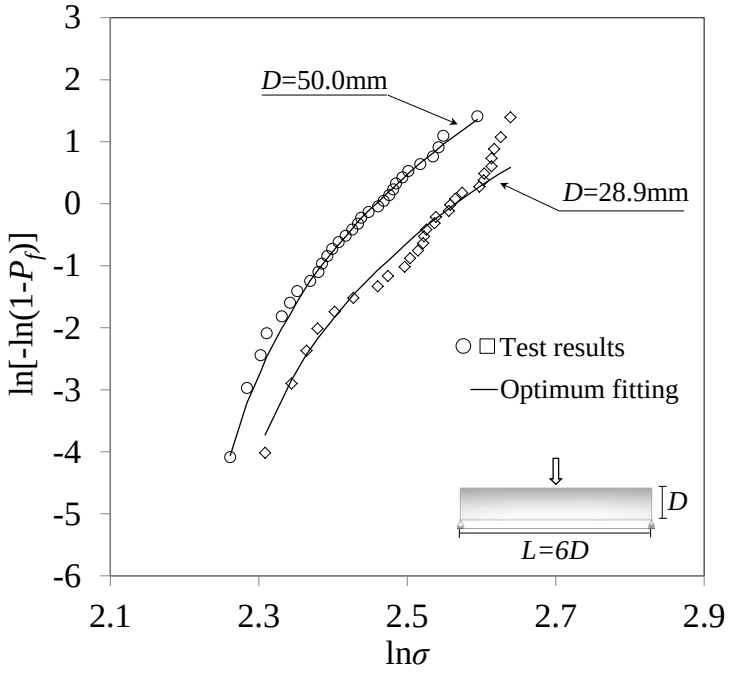

Figure 4.10. Optimum fitting of strength histograms by the three-parameter Weibull distribution

The three-parameter Weibull distribution can be used to predict the mean structural strength of beam series *A* and of the direct tensions specimens, which are $\overline{\sigma}_N = 14.51\,\text{MPa}$ and $\overline{\sigma}_N = 8.84\,\text{MPa}$, while the experimental values are $\overline{\sigma}_N = 14.31\,\text{MPa}$ and $\overline{\sigma}_N = 8.18\,\text{MPa}$, respectively. Such results indicate that the three-parameter Weibull distribution does not to accurately predict the mean strength of DT specimens.

A more comprehensive understanding can be obtained by comparing the mean size effect curves predicted by three-parameter Weibull distribution and by the finite WLM (Figure 4.11). At the large size limit, there is a significant deviation between the two strength size effects; the three-parameter Weibull distribution approaches to its threshold while the WLM follows a power law as structure size increases. This further

confirms that the finite WLM provides better fitting and prediction of size effect for quasi brittle materials.

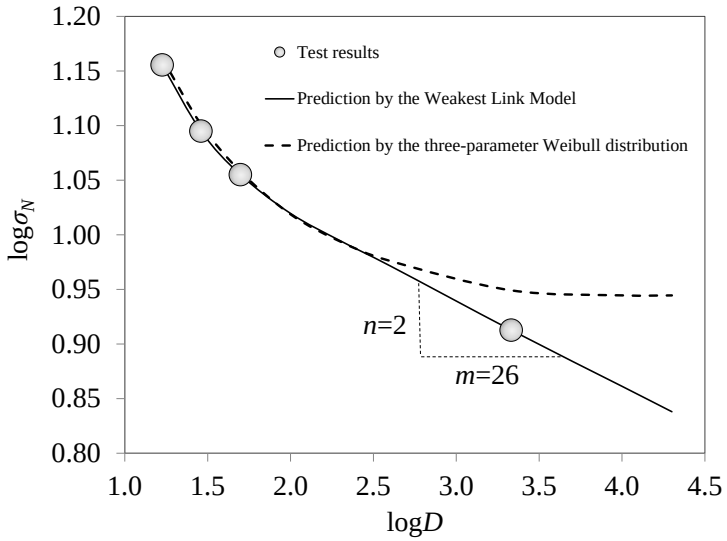

Figure 4.11. Comparison of mean size effect curves: 1) experimental measurements, 2) prediction by the three-parameter Weibull distribution, and 3) prediction by the finite WLM

Therefore, when a limited number of specimens is tested, the three-parameter Weibull distribution can fit the measured strength histograms in the small-intermediate size range. However, for experimental histograms obtained over a large number of replicates, the three-parameter Weibull distribution would not give an optimum fitting, as shown by Bažant and Pang (*2007*). This implies that, for quasibrittle structures, histogram testing should be used with caution in determining the failure distributions, unless a large number of specimens are used. On the other hand, the mean size effect analysis provides a more complete verification as it implicitly checks the strength statistics of structures of different sizes. This requires a large size range, which can be achieved by considering different specimen geometries, such as DT specimens to obtain

the large-size limit of the size effect curve. Nevertheless, this may not be always possible and practical due to specimens' preparation and testing device availability.

4.5.2. Determination of the Large-Size Asymptotic Properties of Size Effect Curve

Due to the limited dimensions of the slabs sample and of the climatic chamber used for the experimental phase of this study, mean strength test were performed on single-size direct tension specimens. However, this was not sufficient for obtaining the large-size asymptote of the size effect curve of mean strength, and, consequently, for directly determining the Weibull modulus m and constant C_2 of equation [4.3]. In this dissertation, the Weibull modulus m was estimated from the measured strength histograms (forward approach) and then used in the inverse problem analysis, in which the constant C_2 was subsequently calculated from the Weibullian mean of the strength of direct tension specimens.

In the case of the back-calculation analysis, this would not be necessary if mean strength tests were performed on direct tension specimens of two different sizes, or possibly on beam specimens with sufficiently large sizes.

Let's assume that, together with the current mean strength, $\overline{\sigma}_N^T$, obtained from a DT prism having N_T RVEs, a second mean strength value, $\overline{\sigma}_{N,2}^T$, was measured on another DT set of specimens having sufficiently large size and $N_{T,2}$ RVEs. Based on Weibull statistics, (equation [4.30]), the Weibull modulus m could be simply determined as:

$$m = \frac{\ln(N_{T,2}) - \ln(N_T)}{\ln(\overline{\sigma}_{N,2}^T) - \ln(\overline{\sigma}_N^T)} \qquad [4.38]$$

Based on the calculated *m* and by using equation [4.34], it is then possible to obtain the equivalent sizes of the three-point bending beams corresponding to these two direct tension specimen sizes. These two points would certainly form the large-size asymptote of the size effect curve, from which the constant C_2 could be easily determined by fitting equation [4.3] or directly from equation [4.7].

4.5.3. Comparison of Forward and Inverse Size Effect Analysis

Previous studies (*Bažant and Pang 2007, Bažant et al. 2009, Le et al. 2011*) showed that the strength distribution of one RVE can be determined by fitting the WLM to the experimental strength histogram; this was demonstrated in section 4.3 of this thesis.

In section 4.4 a back-calculation solution for obtaining the strength cdf of one RVE from mean size effect curve was presented. It is now worthwhile comparing the two methods with the objective of determining which one is more convenient and suitable for strength size effect analysis.

Table 4.3 presents a summary of the parameter of the RVE cdf and of the mean strength curve (equation [4.3]) obtained with the two methods. Figure 4.12 and 4.13 provide a graphical comparison of the predicted/fitted strength histograms and mean size effect curves calculated with forward and inverse analysis.

Table 4.3. Parameters of RVE cdf and mean strength size effect curve

	RVE cdf				Mean size effect curve		
	μ_G (MPa)	δ_G (MPa)	s_0 (MPa)	m	C_2	C_1	r
Forward Analysis	44.49	14.89	12.68	26	1.56×10^{15}	45.34	1.00
Back-calculation	45.24	14.82	12.68	26	1.56×10^{15}	49.49	1.01

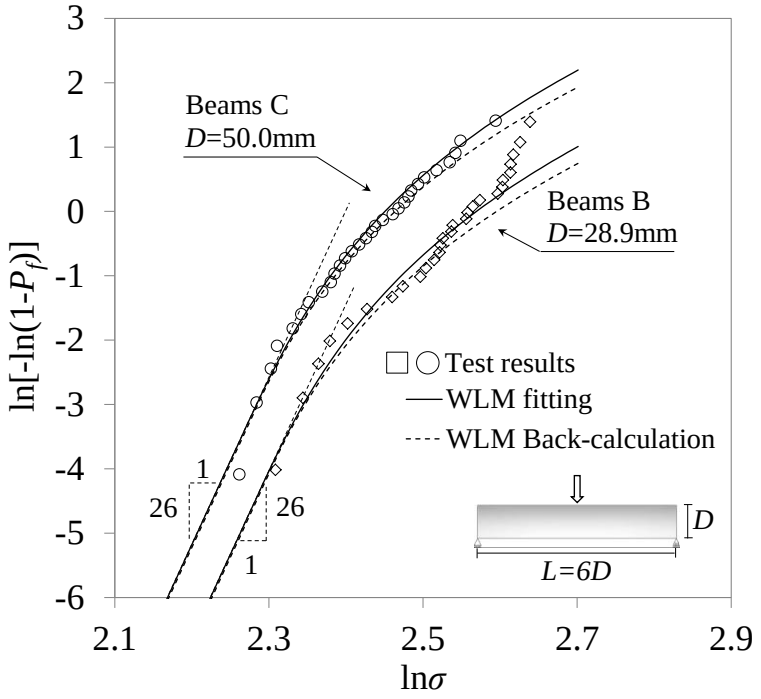

Figure 4.12. Strength histogram – forward and back-calculation analysis

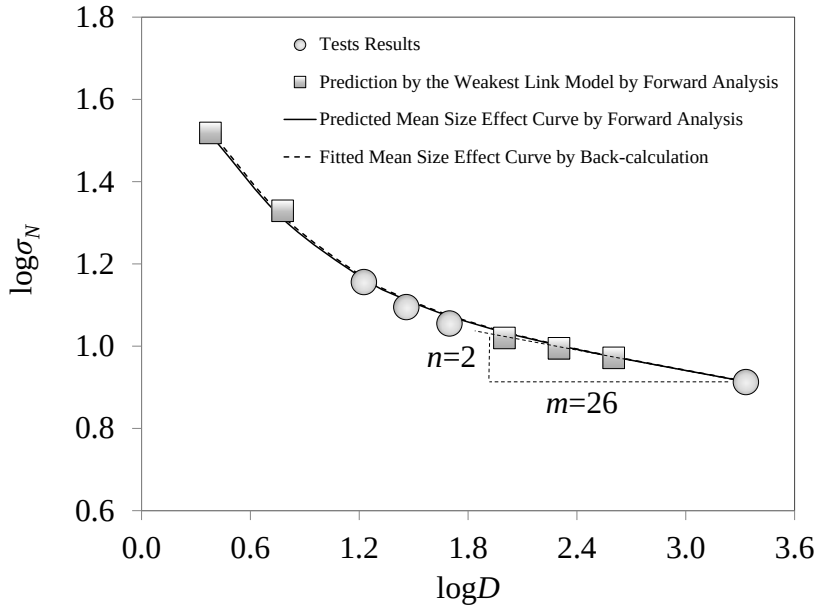

Figure 4.13. Mean size effect curve – forward and back-calculation analysis

The values of μ_G, δ_G, C_1, C_2, and r obtained from forward and inverse analysis are very close, while in the case of m and s_0 are identical since they are both estimated by fitting the lower straight part of the strength histogram. The back-calculation approach tends to slightly overestimate the mean strength of beam series *C* and *B*. This is clearly showed by the lower histogram curves, dashed lines, compared to the solid ones, which indicates the forward analysis, on the Weibull scale (Figure 4.12). The fitted mean size effect curve (dashed curve) further confirms this trend, which is more pronounced at the small-size limit, even though visually not very appreciable. Nevertheless, fitted (from back-calculation analysis) and predicted (from forward analysis) mean strength curves are very close and overlap at the large-size limit. Therefore from a quantitative point of view the two methods can be considered as equivalent, when the experimental phase is carefully prepared and conducted.

From a practical and experimental point of view, one advantage of the back-calculation method over the histogram testing method (forward analysis) is the number of specimens needed. The inverse method only requires testing on the mean strengths of geometrically similar specimens with several different sizes, where 3-5 specimens are needed for each structure size, and the size effect test should involve about 4-5 different sizes. The total number of specimens required for the proposed back-calculation method can, therefore, be limited to about 20 specimens, which is significantly less than the number of specimens required for the conventional histogram testing. Another advantage of the inverse analysis is that the mean strength is less prone to experimental errors due to the averaging, whereas, the strength histogram is sensitive to the experimental errors,

unless a large number of specimens is used, and each point on the histogram represents the average strength of a group of several specimens.

On the other hand, the back-calculation analysis requires the mean size effect curve with a large size range. Mean strength in the small-size range is usually easy to be obtained experimentally. This may not be the case for the large size asymptote, which is fundamental for the estimating the Weibull modulus m and constant C_2; this is generally due to the challenges imposed by the preparation of large specimens and to the size constraint of the loading machine (e.g. three-point beams considered in this dissertation). As showed in this chapter, one solution to overcome such a difficulty is to consider the specimens of different sizes under different loading modes. However, this would require a different test set-up.

In general, there is not a definite answer to whether the back-calculation method is better than the conventional histogram testing method. The choice mainly depends on the type of materials to be tested and the testing facilities and tests device available. For some materials, such as ceramics (e.g. silicon nitride), where it is very expensive to produce large-size specimens, the histogram testing method may be a better approach. On the other hand, for materials such as sandstones, histogram testing requires a large amount work of specimen cutting and grinding, which makes the inverse method more attractive.

In the specific case of asphalt mixture, the fabrication of large specimens is mainly constrained by the dimension of the climatic chamber and by the availability of a slab compactor or a linear kneading compactor. Such devices are not commonly available in asphalt materials laboratory since the gyratory compactor (GC) is the standard device

for asphalt mixture compaction. GC is used to prepare cylindrical specimens with a diameter of 150mm and a maximum height of 170mm. Given the limited dimension of the type of specimens that can be cut out of such a cylindrical sample, a forward analysis, based on the classical histogram tests, becomes more convenient for investigating the size effect of asphalt mixture.

Chapter 5. BBR Asphalt Mixture Strength

In this Chapter the possibility of obtaining low temperature strength by testing small beam of asphalt mixture with the Bending Beam Rheometer (*AASHTO T313-10-UL 2010, Marasteanu et al. 2012*) is investigated. First, mean strength test are performed and the effect of factors such as cooling medium, conditioning time, binder type, and the use of reclaimed asphalt material are evaluated. Then, histogram testing is performed for one mixture and based on size effect theory for quasibrittle materials (*Bažant and Pang 2007, Bažant et al. 2009, Le et al. 2011*), the BBR failure distribution of material strength is discussed. From the experimental results and the mathematical bundle model (*Bažant and Pang 2007*), a sub-structure of the material RVE is proposed and used to predict the three-point bending strength of larger specimens of asphalt mixture.

5.1. Materials and Experimental Procedure

Five asphalt mixtures prepared with four different asphalt binders, were used in the experimental work. All mixtures had a nominal maximum aggregate size, NMAS=12.5mm. Since in Chapter 3 it was found that the cooling fluid used in the BBR conditioning bath significantly influenced the failure response of asphalt binder, the same three cooling media were considered: ethanol (E) (control), potassium acetate (PA) and air (A). Conditioning time (CT) was also investigated at two levels, 1h (control) and 20h. For one asphalt mixture, the effect of RAP addition was also evaluated. Table 5.1 presents the summary of the details of the five asphalt mixtures and the experimental design used for investigating the BBR mean strength.

Table 5.1. Asphalt mixtures details and experimental design for BBR testing

Mixture ID	Binder	RAP	Cooling Medium	Conditioning Time
RAP	MIF PG58-34 Elvaloy	20%	E (control) – PA - Air	1h (control)
Virgin	MIF PG58-34 Elvaloy	0% (control)	E (control) – PA - Air	1h (control)
Citgo	Citgo PG58-28 plain	0% (control)	E (control) – PA - Air	1h (control) – 20h
Marathon	Marathon PG58-28 plain	0% (control)	E (control) – PA - Air	1h (control) – 20h
Valero	Valero PG58-28 plain (control)	0% (control)	E (control) – PA - Air	1h (control) – 20h

Asphalt mixture beams were prepared according to the method proposed by Marasteanu et al. (*2009*). This procedure includes several cutting steps from a gyratory compacted (GC) cylinder samples to the actual BBR beams (Figure 5.1). The dimension of the beam specimens are 125mm x 12.5mm x 6.25mm and the span is L=101.6mm.

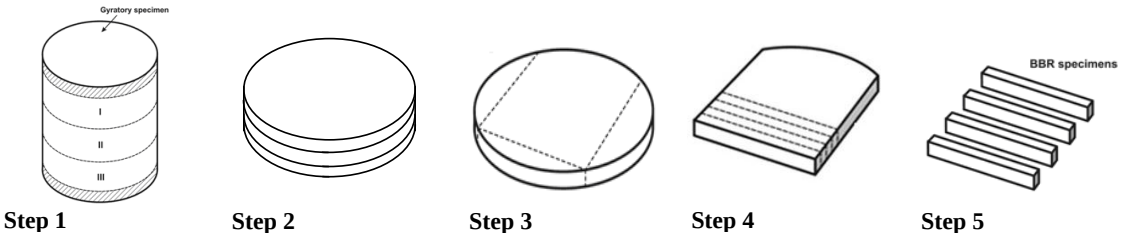

Figure 5.1. BBR asphalt mixture beams cutting procedure (*Marasteanu et al. 2012*)

BBR strength tests, mean and histogram, were performed with the BBR-Pro device described in Chapter 3. Testing temperature was set to T=-12°C for all the five asphalt mixtures used. In order to minimize the loading rate effect and impose a constant loading rate of the fracture process zone (FPZ), a time to failure of about 5 minutes was set for all the five mixtures.

5.2. Mean Strength Results

BBR nominal strength of asphalt mixture, σ_N, and corresponding strain at failure, ε_N, were calculated from the mean obtained over six replicates per each testing condition with the same formulas used for the BBR asphalt binder strength:

$$\sigma_N = \frac{3P_N L}{2bh^2} \quad [5.1]$$

$$\varepsilon_N = \frac{6\delta_N h}{L^2} \quad [5.2]$$

where σ_N is the nominal strength (MPa), ε_N is the strain at failure, P_N is the maximum measured load (N), L is the span length (101.6 mm), b is the width of the beam (12.5 mm), h is the thickness of the beam (6.25 mm) and δ_N is the deflection (mm) of the beam corresponding to the peak load P_N. Figure 5.2 shows the mean strength obtained from BBR testing for all the factor-level combination given in Table 5.1; CoV stands for coefficient of variation (%). Figures 5.3a and 5.3b present examples of stress strain curve.

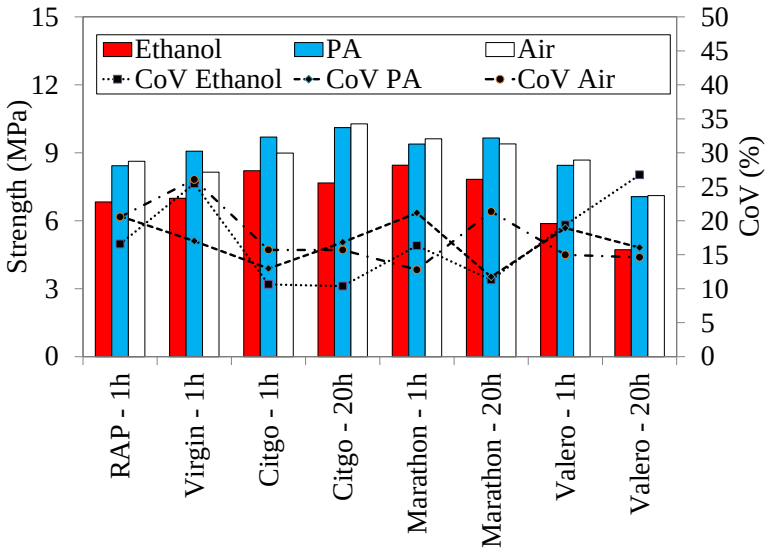

Figure 5.2. BBR mean strength for asphalt mixture

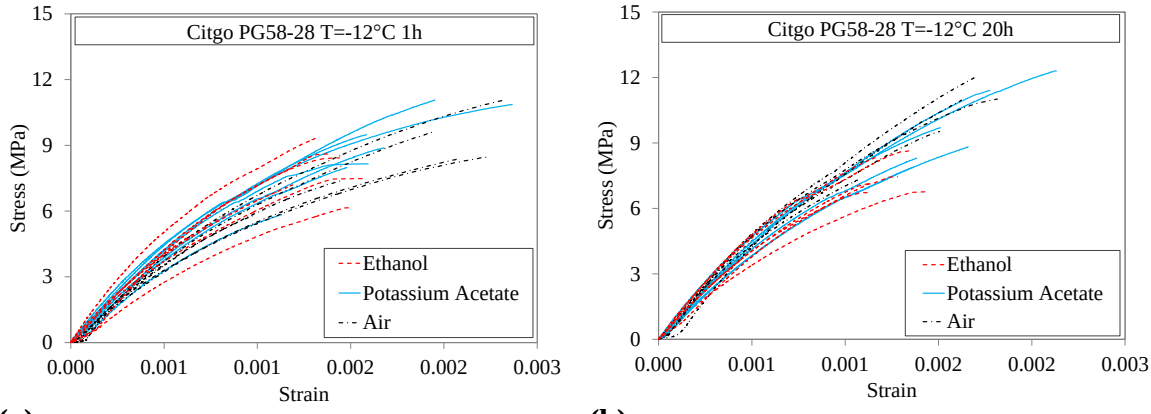

(a) **(b)**

Figure 5.3. BBR stress-strain curve for asphalt mixture Citgo (a) 1h and (b) 20h conditioning

A visual inspection of the bar chart (Figure 5.2) indicates there is an increase in mixture strength for tests performed in PA and air compared to those in ethanol, while similar strength values are obtained for PA and air. However, a significant difference among the stress strain curves for the different cooling media is not visually appreciable.

5.2.1. Statistical Analysis of BBR Mean Strength

In a previous research, *Turos et al.* (*2012*) found that asphalt mixture strength presents a failure distribution (cdf) with a Weibull left tail (*Weibull 1939*). In Chapter 4 of this thesis, it was shown that asphalt mixture gradually change failure distribution as the structure size increases. To better take into account these fact, a non-parametric statistical analysis (*Moore et al. 2009*) based on ANOVA (*Oehlert 2000*) was performed to evaluate the significance of the different factors assumed in the experimental design (Table 5.1). Asphalt mixture air voids, determined through digital image processing (DIP) of asphalt mixture BBR beam images (*Marasteanu et al. 2012*), were also included in the analysis

as co-variate. Table 5.2 summarizes the statistical analysis results for the significant factors.

Table 5.2. Statistical analysis of BBR asphalt mixture strength

Factor	Coefficients	Estimate	*t*	*p*-value
	Intercept	13.065	11.3	10E-8
	Air Voids	-1.445	-6.5	10E-8
Binder Type	Citgo	1.737	4.6	**10E-8**
	MIF	1.282	4.4	**10E-8**
	Marathon	1.734	4.6	**10E-8**
	Valero	Control	-	-
Cooling Medium	Potassium Acetate	1.813	7.6	**10E-8**
	Air	1.718	7.1	**10E-8**
	Ethanol	Control	-	-

The very low *p*-values indicates that the specific factor-level combination is highly statistical significant at 0.05 level. ANOVA shows that conditioning time and RAP are not affecting the BBR strength of asphalt mixture. An increase in air voids results in a decrease of the mixture strength. The response is highly binder dependent, and strongly affected by the cooling medium (*Marasteanu et al. 2012*), with higher values for potassium acetate and air. Tukey–Kramer method (*Oehlert 2000*) further provides evidence that strength results in air and potassium acetate are statistically comparable.

The statistical analysis suggests that, as hypothesized in Chapter 3 for BBR asphalt binder strength, ethanol leads to environmental stress cracking and, therefore, is not suitable for BBR strength tests on asphalt mixtures. Measurements in potassium acetate and air show similar values. For these reasons histogram tests used for size effect analysis were performed only in air.

5.3. Histogram Testing and Size Effect Analysis

BBR strength histogram testing (20 replicates) was performed in air at T=-12°C on the mixture containing RAP (Table 5.1), and the results were used to investigate the distribution of material strength and to evaluate the possibility of extrapolating the experimental results to larger structures. This mixture was selected since it was prepared with modified asphalt binder, MIF, and because the previous statistical analysis indicated no significant difference in mean strength by adding RAP.

In order to understand whether BBR beams are representative of the mixture RVE, strength histogram testing of larger beams, LB (125mm x 40mm x 40mm - 28 replicates) made with the same mixture, was performed at the same low temperature, T=-12°C, in air, and then, the BBR results were used to predict the strength distribution of LB. Since a higher failure load was expected for the LB, an MTS servo-hydraulic machine was used for testing. The nominal strength on the LB was calculated with equation [5.1] using the actual beams' dimensions. Figure 5.4 shows the BBR and LB specimens used, while Figure 5.5 presents a schematic of the three-point bending test for the LB specimens.

Figure 5.4. LB and BBR specimens

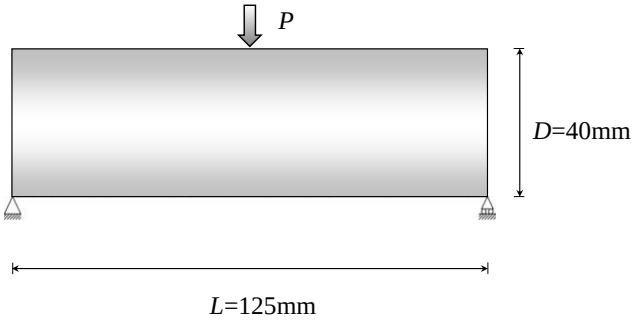

Figure 5.5. Schematic of the three-point bending tests on larger asphalt mixture beams

The time to failure of BBR and LB was set to about 5 minutes to reduce the rate dependence of the FPZ and thus to facilitate the comparison between BBR and LB strength through size effect.

The mean strengths of the two strength histograms were $\bar{\sigma}_{N-BBR} = 9.09\,\text{MPa}$ and $\bar{\sigma}_{N-LB} = 5.65\,\text{MPa}$ for BBR and LB, respectively. Figures 5.6a and 5.6b present the two experimental strength histograms.

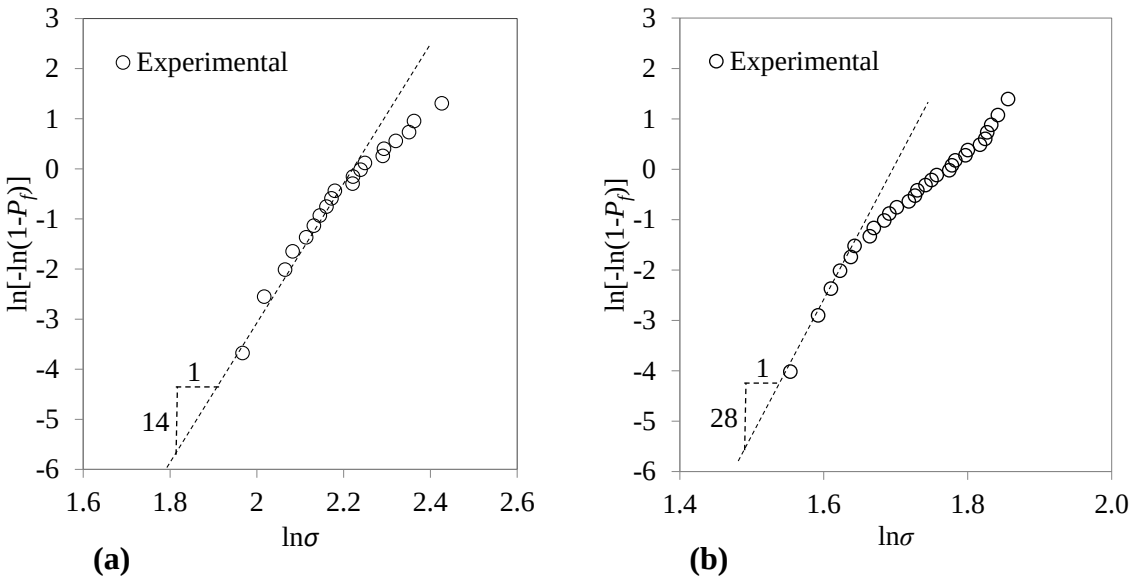

Figure 5.6. (a) BBR and (b) LB strength histograms for asphalt mixture RAP

Both experimental histograms (circle symbols) clearly show that asphalt mixture has a quasibritlle failure distribution with a left Weibull tail and a curved upper part. However, the Weibull modulus, *m*, (slope of the histogram left straight part – dashed line) of the two cdf's are different with BBR having m_{BBR} = 14, which is exactly half of that obtained from the larger beams, m_{LB} = 28. The Weibull modulus of the larger beams has a value which is typical for quasibrittle cementitious materials: e.g. *m* = 24 for Portland cement concrete (*Bažant and Pang 2007*) or, as previously found in Chapter 4, *m* = 26 for asphalt mixture. This suggests that BBR strength results cannot be directly used to predict the strength and the failure distribution of larger structures, since the parameters obtained by fitting the WLM and the grafted distribution (equations [2.22a] and [2.22b]) to BBR strength histogram would not return the parameters of the actual material RVE.

Therefore, it is necessary to find a solution for reconstructing the material RVE structure from the BBR experimental results. Since both BBR and LB strength distributions present a Weibull tail having $m_{LB} = 2 \times m_{BBR}$, one condition to related the cdf of the BBR to cdf of one material RVE is to rise the exponent of the distribution of the BBR tail by a factor of two. This can be done mathematically by using a fiber bundle model (*Bažant and Pang 2007*) (Chapter 2). The brittle fibers bundle model (*Bažant and Pang 2007*) presents a simple solution for such a purpose. The cumulative distribution function of strength σ of a bundle made of *n* brittle fibers can be obtained from the recursive formula (*Daniel 1945*):

$$G_n(\sigma) = \sum_{k=1}^{n} (-1)^{k+1} \binom{n}{k} F^k(\sigma) G_{n-k}\left(\frac{n\sigma}{n-k}\right) \qquad [5.3]$$

where fibers are numbered k = 1, 2...n in the order of increasing random values of strength σ_k, $F_k(\sigma) = [F(\sigma)]^k$, $\sigma > 0$, $G_0 = 1$, $G_n(\sigma)$ is the strength cdf of the entire bundle with n fibers. When the strength cdf of each fiber has a power-law left tail with same exponent p, the cdf of strength of brittle bundle has also a power-law tail, and its exponent is np.

In order to use expression [5.3], the cdf of each fiber composing the bundle needs to be known. Based on this condition, it was decided to model the cdf of BBR strength (Figure 5.5a) using the finite WLM, equation [2.7], and the grafted distribution given by the system of equations [2.22a] and [2.22b]. It was assumed that each element of the BBR beams, which in this dissertation will be called sub-RVE, is a sub-element of each fiber of the material RVE, and that the cdf of such a sub-element can be approximated by equations [2.22a] and [2.22b].

To obtain the four parameters (m_{BBR}, $s_{0\text{-}BBR}$, $\mu_{G\text{-}BBR}$ and $\delta_{G\text{-}BBR}$) of strength cdf of the BBR sub-RVE, the BBR beam was discretized into a grid of n equal elements, and the WLM together with equations [2.22a] and [2.22b] were fitted to the BBR experimental strength histogram (Figure 5.6a). The characteristic size, $l_{0\text{-}BBR}$, of the BBR sub-RVE was first assumed in the range of 0.3-0.5mm for a 2D scaling; this ensures a sufficient number of BBR sub-RVEs with respect to the thickness of the BBR beam. Based on best fitting the characteristic size of the BBR sub-element was next adjusted to $l_{0\text{-}BBR}$ = 0.39mm, which correspond to a volume $V_{0\text{-}BBR}$ = 1.90mm^3, resulting in a total number of sub-RVE n=4175. The solid line in figure 5.7 represents the best fitting of the WLM to the BBR experimental data using the following set of parameters: m_{BBR}=14, $s_{0\text{-}BBR}$=10.70MPa, $\mu_{G\text{-}BBR}$=17.09MPa and $\delta_{G\text{-}BBR}$ =4.75MPa.

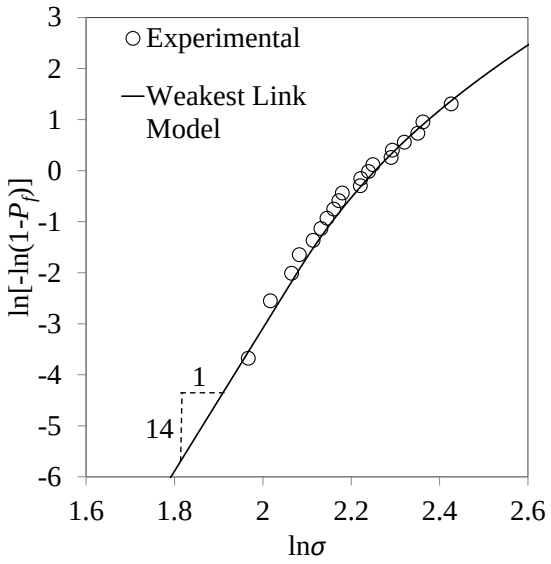

Figure 5.7. BBR strength histogram for asphalt mixture RAP and WLM fitting

The BBR sub-RVE cdf and the brittle bundle model were next used to mathematically construct the material RVE model. This is based on two chains made of BBR sub-RVEs up to the volume of the real RVE. In Chapter 4 the RVE volume of asphalt mixture was estimated based on the RVE characteristic size, l_0, which was set as twice the aggregate average size (*Bažant and Pang 2007*). The RVE characteristic size for this specific mixture containing RAP is l_0=6.32mm, corresponding to a RVE volume $V_0 = (l_0)^3 = 252.44\text{mm}^3$. Therefore, the total number of sub-RVEs in the two-fiber RVE model is simply obtained dividing the RVE volume by the volume of the sub-RVE: $n_{sub\text{-}RVEs} = V_0 / V_{0\text{-}BBR} = 132$; each fiber is, hence, made of $n_f = 66$ sub-RVEs. Figure 5.8 shows the schematic of the proposed RVE model.

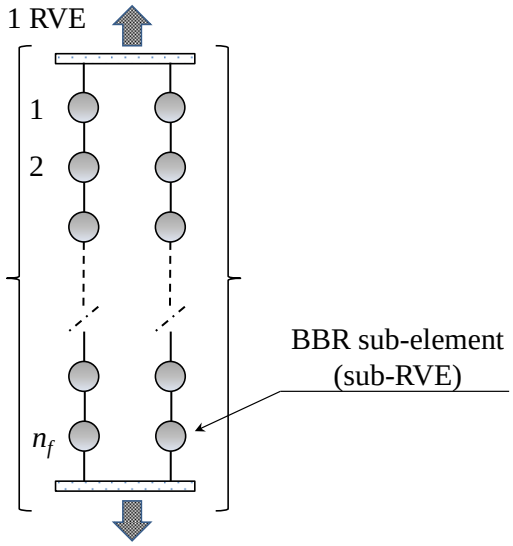

Figure 5.8. RVE bundle model

Based on equation [5.3], it is possible to calculate the cdf $P_1(\sigma)=G_2(\sigma)$ of the entire RVE as:

$$P_1(\sigma) = G_2(\sigma) = \sum_{k=1}^{2} (-1)^{k+1} \binom{2}{k} F^k(\sigma) G_{2-k}\left(\frac{2\sigma}{2-k}\right) \qquad [5.4]$$

$$P_1(\sigma) = G_2(\sigma) = 2F(\sigma)F(2\sigma) - [F(\sigma)]^2 \qquad [5.5]$$

where $F(\sigma)$ is the cdf of each fiber, which is computed using the grafted distribution described by equations [2.22a] and [2.22b] together with the WLM and the BBR sub-RVE (sub-element) parameters. Figure 5.9 shows the failure distribution of the material RVE (solid line) obtained from equations [5.4] and [5.5].

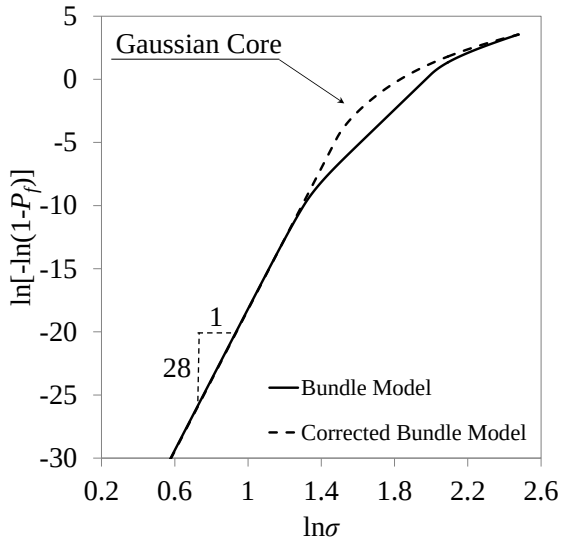

Figure 5.9. Histograms of the failure cdf for the RVE bundle model and RVE corrected bundle model

It can be observed that $P_1(\sigma) = G_2(\sigma)$ presents a very low grafting point with a core having a non-Gaussian distribution. This is due to the limited number of chain (two) necessary to raise the power tail of the RVE cdf from 14 to 28. Therefore, the RVE grafted distribution model (equations [2.22a] and [2.22b]) presents a non-Gaussian core that leads to a severe over prediction of the mean strength of larger beams. Nevertheless, the RVE bundle model still provides the boundaries for the RVE distribution and, thus, the non-Gaussian part of the cdf can be approximated with a Gaussian core, based on normalization condition of the entire RVE cdf: $P_1(\sigma\rightarrow\infty) = G_2(\sigma\rightarrow\infty) = 1$ (Figure 5.9 dashed line). Therefore, it is possible to determine the four RVE parameters of equations [2.22a] and [2.22b] (m, s_0, μ_G and δ_G) and use them to predict the failure distribution of larger beams. Figure 5.10 shows the prediction obtained with such a corrected bundle model and the WLM (equation [2.7]), having the following set of parameters: $m_{RVE} = 28$,

$s_{0\text{-}RVE}$ = 5.22MPa, $\mu_{G\text{-}RVE}$ = 5.99MPa and $\delta_{G\text{-}RVE}$ = 0.74MPa and a total number of RVEs N_{RVE} = 792.

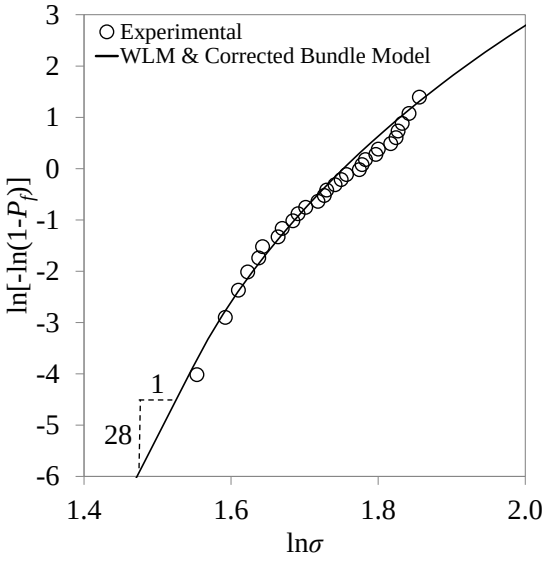

Figure 5.10. Strength histograms for asphalt mixture RAP for larger beams and WLM prediction

The solid curve predicts very well the experimental strength data of the larger beams suggesting that the proposed approximation is a reasonable approach to the size effect analysis of strength data obtained from BBR strength tests. The mean strength prediction for the larger beam is $\bar{\sigma}_{N-LB-prediction} = 5.53\,\text{MPa}$, which is very close to the experimental value $\bar{\sigma}_{N-LB} = 5.65$ MPa.

Chapter 6. Summary and Conclusions

6.1. Summary

In this thesis the strength size effect of asphalt binders and asphalt mixtures was investigated, and the possibility of obtaining three-point bending strength by testing small beam specimens with the Bending Beam Rheometer (BBR) was evaluated. In the first part, a review of the theory of strength size effect for quasibrittle materials was presented. The theoretical framework was then used to analyze and compare the experimental results obtained from strength tests performed on specimens of different sizes and geometries.

Asphalt binder strength obtained with BBR was evaluated for different binder types and different cooling media, ethanol, potassium acetate and air, and statistical analysis was used to estimate the effect of these factors on the material response. Then, histogram strength testing was performed and size effect theory was applied to compare BBR strength with the direct tension test (DTT) strength results.

A forward and inverse analysis of asphalt mixture size effect was also performed. A set of closed-form equations, for directly relating the parameters of failure probability of one material RVE to the parameters of the mean size effect curve of structural strength and vice versa, was derived. The new formulation was experimentally verified by histogram and mean strength testing of mixture specimens of different sizes at low temperature.

Histogram testing and size effect analysis were used to investigate the asphalt mixture strength obtained with BBR. Based on BBR experimental results, the brittle bundle model was used to determine the RVE cumulative distribution function of asphalt

mixture. This RVE model was then verified by comparing the experimental results obtained on larger beam specimens with the prediction obtained from the proposed model. The effect of cooling medium on BBR asphalt mixtures mean strength was also evaluated.

6.2. Conclusions

The main conclusions of this thesis can be summarized as follows:

- BBR asphalt binder strength results indicate that cooling medium strongly affects the response. Statistical analysis shows that the use of potassium acetate and air result in similar strength values, while strength measurements obtained in ethanol are much lower.
- BBR strength histograms indicate a binder dependence of the asphalt binder failure distribution. Plain binder presents a typical Weibull statistics pattern with a brittle behavior, while modified binder shows a quasibrittle trend. This can most likely be attributed to the polymer modification and consequently to the non-negligible dimension of the material RVE, which still remains small.
- Weakest link model can be used as an analysis tool to transform the BBR flexural response into a DTT uniaxial stress; conversion shows that BBR strength obtained in air and DTT strength obtained in potassium acetate are very similar. These findings also indicate that air is a suitable cooling medium to perform BBR strength tests on asphalt binder.
- Forward and inverse analyses of size effect indicate that, at low temperatures, asphalt mixture behaves as a quasibrittle material, showing a Type I mean

strength size effect. The cumulative distribution function can thus be described by a grafted distribution having a Weibull cdf tail and a Gaussian cdf core.

- Both forward and back-calculation methods provide very good predictions of the experimental results. However, for asphalt mixture, a conventional histogram testing (forward analysis) is experimentally more practical. Therefore, strength histogram and size effect theory can be used as an analysis tool also for asphalt mixture when extrapolating data to larger specimens' sizes.
- Asphalt mixture strength obtained on small BBR beams is highly dependent on the asphalt binder type and on the cooling medium with air and potassium acetate giving similar results. Air seems to be a suitable cooling medium for BBR strength tests of asphalt mixtures, as well.
- The BBR beams are not representative of the corresponding asphalt mixture RVE. This is shown by the difference in Weibull modulus between histograms obtained on BBR and on much larger beams. Brittle bundle model, adjusted in the Gaussian core of the failure distribution, can be used to obtain the cdf of the material RVE starting from the BBR experimental data. This model can be further used to extrapolate the BBR strength results to specimens of different sizes and geometries.
- From the experimental work and size effect modeling it can be concluded that strength tests can be performed on asphalt binders and asphalt mixtures with a modified BBR. Cooling in air appears to be the best option for storing and testing both binders and mixtures. Size effect theory can then be used to extrapolate experimental data to structures of different size and geometry.

6.3. Recommendations and Future Work

The results obtained in this investigation indicated that the BBR system can be used to obtain strength properties of asphalt binder and mixtures. A number of important issues need to be further addressed before implementing a test method:

- The experimental results and analyses indicated that using air as a cooling medium would eliminate any issues related to the effect of cooling fluid on material properties. However, controlling air temperature in the BBR cooling chamber is challenging and ice can form on the walls of the chamber. While in this research effort extreme care was taken to control the temperature, this may be difficult to achieve on a routine basis.
- Some asphalt mixtures had strength values in air that exceeded the limits of the load cell. This needs to be further investigated since it may require retrofitting the BBR with a larger load cell.
- Other bundle models, such as plastic and softening bundle fibers, should be evaluated for reconstructing the RVE cdf of asphalt mixture when analyzing BBR strength data. This could avoid the use of the Gaussian approximation when using a brittle bundle fiber model.

References

AASHTO M320-10-UL, Standard Specification for Performance-Graded Asphalt Binder, American Association of State Highway and Transportation Officials, 2010.

AASHTO M323-07-UL, Standard Specification for Superpave Volumetric Mix Design, American Association of State Highway and Transportation Officials, 2007.

AASHTO R028-09-UL, Standard Practice for Accelerated Aging of Asphalt Binder Using a Pressurized Aging Vessel (PAV), American Association of State Highway and Transportation Officials, 2009.

AASHTO T240-09-UL, Standard Method of Test for Effect of Heat and Air on a Moving Film of Asphalt Binder (Rolling Thin-Film Oven Test), American Association of State Highway and Transportation Officials, 2009.

AASHTO T313-10-UL, Determining the Flexural Creep Stiffness of Asphalt Binder Using the Bending Beam Rheometer (BBR), American Association of State Highway and Transportation Officials, 2010.

AASHTO T314-07-UL Standard Method of Test for Determining the Fracture Properties of Asphalt Binder in Direct Tension (DT), American Association of State Highway and Transportation Officials, 2007.

AASHTO T322-07-UL, Standard Method of Test for Determining the Creep Compliance and Strength of Hot Mix Asphalt (HMA) Using the Indirect Tensile Test Device, American Association of State Highway and Transportation Officials, 2007.

Abraham H., Asphalt and Allied Substances, 6th edition, New York, Van Nostrand, 1960.

Anderson D. A., Champion-Lapalu L., Marasteanu M. O., Le Hirn Y. M., Planche J. P. and Martin D., Low-Temperature Thermal Cracking of Asphalt Binders as Ranked by Strength and Fracture Properties, Transportation Research Record, vol. 1766, pp. 1-6, 2001.

Ang A. H-S. and Tang. W. H., Probability Concepts in Engineering Planning and Design vol. II. Decision, Risk and Reliability. J. Wiley, New York, 1984.

Arnold J. C., The Influence of Liquid Uptake on Environmental Cracking of Glassy Polymers, Materials Science and Engineering A, vol. 197, pp. 119-124, 1995.

Batdorf S. B., Tensile Strength of Unidirectionally Reinforced Composites, Journal of Reinforced Plastics and Composites, vol. 1, pp. 153–164, 1982.

Bažant Z. P. He S., Plesha M. E. and Rowlands R. E., Rate Size Effects in Concrete Fracture: Implication for Dams, Proceedings of the International Conference on Dam Fracture, V. Saouma, R. Dungar and D. Morris editions, University of Colorado, Boulder, Colorado, pp. 255-261, 1991.

Bažant Z. P. and Gettu R., Rate Effects and Load Relaxation: Static Fracture of Concrete, ACI Materials Journal, vol. 89, 1992.

Bažant Z. P. and Jirasek M., R-Curve Modeling of Rate and Size Effects in Quasibrittle Fracture, International Journal of Fracture, vol. 62, pp. 355-373, 1993.

Bažant Z. P. and Li Z., Modulus of Rupture: Size Effect Due to Fracture Initiation in Boundary Layer, Journal of Structural Engineering, ASCE, vol. 121(4), pp. 739–746, 1995.

Bažant Z. P. and Li Y-N., Cohesive Crack with Rate-Dependent Opening and Viscoelasticity: I. Mathematical Model and Scaling, International Journal of Fracture, vol. 86, pp. 247-265, 1997.

Bažant Z. P. and Planas J., Fracture and Size Effect in Concrete and Other Quasibrittle Materials, CRC Press, Boca Raton, 1998.

Bažant Z. P. and Novák D., Energetic-Statistical Size Effect in Quasibrittle Failure at Crack Initiation, ACI Materials Journal, vol. 97(3), pp. 381–392, 2000.

Bažant Z. P., Scaling of Structural Strength, Elsevier, London, 2005.

Bažant Z.P. and Pang S-D., Activation Energy Based Extreme Value Statistics and Size Effect in Brittle and Quasibrittle Fracture, Journal of the Mechanics and Physics of Solids, vol. 55, pp. 91-131, 2007.

Bažant Z.P., Le J-L. and Bažant M. Z., Scaling of Strength and Lifetime Distributions of Quasibrittle Structures Based on Atomistic Fracture Mechanics, Proceedings of the National Academy of Science USA, vol. 106, pp. 11484-11489, 2009.

Bell C., Summary Report on Aging of Asphalt-Aggregate Systems, SHRP Report A-305, Washington D. C., National Research Council, 1989.

Berryman, J. G., Measurement of Spatial Correlation Functions Using Image Processing Techniques, Journal of Applied Physics, vol. 57, pp. 2374-2384, 1985.

Bonemazzi F., Braga V., Corrieri R., Giavarini C. and Sartori F., Characteristics of Polymers and Polymer-Modified Binders, Transportation Research Record, vol. 1535, pp.36–47, 1996.

Bouchaud J.-P. and Potters M., Theory of Financial Risks: From Statistical Physics to Risk Management, Cambridge University Press, Cambridge, UK, 2000.

Branthaver J.F., Petersen J.C., Robertson R.E., Duvall J.J., Kim S.S., Harnsberger P.M., Binder Characterization and Evaluation – vol. 2 Chemistry, SHRP Report A-368, Washington D. C., National Research Council, 1994.

Bulmer M.G., Principles of Statistics, Dover, New York, 1967.

Cannone Falchetto A., Marasteanu M. O. and Di Benedetto H., Analogical Based Approach to Forward and Inverse Problems for Asphalt Materials Characterization at low Temperatures, Journal of the Association of Asphalt Paving Technologists, vol. 80, pp. 549-582, 2011.

Cannone Falchetto A., Montepara A., Tebaldi G. and Marasteanu M. O., Microstructural and Rheological Investigation of Asphalt Mixtures Containing Recycled Asphalt Materials, Construction and Building Materials, vol 35, pp. 321-329, 2012a.

Cannone Falchetto A., Montepara A., Tebaldi G. and Marasteanu M. O., Microstructural Characterization of Asphalt Mixtures Containing Recycled Asphalt Materials. Journal of Materials in Civil Engineering, ASCE, 2012b (in press).

Carpinteri A. and Chiaia B., Fracture Mechanics of Concrete Structures, Proceedings of FraMCoS-2, Wittmann FH, Aedificatio Publisher, Freiburg, pp. 581-596, 1995.

Chen W-F., and Yuan R. L., Tensile Strength of Concrete: Double Punch Test, Journal of the Structural Division, vol. 106, pp. 1673-1693, 1980.

Christensen D., Pellinen T., Bonaquist R. F. Hirsch Model for Estimating the Modulus of Asphalt Concrete, Journal of Association of Asphalt Paving Technologists, vol. 72, pp. 97-121, 2003.

Christensen D. W. and Bonaquist, R. F., Evaluation of Indirect Tensile Test (IDT) Procedures for Low-Temperature Performance of Hot Mix Asphalt, NCHRP Report 530, Washington D.C., 2004.

Corbett L.W., Composition of Asphalt Based on Generic Fractionation, Using Solvent Deasphaltening, Elution-adsorption Chromatography and Densimetric Characterization, Analytical Chemestry, vol. 41, pp. 576–579, 1969.

Craus J., Ishai I. and Por N., Selective Sorption in Filler-Bitumen Systems, Journal of the Materials Science, vol. 14, pp. 2195–204, 1979.

Daniels E., The Statistical Theory of the Strength of Bundles and Threads, Proceedings of the Royal Society A, vol. 183, pp. 405–435, 1945.

Dickie J. P., Yen T. F., Macrostructure of the Asphaltic Fractions by Various Instrumental Methods, Analytical Chemestry, vol. 39, pp. 1847–1852, 1967.

da Vinci L., The Notebboks of Leonardo da Vinci, 1500s. Edward MvCurdy, London, 1945.

Di Benedetto H., Olard F., Sauzéat C., Delaporte B., Linear Viscoelastic Behaviour of Bituminous Materials : from Binders to Mixes, Road Material and Pavement Design, vol. 5 – Special Issue, pp.163-202, 2004.

Dongré J. and D'Angelo J., Effect of New Direct Tension Test Protocol on the Superpave Low-Temperature Specification for Bitumen Binders, Bearing Capacity of Roads and Airfields, 1998.

Duffy S. F., Powers L. M. and Starlinger. A., Reliability Analysis of Structural Ceramic Components Using a Three-parameter Weibull Distribution, ASME Journal Engineering for Gas Turbines and Power, vol. 115, pp. 109–116, 1993.

EN 12597, Bitumen and Bituminous Binders – Terminology, European Committee for Standardization, 2000.

EN 12697, Bituminous mixtures - Test methods for hot mix asphalt - Part 46: Low temperature cracking and properties by uniaxial tension tests, European Committee for Standardization, 2012.

Fisher R. A. and Tippet L. H. C., Limiting Forms of the Frequency Distribution of the Largest and Smallest Number of a Sample, Proceeding of the Cambridged Philosophical Society, vol. 24, pp. 180-190, 1928

Fréchet M., Sur la Loi de Probabilité de l'Écart Maximum. Annales Societatis Mathematicae Polonae, vol. 6, pp. 93–116, 1927.

Galilei G., Discorsi e Dimostrazioni Matematiche intorno a Due Nuove Scienze, 1638. Elsevirii Leiden, English transaltion by T. Weston, London, pp. 178-181, 1730.

Gawrys K. L. and Kilpatrick P. K., Asphaltene Aggregation: Techniques for Analysis, Journal of the Instrumentation Science and Technology, vol. 32, pp. 247–253, 2004.

Grassl P. and Bažant Z. P., Random Lattice-Particle Simulation of Statistical Size Effect in Quasi-Brittle Structures Failing at Crack Initiation, Journal of Engineering Mechanics, ASCE, vol. 135(2), 85–92, 2009.

Gross B., Least Squares Best Fit method for the Three Parameter Weibull Distribution: Analysis of Tensile and Bend Specimens with Volume or Surface Flaw Failure, NASA TM-4721, pp. 1-21, 1996.

Gumbel E. J., Statistics of Extremes. Columbia University Press, New York, 1958.

Haldar A. and Mahadevan S., Probability, Reliability, and Statistical Methods in Engineering Design, Wiley, New York, 2000.

Hase M., Oelkers C., Influence of Low Temperature Behaviour of PmB on Life Cycle, Proceding of the 7th International RILEM Symposium ATCBM09 on Advanced Testing and Characterization of Bituminous Materials, pp. 23-32, 2009.

Hasegawa T., Shioya T. and Okada T., Size Effect on Splitting Tensile Strength of Concrete, Proceeding of Japan Concrete Institute 7th Conference, pp. 309-312, 1985.

Hilleborg A., Modéer M. and Petersson P. E., Analysis of Crack Formation and Crack Growth in Concrete by Means of Fracture mechanics and Finite Elements, Cement and Concrete Research, vol. 6, pp. 773-782, 1976.

Hirsch T. J., Modulus of elasticity of concrete affected by elastic moduli of cement paste matrix and aggregate, Journal of the American Concrete Institute vol. 59(3), pp. 427-452, 1962.

Hoare T. R. and Hesp S. A. M., Low-temperature Fracture Testing of Asphalt Binders, Transportation Research Record, vol. 1728, pp. 36-42, 2000.

Huet, C., Etude par une méthode d'impédance du comportement viscoélastique des matériaux hydrocarbonés. Thèse de doctorat d'ingénieur, Faculté des Sciences de l'Université de Paris, pp. 69, October 1963, [In French].

Isaccson U. and Zeng H., Cracking of Asphalt at Low Temperature as Related to Bitumen Rheology, Journal of Material Science, vol. 33 pp. 2165–2170, 1998.

Jäger A., Lackner R., Eisenmenger-Sittner C. and Blab R., Identification of Microstructural Components of Bitumen by Means of Atomic Force Microscopy

(AFM), Proceedings in Applied Mathematics and Mechanics vol. 4, pp. 400–401, 2004.

Jennings P.W., Desando M.A., Raub M.F., Moats R., Mendez T.M., Stewart F.F., NMR Spectroscopy in the Characterization of Eight Selected Asphalts, Fuel Science & Technology International vol. 10, pp. 887–907, 1992.

Khedoe R., Molenaar A. and Ven M., Low Temperature Behavior of Very Hard Bituminous Binder Material for Road Applications, Proceeding of the 6th RILEM Conference on Cracking in Pavement, pp. 481-490, 2008.

Kim J-K., Size Effect on the Splitting Tensile Strength of Concrete and Mortar, Report No. CM 89-3, Korea Advanced Institute of Science and Technology, Seoul, 1989.

Koh C., *Lopp G.* and *Roque R.*, Development of a Dog-Bone Direct Tension Test (DBDT) for Asphalt Concrete, Proceding of the 7th International RILEM Symposium ATCBM09 on Advanced Testing and Characterization of Bituminous Materials, pp. 585-596, 2009.

Koots J. A. and Speight J. G., Relation of Petroleum Resins to Asphaltenes, Fuel, vol. 54, pp. 179–84, 1975.

Lay M. G., Ways of the World. New Brunswick, Rutgers University Press, 1992.

Le J-L. and Bažant Z. P., Finite Weakest Link Model with Zero Threshold for Strength Distribution of Dental Restorative Ceramics", Dental Materials, vol. 25(5), pp. 641-648, 2009.

Le J-L., Bažant Z. P. and Bažant M. Z., Unified Nano-mechanics Based Probabilistic Theory of Quasibrittle and Brittle Structures: I. Strength, Static Crack Growth, Lifetime and Scaling, Journal of the Mechanics and Physics of Solids 59, pp. 1291–1321, 2011

Le J-L., Eliáš, J. and Bažant, Z. P., Computation of Probability Distribution of Strength of Quasibrittle Structures Failing at Macro-Crack Initiation, Journal of Engineering Mechanics, ASCE, vol. 138(7), pp. 888-899, 2012.

Lee N. K., and Hesp S. A. M., Low Temperature Fracture Toughness of Polyethylene-Modified Asphalt Binders, Transportation Research Record vol. 1436, pp. 54-59, 1994.

Leicester R. H., The Size Effect of Notches, Proceedings of the 2nd Australian Conference of Mechanics of Structures and Materials, Melbourne, pp. 4.1–4.20, 1969.

Lesueur D., Gérard J. F., Claudy P., Létoffé J. M., Planche J. P., Martin D., A Structurerelated Model to Describe Asphalt Linear Viscoelasticity, Journal of Rheology, vol. 40, pp. 813–836, 1996.

Lesueur D., The Colloidal Structure of Bitumen: Consequences on the Rheology and on the Mechanisms of Bitumen Modification, Advances in Colloid and Interface Science, vol. 145, pp. 42–82, 2009.

Loeber L., Sutton O., Morel J., Valleton J. M. and Muller G., New Direct Observations of Asphalts and Asphalt Binders by Scanning Electron Microscopy and Atomic Force Microscopy, Journal of Microscopy, vol. 182, pp. 32–39, 1996.

Lohbauer U., Petchelt A. and Greil P., Lifetime Prediction of CAD/CAM Dental Ceramics, Journal of Biomedical Materials Research, vol. 63(6), pp. 780–785, 2002.

Lu X., Langton M., Olofsson P. and Redelius P., Wax Morphology in Bitumen, Journal of Materials Science, vol. 40 pp.1893–1900, 2005.

Mahesh S. and Phoenix S. L., Lifetime Distributions for Unidirectional Fibrous Composites Under Creep-Rupture Loading, International Journal of Fracture, vol. 127, pp. 303–360, 2004.

Marasteanu M. O., Zofka A., Turos M., Li X., Velasquez R., Li X., (University of Minnesota), Buttlar W., Paulino P., Braham A., Dave E., (University of Illinois), Ojo J., Bahia H., (University of Wisconsin, Madison), Williams C., Bausano J., Kvasnak A., (Iowa State University), Gallistel A., McGraw J., (Mn/DOT Office of Materials), Investigation of Low Temperature Cracking in Asphalt Pavements, National Pooled Fund Study 776, Final Report, Minneapolis, MN, October 2007.

M. Marasteanu M. O., Velasquez R., Cannone Falchetto A. and Zofka A., Development of a Simple Test to Determine the Low Temperature Creep Compliance of Asphalt Mixtures, IDEA Program Final Report, NCHRP-133, June 2009.

Marasteanu M.O., Cannone Falchetto A., Turos M. and Le J.-L., Development of a Simple Test to Determine the Low Temperature Strength of Asphalt Mixtures and Binders, IDEA Program Final Report NCHRP 151, July 2012 (in press).

Mariotte E., Traité du Mouvement des Eaux, Posthumously, 1686, edited by J.T. Desvaguliers London, 1918.

Masson J. F., Leblond V. and Margeson J., Bitumen Morphologies by Phase-detection Atomic Force Microscopy, Journal of Microscopy, vol. 221, pp. 17–29, 2006.

Milton G. W., Bounds on the Electromagnetic, Elastic, and Other Properties of Two-Component Composites, Physical Review Letters, vol. 46(8), pp. 542-545, 1981.

Monismith, C. L., Secor, K. E., Viscoelastic behavior of asphalt concrete pavements, Journal of the Association of Asphalt Paving Technologists, vol. 34, pp. 248-285, 1962.

Moore D. S., McCabe G. P. and Craig B. A., Introduction to the Practice of Statistics, W. H. Freeman and Company, New York, 2009.

Moskala E. J., A Fracture Mechanics approach to Environmental Stress Cracking in Poly(ethyleneterephtalate), Polymer, vol. 39(3), pp. 675-680, 1998.

Mullins O., Optical Interrogation of Aromatic Moieties in Crude Oils and Asphaltenes, In: Mullins O., Sheu E. Y., editors, Structures and Dynamics of Asphaltenes, New-York, Plenum Press, pp. 21–77, 1998.

Munz D. and Fett T., Ceramics: Mechanical Properties, Failure Behavior, Materials Selection, Springer-Verlag, Berlin, 1999.

NCAT - National Center for Asphalt Technology, Hot Mix Asphalt Materials, Mixture Design and Construction, 2009.

Nellensteyn F. J., The Constitution of Asphalt, Journal of the Institution of Petroleum Technologists, vol. 10, pp. 311–325, 1924.

Olard F. and Di Benedetto H., Fracture Toughness and Fracture Energy of Bituminous Binders at Low Temperatures, Proceedings of 5th RILEM International Conference on Cracking in Pavements, Limoges, France,May 5-7, 2004.

Oehlert G. W., A First Course in Design and Analysis of Experiments, W. H. Freeman; 1st edition, January 19, 2000.

Petersen J. C., Plancher H. and Harnsberger P. M., Lime Treatment of Asphalt to Reduce Age-Hardening and Improve the Flow Properties, Journal of the Association of Asphalt Paving Technologists, vol. 56, pp. 632–653, 1987.

Pfeiffer J. P. and Saal R. N. J,. Asphaltic Bitumen as Colloid Systems, Journal of Physical Chemistry, vol. 44 pp. 139–149, 1940.

Phoenix S.L. and Tierney L.-J., A Statistical Model for the Time Dependent Failure of Unidirectional Composite Materials Under Local Elastic Load-Sharing Among Fibers, Engineering Fracture Mechanics, vol. 18 (1), pp. 193–215, 1983.

PIARC - World Road Association, Use of Modified Bituminous Binders, Special Bitumens and Bitumens with Additives in road Pavements, Routes/Roads 303, 1999.

Portillo O. and Cebon D., An Experimental Investigation of the Fracture Mechanics of Bitumen and Asphalt, Proceeding of the 6th RILEM Conference on Cracking in Pavement, pp. 627-636, 2008.

Read J. and Whiteoak D., The Shell Bitumen Handbook, 5th edition, London, Thomas Telford Publishing, 2003.

Rigden D. J., Mineral Fillers in Bituminous Road Surfacings: a Study of Filler/Binder Systems in Relation to Filler Characteristics, Journal of the Society of Chemical Industry, vol. 66, pp.299–309, 1947.

Rinne H., The Weibull Distribution: A Handbook. CRC Press Taylor and Francis, 2009.

Rocco C., Guinea G. V., Planas J. and Elices M., The Effect of Boundary Conditions on the cylinder Splitting Strength, in Fracture Mechnaics of Concrete Structures, F. H. Wittmann edition, Aedification Publisher, Freiburg , Germany, pp.75-84, 1995.

Rocco C., Influencia del Tamaño y Mecanismos de Rotura del Ensayo de Compresion Diametral, Doctoral Thesis, Dep. Ciencia de Materiales, Universidad Politecnica de Madrid, ETS de Ingenieros de Caminos, Ciudad Universitaria, 28040 Madrid, Spain, 1996.

Rosinger A., Beiträge zur Kolloidchemie des Asphalts. Kolloid-Z, vol.15 pp. 177–179, 1914.

Sabnis G. M. and Mirza S. M., Size Effects in Model Concretes, Journal of the Structural Division, vol. 105(6), pp. 1007-1020, 1979.

Soong T. T., Fundamentals of Probability and Statistics for Engineers, Wiley, New York, 2004.

Speight J. G., Petroleum Asphaltene, Part 1, Asphaltenes, Resins and the Structure of Petroleum, Oil Gas Science and Technology, vol. 59, pp. 467–477, 2004.

Stanley P. and Inanc E. Y., Assessment of Surface Strength and Bulk Strength of a Typical Brittle Material, In: S. Eggwertz and N.C. Lind, Editors, Probabilistic Methods. I. The mechanics of Solids and Structures, Springer-Verlag, Berlin, pp. 231–251, 1985.

Storm D. A., Sheu E. Y., De Tar M. M., Macrostructure of Asphaltenes in Vacuum Residue by Small-angle X-Ray Scattering, Fuel, vol. 72, pp. 977–981, 1993.

Swartz S. E. and Siew H. C., Is Load Control Suitable for Fracture-Energy Measurements for Concrete, Experimental Mechanics, vol. 27(4), pp. 359-365, 1987.

Tinschert J., Zwez D., Marx R. and Ausavice K. J., Structural Reliability of Alumina-, Feldspar-, Leucite-, Mica- and Zirconia-based Ceramic,s Journal of Dentistry, vol. 28, pp. 529–535, 2000.

Torquato S., Random Heterogeneous Materials, Springer-Verlag, New York, 2002.

Turner T. F., Branthaver J. F., DSC Studies of Asphalts and Asphalts Components. In: Usmani A. M., editor. Asphalt Science and Technology. New York, Marcel Dekker, pp. 59–101, 1997.

Turos M, Cannone Falchetto A, Tebaldi G. and Marasteanu M. O., The Flexural Strength of Asphalt Mixtures Using the Bending Beam Rheometer, Proceeding of the 7th RILEM Conference on Cracking in Pavements, pp.11-20, 2012.

U.S. Department of Transportation, Research and Innovative Technology Administration Bureau of Transportation Statistics, National Transportation Statistics 2010.

Velasquez R.A., On the Representative Volume Element of Asphalt Concrete with Application to Low Temperature, PhD Thesis, University of Minnesota, Minneapolis, July 2009.

Velasquez R.A., Tabatabaee H. and Bahia H., Low Temperature Cracking Characterization of Asphalt Binders by Means of the Single-Edge Notch Bending (SENB) Test, Journal of Association of Asphalt Paving Technologists, vol. 80, pp. 583-614, 2011.

Walsh P.F., Fracture of Plain Concrete, Indian Concrete Journal, vol 46 (11), 1972.

Weibull W., The Phenomenon of Rupture in Solids, Proceedings of Royal Swedish Institute of Engineering Research, vol. 151, Stockholm, pp. 1–45, 1939.

Zofka A., Marasteanu M., Development of Double Edge Notched Tension (DENT) Test for Asphalt Binders, Journal of Testing and Evaluation, ASTM, vol. 35/3, pp. 259-265, May 2007.